Eur. Phys. J. A **10**, 395–446 (2001)

THE EUROPEAN PHYSICAL JOURNAL A

The light-baryon spectrum in a relativistic quark model with instanton-induced quark forces

The non-strange–baryon spectrum and ground states

U. Löring[a], B.Ch. Metsch, and H.R. Petry

Institut für Theoretische Kernphysik, Universität Bonn, Nußallee 14-16, D-53115 Bonn, Germany

Received: 27 March 2001
Communicated by V.V. Anisovich

Abstract. This is the second of a series of three papers treating light-baryon resonances up to 3 GeV within a relativistically covariant quark model based on the three-fermion Bethe-Salpeter equation with instantaneous two- and three-body forces. In this paper we apply the covariant Salpeter framework (which we developed in the first paper, U. Löring, K. Kretzschmar, B.Ch. Metsch, H.R. Petry, Eur. Phys. J. A **10**, 309 (2001)) to specific quark model calculations. Quark confinement is realized by a linearly rising three-body string potential with appropriate spinorial structures in Dirac space. To describe the hyperfine structure of the baryon spectrum we adopt 't Hooft's residual interaction based on QCD-instanton effects and demonstrate that the alternative one-gluon exchange is disfavored on phenomenological grounds. Our fully relativistic framework allows to investigate the effects of the full Dirac structures of residual and confinement forces on the structure of the mass spectrum. In the present paper we present a detailed analysis of the complete non-strange–baryon spectrum and show that several prominent features of the nucleon spectrum such as, *e.g.*, the Roper resonance and approximate "parity doublets" can be uniformly explained due to a specific interplay of relativistic effects, the confinement potential and 't Hooft's force. The results for the spectrum of strange baryons will be discussed in a subsequent paper, see U. Löring, B.Ch. Metsch, H.R. Petry, this issue, p. 447.

PACS. 11.10.St Bound and unstable states; Bethe-Salpeter equations – 12.39.Ki Relativistic quark model – 12.40.Yx Hadron mass models and calculations – 14.20.-c Baryons (including antiparticles)

1 Introduction

In the previous paper [1] we analyzed the three-fermion Bethe-Salpeter equation [2,3] with instantaneous two- and three-body interaction kernels. Without being too specific concerning the interaction kernels, we derived the three-fermion Salpeter equation [4]. We now want to apply this covariant formalism to a system of three light quarks with flavors up, down and strange and thus use this fully relativistic framework as basis for a quark model of light baryons. In fact, the reduced Salpeter equation provides a suitable, fully relativistic framework, which nonetheless keeps as close as possible to the rather successful non-relativistic potential models: On the one hand, we found a one-to-one correspondence of the Salpeter amplitudes with the ordinary states of the non-relativistic quark model meditated by the embedding map of non-relativistic three-quark Pauli spinors to full three-quark Dirac spinors. On the other hand, this approach adopts the concept of constituent quarks with an effective mass where the underlying interactions are described by inter-quark potentials in the rest frame of the baryons. Hence, we basically have the same input describing the quark dynamics as in non-relativistic quark models, in particular the number of parameters remains exactly the same as in a corresponding non-relativistic approach [1]. To be specific, we now have to fill in the details of the underlying quark interactions, *i.e.* we have to specify the three- and two-body potentials $V^{(3)}$ and $V^{(2)}$, respectively, which we

[a] e-mail: loering@itkp.uni-bonn.de

[1] It is worth mentioning here that this is quite in contrast to other attempts like the so-called "relativized" quark models [5,6] which just parameterize relativistic effects and therefore introduce additional parameters.

use as instantaneous interaction kernels. We then solve the resulting Salpeter equation numerically. The fact that this equation can be cast in Hamiltonian form allows for the use of a variational principle: We expand our wave functions in terms of harmonic-oscillator functions and diagonalize the Hamiltonian with respect to a truncated wave function basis checking carefully numerical stabilities.

One of our aims is to extend a covariant quark model for mesons [7–13] which is based on the quark-antiquark Bethe-Salpeter equation with instantaneous two-body interaction kernels. In this model the interaction between quark and antiquark included a linearly rising (string-like) confinement potential provided with a suitable spinorial form (Dirac structure), which was combined with the effective residual interaction first computed by 't Hooft from instanton effects in QCD [14]. In fact, it turned out that this relativistic approach, which employs 't Hooft's force as residual interaction, provides significant improvements with respect to other, non-relativistic or "relativized" approaches which in general use parts of the residual one-gluon exchange in addition to a confining central potential. In particular, this model allows for a consistent and complete description of the whole mesonic mass spectrum but at the same time also for the description of dynamical observables such as form factors, where a fully covariant treatment of the quark dynamics becomes particularly crucial. The results are rather encouraging to extend this approach to baryons. Thus, our main choice for $V^{(2)}$ is 't Hooft's instanton-induced quark interaction. However, in appendix A we will also show the result of calculations with a one-gluon exchange potential, demonstrating that from a phenomenological point of view it should be discarded.

Similar to the Salpeter model for mesons, quarks in baryons shall be confined by a linearly rising string potential. Generalizing the linear quark-antiquark confinement for mesons our quark confinement for baryons will be produced by a three-quark string potential $V^{(3)}$ provided with an appropriate Dirac structure. As in the meson model [7,8,12,13] we use in addition 't Hooft's two-quark interaction mentioned before as residual two-body force $V^{(2)}$. A non-relativistic version with these dynamics has been applied already by Blask *et al.* [15–17] for the calculation of baryon (and meson) mass spectra. We would like to note that this model could satisfactorily account for the gross features of the light-baryon spectrum with only seven parameters. In particular, it was able to explain the sign and the rough size of hyperfine splittings of ground-state baryons as well as the right size of splittings of negative-parity excited baryons. However, a closer look at the mass spectra reveals that special features, such as, *e.g.*, the conspicuously low-lying first scalar/isoscalar excitations of the octet ground states (Roper resonances) or the highest members of Regge trajectories cannot be accounted for in the non-relativistic framework. In particular, these issues improve in the present relativistic approach. We will not always comment in detail on calculations in alternative baryon models; for an excellent review see ref. [18].

In this paper baryon resonances are treated as bound states and no calculation of widths is performed. This is certainly questionable, but so far is due to technical limitations. To improve this situation, one has to specify the decay channels and perform at least a perturbative calculation of the decay widths [19]. Very often this is not sufficient since final-state interactions may also change (non-perturbatively) the resonance positions appreciably [20–25]. As long as this shift is approximately uniform, it can be absorbed in the potential parameters of the quark model. We are aware of the fact that this is true in many, but not all cases [20–25].

Our paper is organized as follows: In sect. 2 we specify the explicit form of the instantaneous three-quark confinement kernel $V^{(3)}$. We introduce two alternative confinement models (model $\mathcal{A}$ and model $\mathcal{B}$) which essentially differ in the choice of the Dirac structures only. Both versions shall be tested in the subsequent investigations in a comparison to the experimental mass spectrum. In sect. 3 we introduce 't Hooft's instanton-induced residual two-quark interaction and discuss its specific structure. In the subsequent sections a detailed discussion of our results in comparison to the phenomenological non-strange–baryon (and ground-state) spectrum is given. We start with some general comments concerning the parameter dependencies in sect. 4. In sect. 5 we investigate the results of our calculations for the Δ spectrum where 't Hooft's interaction gives no contribution. These investigations constitute a first test of the confinement models considered. Section 6 is concerned with the hyperfine structure of the ground-state baryons and the role of the instanton-induced interaction for generating this structure. Section 7 is devoted to an extensive discussion of the excited nucleon spectrum. A principal objective of this discussion is to demonstrate how instanton-induced effects along with the $\Delta - N$ hyperfine splitting simultaneously generate several prominent structures seen in the experimental nucleon spectrum such as, *e.g.*, the low position of the Roper resonance or the occurrence of approximate "parity doublets". Finally we give a summary and a conclusion in sect. 8. A detailed discussion of the corresponding results for the strange baryons will be presented in a subsequent paper [26].

2 Three-body confinement

It is well known that the global structure of the experimental baryon and meson mass spectrum suggests a linearly rising, flavor-independent confinement potential. The appearance of the experimentally observed baryon resonances as nearly degenerate, alternating even- and odd-parity shells motivates the picture that the quarks are moving in a local potential which roughly reflects harmonic forces between the quarks. This picture led to the naive quark oscillator shell model. Moreover, phenomenological analyses of the experimental baryon (and also meson) spectra up to highest orbital excitations show a remarkable empirical connection between the total spin J and the squared mass M^2 of the states, namely that certain states, within a so-called Chew-Frautschi plot of M^2

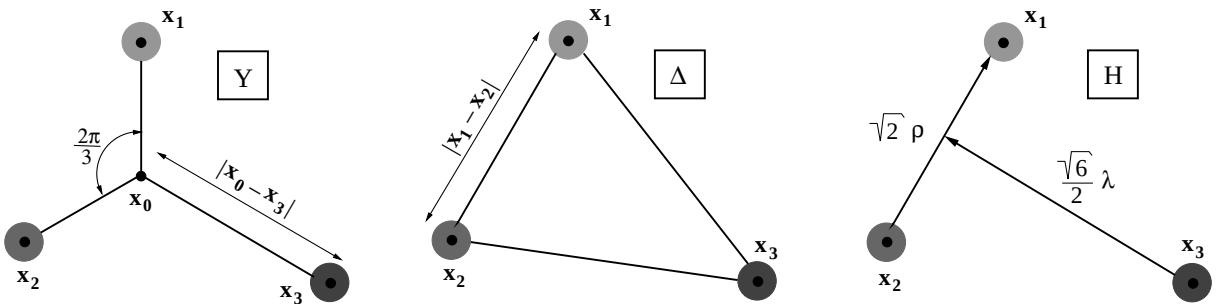

Fig. 1. The Y-type (left), Δ-type (middle) and hyperspherical (right) string-like confinement interaction between all three quarks.

vs. J, lie on linear Regge trajectories $M^2 \sim J$. The interpretation of this empirical feature motivates a string picture for the confinement mechanism, where the quarks are connected by gluonic strings (flux tubes) such that the effective confining potential rises linearly with the string length for large distances of the quarks. A further confirmation of this scenario stems from lattice QCD calculations, which in fact indicate a string-like realization of the confinement force in the static limit of heavy quarks; for a review of these issues we refer to [27] and references therein.

We therefore choose a three-body confinement force which in the rest frame of the baryon takes the form:

$$\begin{aligned} &V^{(3)}(x_1,x_2,x_3;\ x_1',x_2',x_3') = \\ &V^{(3)}_{\rm conf}(\mathbf{x}_1,\mathbf{x}_2,\mathbf{x}_3)\delta^{(1)}(x_1^0-x_2^0)\delta^{(1)}(x_2^0-x_3^0) \\ &\times\delta^{(4)}(x_1-x_1')\ \delta^{(4)}(x_2-x_2')\ \delta^{(4)}(x_3-x_3'). \end{aligned} \tag{1}$$

Here $V^{(3)}_{\rm conf}(\mathbf{x}_1,\mathbf{x}_2,\mathbf{x}_3) = V^{(3)}_{\rm conf}(r_{3q}) \sim r_{3q}$ denotes the local three-quark potential whose radial dependence is assumed to be linearly increasing with some "collective" radius $r_{3q} = r_{3q}(\mathbf{x}_1,\mathbf{x}_2,\mathbf{x}_3)$ (string picture). (As will be discussed below such a three-quark distance can be realized in various ways.) In contrast to non-relativistic quark models, in our fully relativistic framework the radial dependence has to be provided with an appropriate spinorial three-quark Dirac structure $\mathcal{W}$. Thus, the most general ansatz for a flavor-independent confinement potential $V^{(3)}_{\rm conf}$, which rises linearly with the inter-quark distance r_{3q}, is given by

$$V^{(3)}_{\rm conf}(\mathbf{x}_1,\mathbf{x}_2,\mathbf{x}_3) = [a\mathcal{W}_{\rm off} + b\ r_{3q}(\mathbf{x}_1,\mathbf{x}_2,\mathbf{x}_3)\mathcal{W}_{\rm str}]\,, \tag{2}$$

where a is an overall constant offset associated with a three-quark Dirac structure $\mathcal{W}_{\rm off}$ and b is the slope of the linearly rising part which is associated with the Dirac structure $\mathcal{W}_{\rm str}$. In general the spin structures $\mathcal{W}_{\rm off}$ and $\mathcal{W}_{\rm str}$ of the constant and linear part can be chosen differently (see discussion below).

As illustrated in fig. 1, there are several possibilities to define the linear inter-quark distance, which we refer to as Y-type, Δ-type and hyperspherical (H) string. The first type was proposed by Carlson *et al.* [28,29] and is intimately related to the color-$SU(3)$ group: In a color singlet qqq system, each quark acts as a source of one flux tube. For $SU(3)$ gauge fields the flux tubes can merge at a single point $\mathbf{x}_0$, which in the adiabatic approximation is chosen such that the energy and hence the length $r_{3q} = r_{\rm Y}$ of the connecting path is minimized to

$$r_{3q}(\mathbf{x}_1,\mathbf{x}_2,\mathbf{x}_3) = r_{\rm Y} := \min_{\mathbf{x}_0} \sum_{i=1}^{3} |\mathbf{x}_i - \mathbf{x}_0|. \tag{3}$$

Then the straight lines emanating from the quarks will meet at an angle $2\pi/3$ at the central junction point $\mathbf{x}_0$ (see fig. 1), unless one of the angles within the baryonic triangle exceeds the value $2\pi/3$, in which case a linear geometry is preferred. An alternative three-quark distance $r_{3q} = r_\Delta$ is defined by the Δ string configuration, in which case the string is formed by the sum of two-body strings between each quark pair:

$$r_{3q}(\mathbf{x}_1,\mathbf{x}_2,\mathbf{x}_3) = r_\Delta := \sum_{i<j} |\mathbf{x}_i - \mathbf{x}_j|. \tag{4}$$

Rescaling this quark distance with a factor $f \simeq 0.5493$ [6, 30,16], its length $f\,r_\Delta$ constitutes a fairly good approximation to the Y-type string potential

$$r_{\rm Y} \approx f\,r_\Delta, \quad \text{where } f = 0.5493 \quad \left(\frac{1}{2} < f < \frac{1}{\sqrt{3}}\right). \tag{5}$$

Obviously, whenever the three quarks are collinear, the factor is exactly $1/2$, while for the other extreme case of an equilateral triangle the factor is $1/\sqrt{3}$. The choice $f = 0.5493$ lies between these two extremes. This particular ratio is chosen such that it minimizes the size of the expectation value of $|r_{\rm Y} - f\,r_\Delta|$ in the harmonic-oscillator basis [6,16] and moreover is also favored by some investigations of flux tubes on the lattice [30]. Only a few lattice results on static baryonic potentials (see [27] and references therein) exist so far with statistical errors too large to rule out either possibility. In a more recent study (see [27]), however, clear evidence in

$$\Delta\mathcal{L}_{\rm eff}(y) = \int_0^{\rho_c} {\rm d}\rho\, \frac{d_0(\rho)}{\rho^5} \Bigg\{ \left(m_u^0\rho - \frac{4}{3}\pi^2\rho^3\,(\overline{\Psi}_{uR}\Psi_{uL})\right)\left(m_d^0\rho - \frac{4}{3}\pi^2\rho^3\,(\overline{\Psi}_{dR}\Psi_{dL})\right)\left(m_s^0\rho - \frac{4}{3}\pi^2\rho^3\,(\overline{\Psi}_{sR}\Psi_{sL})\right)$$
$$+\frac{3}{32}\left(\frac{4}{3}\pi^2\rho^3\right)^2 \Bigg[\left((\overline{\Psi}_{uR}\lambda^a\Psi_{uL})(\overline{\Psi}_{dR}\lambda^a\Psi_{dL}) - \frac{3}{4}(\overline{\Psi}_{uR}\sigma_{\mu\nu}\lambda^a\Psi_{uL})(\overline{\Psi}_{dR}\sigma^{\mu\nu}\lambda^a\Psi_{dL})\right)$$
$$\times\left(m_s^0\rho - \frac{4}{3}\pi^2\rho^3\,(\overline{\Psi}_{sR}\Psi_{sL})\right) + \frac{9}{40}\left(\frac{4}{3}\pi^2\rho^3\right)\, d^{abc}\,(\overline{\Psi}_{uR}\sigma_{\mu\nu}\lambda^a\Psi_{uL})(\overline{\Psi}_{dR}\sigma^{\mu\nu}\lambda^b\Psi_{dL})(\overline{\Psi}_{sR}\lambda^c\Psi_{sL})$$
$$+\text{cycl. perm. of } (uds)\Bigg] + \frac{9}{320}\left(\frac{4}{3}\pi^2\rho^3\right)^3\, d^{abc}\,(\overline{\Psi}_{uR}\lambda^a\Psi_{uL})(\overline{\Psi}_{dR}\lambda^b\Psi_{dL})(\overline{\Psi}_{sR}\lambda^c\Psi_{sL})$$
$$+\frac{9}{256}\,{\rm i}\left(\frac{4}{3}\pi^2\rho^3\right)^3\, f^{abc}\,(\overline{\Psi}_{uR}\sigma_\mu^\nu\lambda^a\Psi_{uL})(\overline{\Psi}_{dR}\sigma_\nu^\gamma\lambda^b\Psi_{dL})(\overline{\Psi}_{sR}\sigma_\gamma^\mu\lambda^c\Psi_{sL}) \;+\; (L\leftrightarrow R)\Bigg\}. \tag{11}$$

support of the Δ configuration has been found. A further example is a hyperspherical ansatz [31,32], which increases linearly with the hyperradius

$$r_{3q}(\mathbf{x}_1,\mathbf{x}_2,\mathbf{x}_3) = r_{\rm hyp} := \sqrt{|\boldsymbol{\rho}|^2+|\boldsymbol{\lambda}|^2},$$
$$\text{where}\quad \begin{aligned}\boldsymbol{\rho} &:= \tfrac{1}{\sqrt{2}}(\mathbf{x}_1-\mathbf{x}_2),\\ \boldsymbol{\lambda} &:= \tfrac{1}{\sqrt{6}}(\mathbf{x}_1+\mathbf{x}_2-2\mathbf{x}_3).\end{aligned} \tag{6}$$

We would like to note at this stage that we have tested the various radial dependencies (3), (4) and (6) in our Salpeter model. Our investigations, however, clearly showed that the structure of resulting spectra depends only slightly on the various radial dependencies chosen. It turned out that the slope parameter b can always be appropriately rescaled (as, *e.g.*, in eq. (5) with the factor f) to obtain almost the same spectrum for all three choices. We therefore prefer for our model the Δ-shape string potential rising linearly with $r_\Delta(\mathbf{x}_1,\mathbf{x}_2,\mathbf{x}_3) = \sum_{i<j}|\mathbf{x}_i-\mathbf{x}_j|$ which, on the one hand, is favored by the most recent lattice studies anyway and, on the other hand, is also much easier to handle numerically. We found, however, that the structure of the resulting spectra depends much more on the Dirac structure chosen, which we shall consider next.

The gross features of the baryon resonances seem to indicate that the dominating confinement forces should be spin-independent, at least in the non-relativistic limit. This property can be realized exactly if and only if $\mathcal{W}_{\rm off}$ and $\mathcal{W}_{\rm str}$ have the form

$$\mathcal{W}_{\rm str} = \alpha_{\rm str}\mathbb{1}\otimes\mathbb{1}\otimes\mathbb{1}+\beta_{\rm str}\left(\gamma^0\otimes\gamma^0\otimes\mathbb{1}+\text{cycl. perm.}\right), \tag{7}$$

$$\mathcal{W}_{\rm off} = \alpha_{\rm off}\mathbb{1}\otimes\mathbb{1}\otimes\mathbb{1}+\beta_{\rm off}\left(\gamma^0\otimes\gamma^0\otimes\mathbb{1}+\text{cycl. perm.}\right). \tag{8}$$

(The appearance of $\gamma^0\otimes\gamma^0$ is allowed because the potential is defined in the rest frame of the baryon!) In this paper we show results only for the following model choices:

– *Model* $\mathcal{A}$

$$V_{\rm conf}^{(3)}(\mathbf{x}_1,\mathbf{x}_2,\mathbf{x}_3) = 3\,a\;\frac{1}{4}\left[\mathbb{1}\otimes\mathbb{1}\otimes\mathbb{1}+\gamma^0\otimes\gamma^0\otimes\mathbb{1}+\text{cycl. perm.}\right] + b\sum_{i<j}|\mathbf{x}_i-\mathbf{x}_j| \times\frac{1}{2}\left[-\mathbb{1}\otimes\mathbb{1}\otimes\mathbb{1}+\gamma^0\otimes\gamma^0\otimes\mathbb{1}+\text{cycl. perm.}\right], \tag{9}$$

– *Model* $\mathcal{B}$

$$V_{\rm conf}^{(3)}(\mathbf{x}_1,\mathbf{x}_2,\mathbf{x}_3) = \left[3a + b\sum_{i<j}|\mathbf{x}_i-\mathbf{x}_j|\right] \times\frac{1}{4}\left[\mathbb{1}\otimes\mathbb{1}\otimes\mathbb{1}+\gamma^0\otimes\gamma^0\otimes\mathbb{1}+\text{cycl. perm.}\right], \tag{10}$$

which have in common that they give the same non-relativistic limit and that they produce equivalent results in flavor-symmetric states. The offset constant a and the slope b enter as free parameters in our models.

3 't Hooft's instanton-induced interaction

As originally shown by 't Hooft [14], instantons lead to an effective contribution to the interaction of quarks. The corresponding effective Lagrangian $\Delta\mathcal{L}_{\rm eff}$ which has been calculated by 't Hooft for the case of the $SU(2)$ gauge group has been generalized to the case of the $SU(3)$ gauge group by Shifman, Vainshtein and Zakharov [33]. They have shown that the contribution of a single instanton and antiinstanton configuration to the effective quark Lagrangian in the case of the $SU(3)$ color group and three light quarks with flavors up (u), down (d) and strange (s) is given by [33]

see equation (11) *above*

Here m_f^0 are the current quark masses for the various light flavor degrees of freedom $f = u, d$ and s. λ^a $(a = 1,\ldots,8)$

denote the standard $SU(3)$ color Gell-Mann matrices and f^{abc}, d^{abc} are the $SU(3)$ structure constants defined by the commutators and anticommutators

$$[\lambda^a,\lambda^b]=\mathrm{i}2f^{abc}\lambda^c,\qquad \{\lambda^a,\lambda^b\}=\frac{4}{3}\delta^{ab}\mathbb{1}+2d^{abc}\lambda^c. \quad (12)$$

$\Psi_{f\,L,R}\equiv\Psi_{f\,L,R}(y)$ are the projections on left- and right-handed components of the quark field operators:

$$\Psi_{f\,L}:=\frac{\mathbb{1}+\gamma^5}{2}\,\Psi_f\qquad \Psi_{f\,R}:=\frac{\mathbb{1}-\gamma^5}{2}\,\Psi_f. \quad (13)$$

An important quantity entering eq. (11) as a generic weight is the reduced instanton density $D(\rho)=d_0(\rho)/\rho^5$ which describes the vacuum-to-vacuum tunneling probability in the presence of an instanton with size ρ. In the case of three colors and three flavors $d_0(\rho)$ is given by [34]

$$d_0(\rho)=(3.63\cdot10^{-3})\,\left(\frac{8\pi^2}{g^2(\rho)}\right)^6\exp\left(-\frac{8\pi^2}{g^2(\rho)}\right). \quad (14)$$

The function $g(\rho)$ denotes the ρ-dependent running coupling constant, which in two-loop accuracy reads

$$\frac{8\pi^2}{g^2(\rho)}=9\ln\left(\frac{1}{\rho\,\Lambda_{\mathrm{QCD}}}\right)+\frac{32}{9}\ln\left[\ln\left(\frac{1}{\rho\,\Lambda_{\mathrm{QCD}}}\right)\right], \quad (15)$$

where Λ_{QCD} is the QCD scale parameter. Unfortunately, using the semi-classical 't Hooft formula (14), large-size instantons make the integration diverge due to the power law behavior of the reduced instanton size distribution $D(\rho)=d_0(\rho)/\rho^5$. This is known as the so-called "*infrared problem*". To cure this problem, we cut the ρ integral for the moment by hand [35], introducing a critical instanton size ρ_c for which the ln ln-term of (15) is still reasonably small compared to the ln-term.

The interaction described before is chirally invariant if the current quark masses are strictly zero. As is well known, it is no longer $U_A(1)$-invariant and thus exhibits the characteristic breaking of this symmetry in QCD. In addition we must take the spontaneous breaking of chiral invariance into account which is most easily done by normal ordering $\Delta\mathcal{L}_{\mathrm{eff}}$ with respect to a vacuum of massive quarks with constituent quark masses. The result is

$$\Delta\mathcal{L}_{\mathrm{eff}}=\epsilon+\Delta\mathcal{L}^{(1)}_{\mathrm{eff}}+\Delta\mathcal{L}^{(2)}_{\mathrm{eff}}+\Delta\mathcal{L}^{(3)}_{\mathrm{eff}}. \quad (16)$$

1. Here ϵ is a constant (a shift in the vacuum energy).
2. $\Delta\mathcal{L}^{(1)}_{\mathrm{eff}}$ is a mass term:

$$\Delta\mathcal{L}_{\mathrm{eff}}(1)=-\Delta m_n\left(:\overline{\Psi}_u\Psi_u:+:\overline{\Psi}_d\Psi_d:\right)-\Delta m_s:\overline{\Psi}_s\Psi_s:, \quad (17)$$

with

$$\Delta m_n:=\int_0^{\rho_c}\mathrm{d}\rho\frac{d_0(\rho)}{\rho^5}\frac{4}{3}\pi^2\rho^3\Big(m_n^0\rho-\frac{2}{3}\pi^2\rho^3\langle\overline{\Psi}_n\Psi_n\rangle\Big)\times\Big(m_s^0\rho-\frac{2}{3}\pi^2\rho^3\langle\overline{\Psi}_s\Psi_s\rangle\Big), \quad (18)$$

$$\Delta m_s:=\int_0^{\rho_c}\mathrm{d}\rho\frac{d_0(\rho)}{\rho^5}\frac{4}{3}\pi^2\rho^3\,\Big(m_n^0\rho-\frac{2}{3}\pi^2\rho^3\langle\overline{\Psi}_n\Psi_n\rangle\Big)^2, \quad (19)$$

where $m_n:=m_n^0+\Delta m_n$ and $m_s:=m_s^0+\Delta m_s$ are naturally identified with the non-strange and strange constituent quark masses (if possible contributions from the confining forces are excluded). In the following we will treat the effective constituent quark masses m_n and m_s as free parameters which we fit to the experimental baryon spectrum.

3. $\Delta\mathcal{L}^{(2)}_{\mathrm{eff}}$ is a two-body interaction which can be cast in the more convenient form

$$\begin{aligned}\Delta\mathcal{L}^{(2)}_{\mathrm{eff}}=&-2:\overline{\Psi}\otimes\overline{\Psi}\left[\left(\mathbb{1}\otimes\mathbb{1}+\gamma^5\otimes\gamma^5\right)\mathcal{P}^{\mathcal{D}}_{S=0}\right.\\&\left.\otimes\left(g_{nn}\mathcal{P}^{\mathcal{F}}_{\mathcal{A}}(nn)+g_{ns}\mathcal{P}^{\mathcal{F}}_{\mathcal{A}}(ns)\right)\otimes\mathcal{P}^{\mathcal{C}}_{\bar{\mathbf{3}}}\right]\Psi\otimes\Psi:\\&-:\overline{\Psi}\otimes\overline{\Psi}\left[\left(\mathbb{1}\otimes\mathbb{1}+\gamma^5\otimes\gamma^5\right)\mathcal{P}^{\mathcal{D}}_{S=1}\right.\\&\left.\otimes\left(g_{nn}\mathcal{P}^{\mathcal{F}}_{\mathcal{A}}(nn)+g_{ns}\mathcal{P}^{\mathcal{F}}_{\mathcal{A}}(ns)\right)\otimes\mathcal{P}^{\mathcal{C}}_{\mathbf{6}}\right]\Psi\otimes\Psi,\end{aligned} \quad (20)$$

where the effective coupling constants $g_{nn}:=3/8g_{\mathrm{eff}}(s)$ and $g_{ns}:=3/8g_{\mathrm{eff}}(n)$ are given by

$$g_{\mathrm{eff}}(f):=\int_0^{\rho_c}\mathrm{d}\rho\,\frac{d_0(\rho)}{\rho^5}\left(\frac{4}{3}\pi^2\rho^3\right)^2\Big(m_f^0\rho-\frac{2}{3}\pi^2\rho^3\langle\overline{\Psi}_f\Psi_f\rangle\Big). \quad (21)$$

This expression in terms of two-quark projection operators in Dirac, flavor and color spaces allows an immediate identification of the diquark channels that in fact are affected by the interaction: In color space $\mathcal{P}^{\mathcal{C}}_{\bar{\mathbf{3}}}$ and $\mathcal{P}^{\mathcal{C}}_{\mathbf{6}}$ denote the projectors onto color antitriplet and color sextet pairs. Since the three quarks within the baryon have to constitute a color singlet, two quarks always have to be in a color antitriplet state. For this reason the second term of the Lagrangian (20), which affects color-sextet quark pairs only, does not contribute in lowest order to the baryon dynamics. In Dirac space, $\mathcal{P}^{\mathcal{D}}_{S=0}$ and $\mathcal{P}^{\mathcal{D}}_{S=1}$ are the projectors onto antisymmetric spin-singlet and symmetric spin-triplet states, respectively, defined by

$$\begin{aligned}\mathcal{P}^{\mathcal{D}}_{S=0}&:=\frac{1}{4}\,\mathbb{1}\otimes\mathbb{1}-\frac{1}{4}\,\boldsymbol{\Sigma}\cdot\otimes\boldsymbol{\Sigma}\\ \text{and}\qquad \mathcal{P}^{\mathcal{D}}_{S=1}&:=\frac{3}{4}\,\mathbb{1}\otimes\mathbb{1}+\frac{1}{4}\,\boldsymbol{\Sigma}\cdot\otimes\boldsymbol{\Sigma},\end{aligned} \quad (22)$$

with $\boldsymbol{\Sigma}\cdot\otimes\boldsymbol{\Sigma}:=\sum_{i=1}^3\Sigma^i\otimes\Sigma^i$ and $\Sigma^i=\mathrm{diag}(\sigma^i,\sigma^i)$, where σ^i are the usual Pauli matrices. In flavor space the operators $\mathcal{P}^{\mathcal{F}}_{\mathcal{A}}(nn)$ and $\mathcal{P}^{\mathcal{F}}_{\mathcal{A}}(ns)$ denote the projectors onto flavor-antisymmetric quarks which either are non-strange (nn), *i.e.* with isospin zero, or non-strange–strange (ns):

$$\begin{aligned}\mathcal{P}^{\mathcal{F}}_{\mathcal{A}}(nn)&:=\left(\mathcal{P}^{\mathcal{F}}_n\otimes\mathcal{P}^{\mathcal{F}}_n\right)\,\mathcal{P}^{\mathcal{F}}_{\mathcal{A}},\\ \mathcal{P}^{\mathcal{F}}_{\mathcal{A}}(ns)&:=\left(\mathcal{P}^{\mathcal{F}}_n\otimes\mathcal{P}^{\mathcal{F}}_s+\mathcal{P}^{\mathcal{F}}_s\otimes\mathcal{P}^{\mathcal{F}}_n\right)\,\mathcal{P}^{\mathcal{F}}_{\mathcal{A}}.\end{aligned} \quad (23)$$

Here $\mathcal{P}^{\mathcal{F}}_n=|u\rangle\langle u|+|d\rangle\langle d|$ and $\mathcal{P}^{\mathcal{F}}_s=|s\rangle\langle s|$ are the projectors for single quark flavors and $\mathcal{P}^{\mathcal{F}}_{\mathcal{A}}=\frac{1}{2}(\mathbb{1}^{\mathcal{F}}-\mathcal{P}^{\mathcal{F}}_{12})$ is the antisymmetrizer in the two-particle flavor space.

Table 1. The parameters of the confinement force, the 't Hooft interaction and the constituent quark masses fitted in the models $\mathcal{A}$ and $\mathcal{B}$.

		Parameter	Model $\mathcal{A}$	Model $\mathcal{B}$
Constituent quark masses	non-strange	m_n	330 MeV	300 MeV
	strange	m_s	670 MeV	620 MeV
Confinement parameters	offset	a	-744 MeV	-1086 MeV
	slope	b	470 MeV fm^{-1}	1193 MeV fm^{-1}
't Hooft interaction	effective range	λ	0.4 fm	0.4 fm
	nn-coupling	g_{nn}	136.0 MeV fm^3	89.6 MeV fm^3
	ns-coupling	g_{ns}	94.0 MeV fm^3	61.7 MeV fm^3

Accordingly, 't Hooft's force acts exclusively on quark pairs which are antisymmetric in flavor and it distinguishes between diquarks of different flavor content (nn) and (ns) by means of the different effective couplings g_{nn} and g_{ns}.

4. $\Delta\mathcal{L}^{(3)}_{\text{eff}}$ is just the original interaction but now with constituent quark field operators. It yields interaction vertices whose contribution within the Bethe-Salpeter equation vanishes for color-free three-quark states, and hence needs no further discussion.

The most interesting contribution stems from the two-body interaction Lagrangian. It is usually used in connection with the solution of the $U_A(1)$-problem. In the framework of calculations for mesons [8,13] we have indeed shown that it yields the correct splitting of the lowest meson nonet and in general of all low-lying meson states. Hence we have good reasons to use it also for the calculation of baryon masses. As in the case of mesons we have to regularize the spatial δ-function dependence of this two-body Lagrangian by a form factor, which we give a Gaussian form:

$$\delta^{(4)}(x) \longrightarrow \frac{1}{\lambda^3\pi^{\frac{3}{2}}}\, e^{-\frac{|\mathbf{x}|^2}{\lambda^2}}\ \delta^{(1)}(x^0). \tag{24}$$

For the moment we make no effort to derive it and treat the effective range λ as well as the couplings g_{nn} and g_{ns} as phenomenological parameters which we fit to the experimental baryon spectrum. Our candidate for the instantaneous two-quark interaction kernel $V^{(2)}$ has then the following form:

$$V^{(2)}(x_1, x_2;\ x_1', x_2') =$$
$$V^{(2)}_{\text{'t Hooft}}(\mathbf{x})\ \delta^{(1)}(x^0)\ \delta^{(4)}(x_1 - x_1')\ \delta^{(4)}(x_2 - x_2'), \tag{25}$$

with $x := x_1 - x_2$ and

$$V^{(2)}_{\text{'t Hooft}}(\mathbf{x}) = \frac{-4}{\lambda^3\pi^{\frac{3}{2}}}\, e^{-\frac{|\mathbf{x}|^2}{\lambda^2}} \left[\mathbb{1}\otimes\mathbb{1} + \gamma^5\otimes\gamma^5\right] \mathcal{P}^{\mathcal{D}}_{S_{12}=0}$$
$$\otimes \left(g_{nn}\mathcal{P}^{\mathcal{F}}_{\mathcal{A}}(nn) + g_{ns}\mathcal{P}^{\mathcal{F}}_{\mathcal{A}}(ns)\right) \otimes \mathcal{P}^{\mathcal{C}}_{\bar{3}}. \tag{26}$$

4 Parameters and general comments

In this (and a consecutive [26]) paper we will present a detailed discussion of the resulting mass spectra of light baryons (with the light-quark flavors "up", "down" and "strange") calculated within our covariant Salpeter framework using the confinement models $\mathcal{A}$ and $\mathcal{B}$ and employing 't Hooft's instanton-induced force as residual interaction.

The seven free parameters entering in the present calculations are listed in table 1. These parameters involve the effective non-strange and strange constituent quark masses m_n and m_s, and the confinement parameters a and b describing the off-set and the string tension of the three-body confinement potential. 't Hooft's instanton-induced interaction is determined by the couplings g_{nn} and g_{ns} and the effective range λ.

Our detailed discussion of the results for the light flavor baryons will be organized according to the specific parameter dependence dictated by the simple characteristic and selective action of the instanton-induced interaction. Due to the simplicity of 't Hooft's force and the induced strong selection rules, a clear-cut identification of the various effects of the long-range confining potential and the short-range residual interaction can be made by comparison with the experimentally observed baryon spectra. Accordingly, the discussion of our results in the subsequent sections will be organized as follows:

As 't Hooft's force acts only on flavor-antisymmetric quark pairs, this residual interaction does not contribute to the non-strange spectrum of Δ-resonances due to their common totally symmetric flavor wave function with isospin $T = 3/2$. Therefore, in our approach (without any additional residual interactions apart from 't Hooft's force) the whole Δ-resonance[2] spectrum is determined by the confining three-body force and the relativistic dynamics alone! This feature thus provides a first test of our phenomenological ansatz for the confinement potential. Furthermore, we can fix the confinement parameters, *i.e.* the off-set parameter a and the slope b, as well as the non-strange quark mass m_n by the positions of the ex-

[2] Of course the same also applies to the whole Ω spectrum. Unfortunately, the only well-established Ω state still is just the decuplet ground state $\Omega\frac{3}{2}^+(1672)$.

perimentally best established Δ-resonances without any influence of the residual interaction. In this respect, the confining three-body interaction kernel, which is a string-like, *i.e.* linearly rising three-body potential with the two distinct Dirac structures of the models $\mathcal{A}$ and $\mathcal{B}$, has to account for the correct description of the positive-parity Δ Regge trajectory $M^2 \sim J$ up to the highest spin known $J = 15/2^+$. At the same time, it should not induce too large spin-orbit effects, for which there is hardly any evidence in the experimental baryon spectrum. The results for the complete Δ spectrum in both model versions will be discussed in sect. 5.

Like the Δ-resonances with the corresponding ground state $\Delta(1232)$, also the remaining strange spin-$(3/2^+)$ decuplet ground states, *i.e.* the hyperons $\Sigma^*(1385)$, $\Xi^*(1583)$ and $\Omega(1672)$, are unaffected by 't Hooft's interaction. Hence, the position of these states then determines the strange constituent quark mass m_s. In this way, all parameters except for those of the 't Hooft interaction are fixed, and in the second step we can then analyze the effect of the instanton-induced interaction on the structure of the remaining baryon spectra.

As already known from non-relativistic potential models, the long-range confinement potential cannot describe the splittings of the spin-(1/2) octet and spin-(3/2) decuplet ground states. Thus, the first feature the 't Hooft interaction has to account for is the hyperfine structure of the ground states, *i.e.* the mass splittings $\Delta(1232) - N(939)$ of the non-strange ground states and the hyperon splittings $\Sigma^*(1385) - \Sigma(1193)$, $\Xi^*(1583) - \Xi(1318)$ and $\Sigma(1193) - \Lambda(1116)$. In this respect we will show that the instanton-induced interaction indeed leads to an at least as satisfactory description as the short-range spin-spin part of the Fermi-Breit interaction, which is generated by the one-gluon exchange (OGE) and is commonly used in non-relativistic (or "relativized") quark models [36,37,6]. In the non-strange sector the $\Delta - N$ mass splitting is explained by 't Hooft's force being attractive for the nucleon, where two (non-strange) quarks can be in a state with trivial spin and isospin. Thus the $\Delta - N$ splitting fixes the coupling g_{nn}. In a similar manner 't Hooft's force is attractive for Σ and Ξ with the strength g_{ns} where a non-strange–strange (ns) quark pair can be in a state with trivial spin and antisymmetric flavor. In this way the splittings $\Sigma^* - \Sigma$ and $\Xi^* - \Xi$ determine the coupling g_{ns}. At the same time, the position of $\Lambda(1116)$, which contains both types $(nn$ and $ns)$ of quark pairs and thus is influenced by both couplings g_{nn} and g_{ns}, should then be properly described in order to get the right experimentally observed $\Sigma - \Lambda$ mass difference. Generating the hyperfine structure of ground-state baryons by 't Hooft's force will be investigated in detail in sect. 6.

All the parameters being fixed, the calculation of all other baryon masses is then parameter-free, *i.e.* the majority of excited mass spectra of N-resonances, Λ-resonances, Σ-resonances, Ξ-resonances and the Ω baryons are thus predictions of our models $\mathcal{A}$ and $\mathcal{B}$. In this paper we restrict our extensive discussion to the predictions for the nucleon sector (sect. 7). The parameter-free predictions for the complete spectrum of excited strange baryons will be discussed in a subsequent paper [26].

A principal objective of our discussion is to demonstrate that the instanton-induced interaction along with a fully relativistic treatment of the quark dynamics within our covariant Salpeter approach plays an important role in the description of the complete spectrum of light baryons, *i.e.* not only for the hyperfine structure of the ground-state baryons as, *e.g.*, the $\Delta - N$ splitting, but especially for distinctive features of the excited spectra. In both confinement models we will explore in detail how and to what extent the striking features of the excited spectra can really be understood by the effect of 't Hooft's force with its parameters g_{nn}, g_{ns} and λ fixed from the hyperfine structure of the octet and decuplet ground-state baryons. Prominent features of the excited baryon spectra that shall be discussed in this context are, for instance, the conspicuously low positions of the first isoscalar/scalar excitations of octet ground states, *i.e.* the Roper-resonance $N\frac{1}{2}^+(1440)$ and its strange counterparts $\Lambda\frac{1}{2}^+(1600)$ and $\Sigma\frac{1}{2}^+(1660)$, or the appearance of approximately degenerate states of the same spin but opposite parity (approximate "parity doublets").

Now let us turn to the discussion of the light-baryon spectra. We begin with the discussion of the Δ spectrum, whose phenomenology reflects the role of the three-body confinement kernel in the Salpeter equation.

5 The Δ spectrum —A first test of the confinement kernel

5.1 Introductory remarks

In this subsection we investigate and discuss the results of both confinement models $\mathcal{A}$ and $\mathcal{B}$ in the sector of Δ-baryons (with isospin $T = \frac{3}{2}$ and strangeness $S^* = 0$). We compare our results with the main features of the complete, hitherto measured Δ-resonance spectrum up to the highest orbital excitations with total spin $J = \frac{15}{2}$. As already mentioned, there is no effect of 't Hooft's force in this sector, because the flavor part of the amplitudes is given by the totally symmetric isospin-(3/2) flavor function. Therefore, the internal quark dynamics of the Δ-baryons is described by the relativistic kinetic energy and the three-body confinement potential only. This offers the possibility to study the role of the confinement force only, *i.e.* without the influence of the residual instanton-induced interaction. Therefore, the calculation of the Δ spectrum constitutes a first important test of the different three-body confinement kernels $\mathcal{A}$ and $\mathcal{B}$. As mentioned before, the phenomenology of Regge trajectories motivates the string picture for confinement, *i.e.* in our case a three-body potential, which rises linearly with the distance between the quarks. In contrast to the radial (string-like) dependence of the confinement mechanism originating, *e.g.*, from the flux tube model [28,29], but also motivated by recent lattice QCD calculations [27], the spinorial (Dirac) structure of three-quark confinement lacks any

clue from first principles or lattice QCD. Thus, an appropriate ansatz for the Dirac structure of the confinement kernel is motivated by phenomenological arguments only. Here the aim is to reproduce the global structure of the Δ spectrum, especially the well-established positive-parity Δ Regge trajectory, with the empirical characteristic $M^2 \propto J$. In particular, the slope of the trajectory should be quantitatively correctly described in order to reproduce the resonance positions even of the highest orbital excitations. At the same time the confinement force has to account for the correct energy gaps between the approximately degenerate bands, which are formed by the radially excited states with different total angular momenta J (corresponding to the even-parity $2\hbar\omega$, $4\hbar\omega$, $6\hbar\omega$ and odd-parity $1\hbar\omega$, $3\hbar\omega$, $5\hbar\omega$ "oscillator shells" of the naive quark oscillator shell model[3]). Moreover, the observed approximate degeneracy in these band structures indicates that spin-orbit effects are rather small. This is an additional experimental feature that we aim to describe in our models. Consequently, the Dirac structures chosen should be such that spin-orbit forces are not too large and compatible with the experimentally observed small intraband splittings of the different shells. In this respect, the spin structures of model $\mathcal{A}$ and $\mathcal{B}$, which in both cases consist of a special combination of a scalar ($\mathbb{1} \otimes \mathbb{1} \otimes \mathbb{1}$) and a time-like vector part ($\gamma^0 \otimes \gamma^0 \otimes \mathbb{1} + \ldots$), have already been selected from a wider class of possible Dirac structures that are all compatible with Lorentz covariance, time-reversal-, parity- and $\mathcal{CPT}$-invariance, as well as the Hermiticity requirements of the Salpeter equation (see ref. [1]). Here we want to verify that both confinement versions can indeed account for the phenomenological features of the Δ spectrum. Then (due to the assumed flavor independence of the confinement force) these should be also appropriate for the other baryon sectors, where in addition instanton effects become substantial. The phenomenology of the Δ spectrum already fixes the offset parameter a and the slope b of the confinement potential, as well as the non-strange quark mass m_n. This is mainly done by fitting the positive-parity Δ Regge trajectory, *i.e.* the ground state $\Delta\frac{3}{2}^+(1232, ****)$, and its orbital excitations $\Delta\frac{7}{2}^+(1950, ****)$ and $\Delta\frac{11}{2}^+(2420, ****)$, which all are well-established four-star resonances with moderate uncertainties in the observed resonance positions. There is evidence of a fourth member of this trajectory, namely the next spin-(15/2) resonance $\Delta\frac{15}{2}^+(2950, **)$, which, however, is only a two-star resonance with quite large experimental uncertainties. Therefore, this member is not used in the fit and thus will be a prediction. In order to achieve the correct gap between the positive-parity ground state $\Delta\frac{3}{2}^+(1232, ****)$ and the first negative-parity (1 $\hbar\omega$) band, we consider also the lowest two, well-established four-star resonances of negative parity, *i.e.* $\Delta\frac{1}{2}^-(1620, ****)$ and $\Delta\frac{3}{2}^-(1700, ****)$, for fixing the three parameters a, b and m_n.

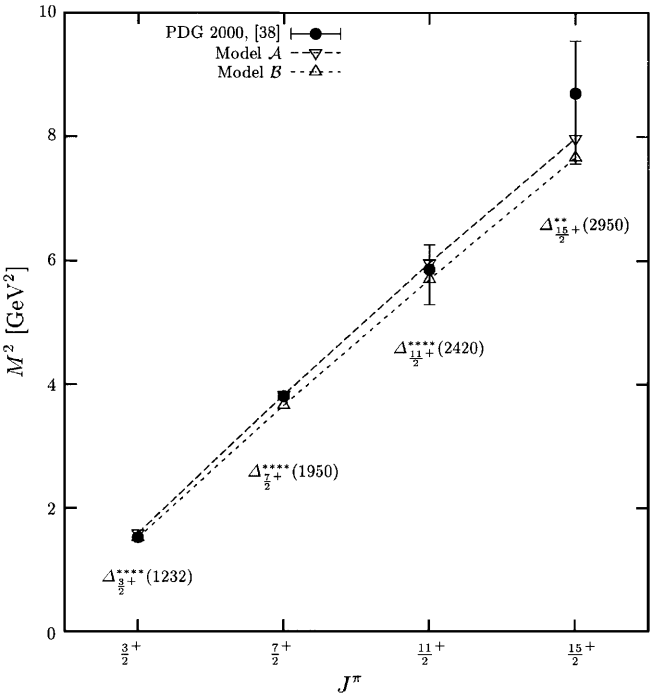

Fig. 2. Chew-Frautschi plot (M^2 *vs.* J) of the positive-parity Δ Regge trajectory ($\Delta\frac{3}{2}^+$, $\Delta\frac{7}{2}^+$, $\Delta\frac{11}{2}^+$, $\Delta\frac{15}{2}^+$), with the parameters of model $\mathcal{A}$ and model $\mathcal{B}$, compared to experimental masses from the Particle Data Group (see [38]). Both models yield the correct linear Regge characteristic $M^2 \sim J$ in good agreement with experiment. See table 2 for numerical values.

5.2 The positive-parity Δ Regge trajectory

Figure 2 shows the Chew-Frautschi plot (M^2 *vs.* J) of the positive-parity Δ Regge trajectory as obtained in models $\mathcal{A}$ and $\mathcal{B}$ with the parameters a, b and m_n given in table 1. Indeed, both models yield excellent Regge trajectories, which show the qualitatively correct linear characteristics.

Due to the correctly reproduced trajectory slope, the experimentally observed resonance positions of the three four-star states $\Delta\frac{3}{2}^+(1232, ****)$, $\Delta\frac{7}{2}^+(1950, ****)$, and $\Delta\frac{11}{2}^+(2420, ****)$ are fairly well described and even the highest observed orbital excitation $\Delta\frac{15}{2}^+(2950, **)$ with total spin $J^\pi = \frac{15}{2}^+$, which is the highest orbital excitation of the whole light-baryon spectrum measured at all,

[3] Due to the one-to-one correspondence of the Salpeter amplitudes with the states of the non-relativistic quark model via the embedding mapping of ordinary non-relativistic Pauli wave functions (see ref. [1]), we will use throughout this work the notation that we assign a model state to that $N\hbar\omega$ oscillator shell at which this state would first appear by counting the states in the non-relativistic oscillator spectrum. Note, however, that this is really just a convenient notation, *i.e.* it does not imply that the wave function of this state is restricted to the configuration subspace of this assigned $N\hbar\omega$ shell. Expanding this state in a (finite $N < N_{\max}$) basis of oscillator states with given flavor, spin and parity, the states of all shells in general mix. On the other hand, it is very likely that the dominant part of the corresponding wave function is made up of $N\hbar\omega$ states.

Table 2. Position of states belonging to the positive-parity Δ Regge trajectory calculated in the models $\mathcal{A}$ and $\mathcal{B}$ in comparison to the experimental resonance positions [38]. For a graphical presentation see fig. 2.

Regge state	Rating	J^π	Experimental Mass [MeV] [38]	Mass [MeV] Model $\mathcal{A}$	Mass [MeV] Model $\mathcal{B}$
$\Delta(1232)$	****	$\frac{3}{2}^+$	1230–1234	1261	1231
$\Delta(1950)$	****	$\frac{7}{2}^+$	1940–1960	1956	1912
$\Delta(2420)$	****	$\frac{11}{2}^+$	2300–2500	2442	2387
$\Delta(2950)$	**	$\frac{15}{2}^+$	2750–3090	2824	2768

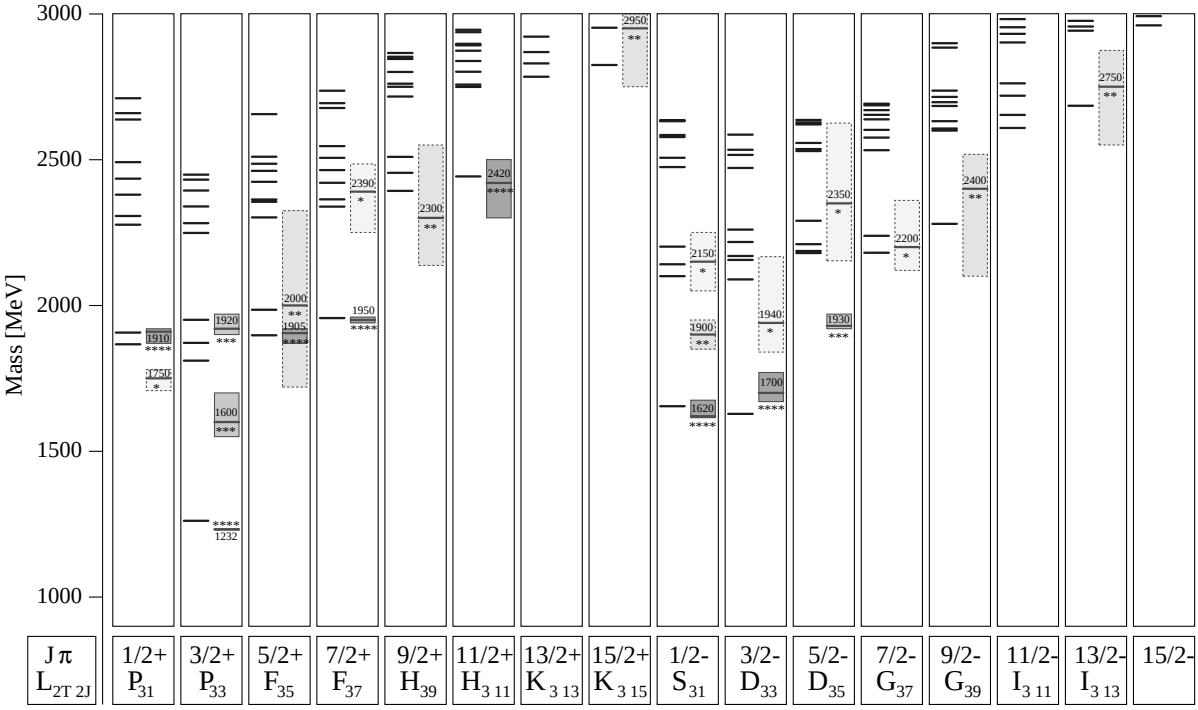

Fig. 3. The calculated positive- and negative-parity Δ-*resonance spectrum* (isospin $T = \frac{3}{2}$ and strangeness $S^* = 0$) in *model* $\mathcal{A}$ (left part of each column) in comparison to the experimental spectrum taken from Particle Data Group [38] (right part of each column). The resonances are classified by the total angular momentum J and parity π. The experimental resonance position is indicated by a bar, the corresponding uncertainty by the shaded box which is darker for better established resonances; the status of each resonance is additionally indicated by stars.

is predicted within the errors of the measured resonance position.

In table 2 the masses calculated in model $\mathcal{A}$ and $\mathcal{B}$ for the Δ Regge states are given explicitly in comparison with the corresponding experimental resonance positions taken from the Particle Data Group [38].

Comparing both models, we find model $\mathcal{A}$ yielding a slightly larger slope of the trajectory (see fig. 2) in somewhat better agreement with experiment than model $\mathcal{B}$ for the high-spin states. On the other hand, model $\mathcal{A}$ predicts the position of the Δ ground state $\Delta\frac{3}{2}^+(1232, ****)$ slightly too high in comparison to the experimentally determined position, whereas model $\mathcal{B}$ fits this resonance position exactly. Altogether, we thus find both models to be of the same good quality. Note that the states $\Delta\frac{3}{2}^+$, $\Delta\frac{7}{2}^+$, $\Delta\frac{11}{2}^+$, $\Delta\frac{15}{2}^+$, ..., belonging to the Regge trajectory, correspond to a sequence of baryons with increasingly large separations of the quarks. Accordingly, this result strongly supports our ansatz of the string-like confinement mechanism in both models. In the following a more detailed discussion of these models concerning the structure of the complete Δ spectrum is presented.

5.3 Discussion of the complete Δ spectrum

Figure 3 shows the resulting positions of positive and negative-parity Δ-baryons (isospin $T = \frac{3}{2}$ and strangeness $S^* = 0$) with total angular momenta up to $J = \frac{15}{2}$ obtained in model $\mathcal{A}$. These are compared to all presently known resonances quoted by the Particle Data Group [38]. Likewise, fig. 4 displays the corresponding results of model $\mathcal{B}$. The resonances in each column are classified by their

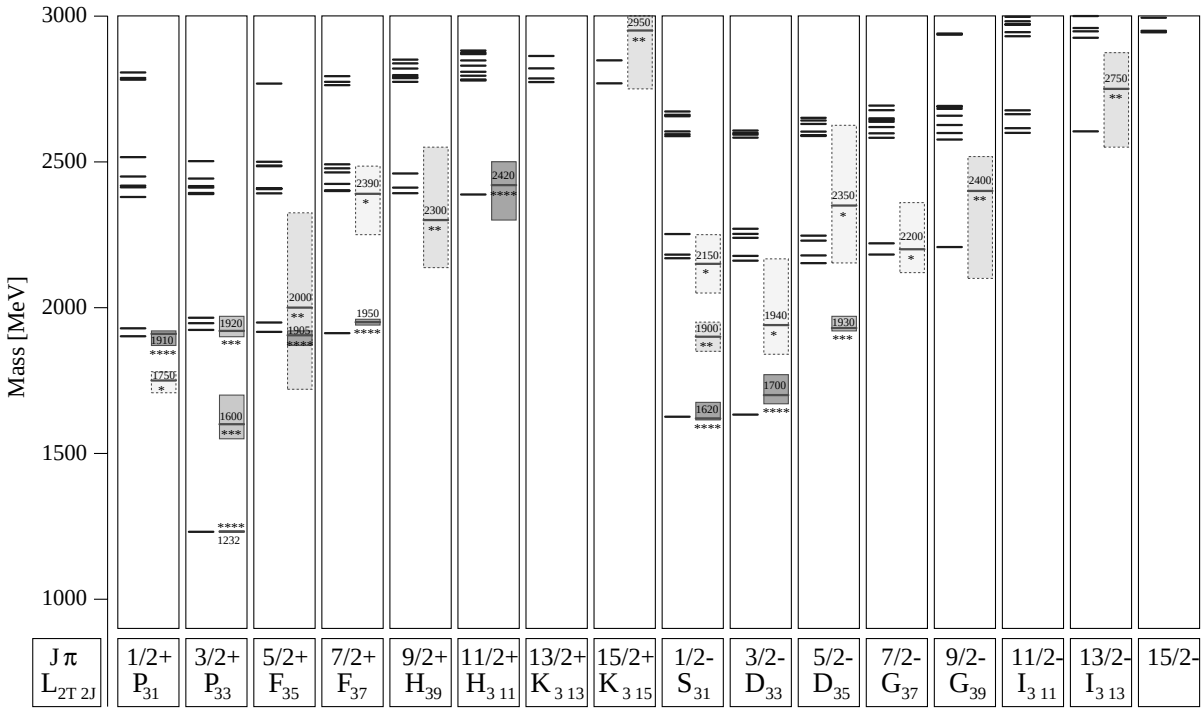

Fig. 4. The calculated positive- and negative-parity Δ-*resonance spectrum* (isospin $T = \frac{3}{2}$ and strangeness $S^* = 0$) in *model* $\mathcal{B}$ (left part of each column) in comparison to the experimental spectrum taken from Particle Data Group [38] (right part of each column). See also caption to fig. 3.

total spin J and parity π. On the left of each column at most the first ten calculated states are shown and can be compared with the experimentally observed positions on the right-hand side of each column. The corresponding uncertainties in the measured resonance positions are indicated by the shaded areas. The status of each resonance is denoted by the corresponding number of stars following the notation of the Particle Data Group [38] and moreover, by the shading of the error box which is darker for better established resonances.

In addition to figs. 3 and 4, the calculated masses of the excited states are summarized according to their assignment to a particular shell in each of the tables 3–8.

5.3.1 Global structure of the Δ spectrum

Before discussing single resonance positions in each shell in detail, let us first focus on the gross structure of the global Δ spectrum. Figures 3 and 4 show that with both variants $\mathcal{A}$ and $\mathcal{B}$, indeed a satisfactory overall description of the global features of the experimentally known resonances can be obtained.

In both models the positions of the shell structures are well reproduced together with the correct position of states that belong to the positive-parity Δ Regge trajectory. The centroids of the various even- and odd-parity bands are in good agreement with the centroids of the corresponding experimentally observed band structures with the exception of the negative-parity states around 1900 MeV. Concerning the structures of the shells themselves it should be noted that model $\mathcal{A}$ exhibits larger intra-band splittings than model $\mathcal{B}$ due to slightly larger spin-orbit effects in model $\mathcal{A}$. In this respect, the Dirac structure (consisting of the scalar and time-like vector part in both models) is combined in model $\mathcal{B}$ such that the spin-orbit forces of both parts cancel and thus these relativistic effects, which arise in connection with the embedding map in the Salpeter amplitudes, are really minimized. Nevertheless, also the intra-band splittings of model $\mathcal{A}$ are still moderate enough to be compatible with the central values for the experimentally observed resonance masses. They even generate the desired feature that the average mass values in each shell rise with total angular momentum J, in contrast to model $\mathcal{B}$, where the states with different spin J are almost degenerate. This produces a slight tilt in the shells of model $\mathcal{A}$ (see, *e.g.*, the positive-parity $2\hbar\omega$ shell), which generally yields higher resonance positions for the states with maximum angular momentum, thus producing positive- and negative-parity Regge trajectories with a slightly bigger slope in model $\mathcal{A}$, in better agreement with the experiment.

Now let us discuss the single resonance positions and the pattern of splittings in the positive- and negative-parity bands of the excited Δ spectrum in some more detail.

Table 3. Calculated positions of Δ states assigned to the negative-parity $1\hbar\omega$ shell in comparison to the corresponding experimental mass values taken from [38]. PW denotes the partial wave and the rating is given according to the PDG classification [38]. Here and throughout this work we use the notation $[B\ J^\pi]_n(M)$ for the predicted model states in model $\mathcal{A}$ and $\mathcal{B}$, respectively, where B denotes the baryon (*i.e.* the flavor), J^π are spin and parity, and M is the predicted mass given in MeV. $n = 1, 2, 3, \ldots$ is the principal quantum number counting the states in each sector J^π beginning with the lowest state.

Experimental state [38]	PW	J^π	Rating	Mass range [MeV] [38]	Model state in model $\mathcal{A}$	Model state in model $\mathcal{B}$
$\Delta(1620)$	S_{31}	$\frac{1}{2}^-$	****	1615-1675	$[\Delta\frac{1}{2}^-]_1(1654)$	$[\Delta\frac{1}{2}^-]_1(1625)$
$\Delta(1700)$	D_{33}	$\frac{3}{2}^-$	****	1670-1770	$[\Delta\frac{3}{2}^-]_1(1628)$	$[\Delta\frac{3}{2}^-]_1(1633)$

5.3.2 States of the $1\hbar\omega$ band

We start with the negative-parity $1\hbar\omega$ band, where our models predict (as usual in constituent quark models) two states which can be uniquely assigned to the two well-established four-star resonances $\Delta\frac{1}{2}^-(1620, ****)$ and $\Delta\frac{3}{2}^-(1700, ****)$. Our results for these states are given explicitly in table 3.

Both models yield the correct center of gravity of this $1\hbar\omega$ band. In particular, the position of $\Delta\frac{1}{2}^-(1620, ****)$ is fairly well reproduced within the experimental range: model $\mathcal{A}$ predicts 1654 MeV and model $\mathcal{B}$ gives 1625 MeV. Note that in quark models, which use the one-gluon exchange as a residual interaction, the Δ ground state is shifted upwards relative to the negative-parity excited states $\Delta\frac{1}{2}^-$ and $\Delta\frac{3}{2}^-$, thus in general predicting the centroid of the $1\hbar\omega$ band too low. Unfortunately, in both models the calculated position of the $\Delta\frac{3}{2}^-$ state turns out to be roughly 70 MeV too low compared to the observed position of the $\Delta\frac{3}{2}^-(1700, ****)$. The splitting of $\Delta\frac{1}{2}^-(1620, ****)$ and $\Delta\frac{3}{2}^-(1700, ****)$ is often interpreted as one of a few possible hints for the relevance of spin-orbit forces in baryon spectroscopy. In this respect, both models cannot account for this splitting: In model $\mathcal{B}$ both states are nearly degenerate and in model $\mathcal{A}$ the splitting $\Delta\frac{3}{2}^- - \Delta\frac{1}{2}^-$ even has the wrong sign. Note however that the experimental indications for the true size of this splitting itself are less clear, since the ranges of possible values for both resonances are even overlapping.

5.3.3 States of the $2\hbar\omega$ band

We now focus on the structure of the positive-parity $2\hbar\omega$ shell. Our results for the states of this shell are given explicitly in table 4. Disregarding for the moment the puzzling low position of the three-star $\Delta\frac{3}{2}^+(1600)$ resonance, figs. 3 and 4 show that both confinement versions predict the centroid of the $2\hbar\omega$ band at around 1900 MeV in very good agreement with experiment. Due to the minimization of spin-orbit effects by the Dirac structure of confinement $\mathcal{B}$, the $2\hbar\omega$ states in model $\mathcal{B}$ hardly show any splitting and all states are clustered within a narrow region between 1900 and 1970 MeV. We thus find for each well-established three- and four-star resonance in this region, *i.e.* the $\Delta\frac{1}{2}^+(1910, ****)$, the $\Delta\frac{3}{2}^+(1920, ***)$, the $\Delta\frac{5}{2}^+(1905, ****)$ and the $\Delta\frac{7}{2}^+(1950, ****)$, a predicted state for a possible assignment. Due to the strong clustering of the predicted states, the experimentally indicated pattern of splittings, *e.g.* $\Delta\frac{1}{2}^+(1910, ****) - \Delta\frac{1}{2}^+(1750, *)$ and $\Delta\frac{5}{2}^+(1905, ***) - \Delta\frac{5}{2}^+(2000, **)$ or even the low position $\Delta\frac{3}{2}^+(1600, ***)$ cannot be described. Concerning the $\Delta\frac{1}{2}^+(1750, *)$ and the $\Delta\frac{5}{2}^+(2000, **)$ note, however, that their rating is only one- and two-star, respectively. On the other hand, the intra-band splittings in model $\mathcal{A}$, which are induced by moderate spin-orbit effects, reproduce the experimentally indicated pattern of splittings in this shell quite well. Consequently, a tentative assignment of the states on the basis of their positions compared to the experimental values is less ambiguous. Let us discuss the intra-band pattern in some more detail (see also table 4).

In the spin-$(1/2^+)$ sector models $\mathcal{A}$ and $\mathcal{B}$ describe the situation very similarly. In model $\mathcal{A}$ we find two close states at 1866 MeV and 1906 MeV, where the latter fits nicely the well-established four-star resonance $\Delta\frac{1}{2}^+(1910, ****)$ within the assigned errors, while the other one overestimates the position of the poorly determined one-star resonance $\Delta\frac{1}{2}^+(1750, *)$. In the sector with $J^\pi = 3/2^+$ model $\mathcal{A}$ generates the largest splittings within the $2\hbar\omega$ band in at least qualitative agreement with the low position of the $\Delta\frac{3}{2}^+(1600, ***)$ resonance. Nevertheless, despite this improvement relative to model $\mathcal{B}$, the role of this state remains still unclear also in model $\mathcal{A}$, since the lowest calculated state in this sector at 1810 MeV is still far away from the PDG reported mass value centered around 1600 MeV. We would like to comment here that this state is often viewed as the analogue of the low-lying Roper resonance. Both states have in common that they are the first scalar excitation of the corresponding ground state, positioned even below the lowest excitations of negative parity. However, in the spirit of our model, which in addition to a proper confinement force uses exclusively 't Hooft's instanton-induced force as residual interaction, the low positions of $\Delta\frac{3}{2}^+(1600, ***)$ and the Roper resonance cannot originate from the same dynamics. In this respect, we should anticipate already here that in the case of the Roper resonance and its strange counterparts (which all appear in the sectors of the spin-$\frac{1}{2}^+$ octet ground-state baryons) the low positions can be nicely explained as an instanton effect due to the attractive action of 't Hooft's

Table 4. Calculated positions of Δ states assigned to the positive-parity $2\hbar\omega$ shell and their tentative assignment to observed resonances due to comparison with experimental mass values taken from [38]. Notation as in table 3.

Experimental state [38]	PW	J^π	Rating	Mass range [MeV] [38]	Model state in model $\mathcal{A}$	Model state in model $\mathcal{B}$
$\Delta(1750)$	P_{31}	$\frac{1}{2}^+$	*	1708–1780	$[\Delta\frac{1}{2}^+]_1(1866)$	
$\Delta(1910)$	P_{31}	$\frac{1}{2}^+$	****	1870–1920	$[\Delta\frac{1}{2}^+]_2(1906)$	$[\Delta\frac{1}{2}^+]_1(1901)$ $[\Delta\frac{1}{2}^+]_2(1928)$
$\Delta(1600)$	P_{33}	$\frac{3}{2}^+$	***	1550–1700	$[\Delta\frac{3}{2}^+]_2(1810)$	
$\Delta(1920)$	P_{33}	$\frac{3}{2}^+$	***	1900–1970	$[\Delta\frac{3}{2}^+]_3(1871)$ $[\Delta\frac{3}{2}^+]_4(1950)$	$[\Delta\frac{3}{2}^+]_2(1923)$ $[\Delta\frac{3}{2}^+]_3(1946)$ $[\Delta\frac{3}{2}^+]_4(1965)$
$\Delta(1905)$	F_{35}	$\frac{5}{2}^+$	****	1870–1920	$[\Delta\frac{5}{2}^+]_1(1897)$	$[\Delta\frac{5}{2}^+]_1(1916)$
$\Delta(2000)$	F_{35}	$\frac{5}{2}^+$	**	1720–2325	$[\Delta\frac{5}{2}^+]_2(1985)$	$[\Delta\frac{5}{2}^+]_2(1948)$
$\Delta(1950)$	F_{37}	$\frac{7}{2}^+$	****	1940–1960	$[\Delta\frac{7}{2}^+]_1(1956)$	$[\Delta\frac{7}{2}^+]_1(1912)$

Table 5. Calculated positions of negative-parity Δ states in the $3\hbar\omega$ shell in comparison to the corresponding experimental mass values taken from [38]. Notation as in table 3.

Experimental state [38]	PW	J^π	Rating	Mass range [MeV] [38]	Model state in model $\mathcal{A}$	Model state in model $\mathcal{B}$
$\Delta(1900)$	S_{31}	$\frac{1}{2}^-$	**	1850–1950		
$\Delta(2150)$	S_{31}	$\frac{1}{2}^-$	*	2050–2250	$[\Delta\frac{1}{2}^-]_2(2100)$ $[\Delta\frac{1}{2}^-]_3(2141)$ $[\Delta\frac{1}{2}^-]_4(2202)$	$[\Delta\frac{1}{2}^-]_2(2169)$ $[\Delta\frac{1}{2}^-]_3(2182)$ $[\Delta\frac{1}{2}^-]_4(2252)$
$\Delta(1940)$	D_{33}	$\frac{3}{2}^-$	*	1840–2167	$[\Delta\frac{3}{2}^-]_2(2089)$ $[\Delta\frac{3}{2}^-]_3(2156)$	$[\Delta\frac{3}{2}^-]_2(2161)$
					$[\Delta\frac{3}{2}^-]_4(2170)$ $[\Delta\frac{3}{2}^-]_5(2218)$ $[\Delta\frac{3}{2}^-]_6(2260)$	$[\Delta\frac{3}{2}^-]_3(2177)$ $[\Delta\frac{3}{2}^-]_4(2239)$ $[\Delta\frac{3}{2}^-]_5(2253)$ $[\Delta\frac{3}{2}^-]_6(2270)$
$\Delta(1930)$	D_{35}	$\frac{5}{2}^-$	***	1920–1970		
$\Delta(2350)$	D_{35}	$\frac{5}{2}^-$	*	2153–2625	$[\Delta\frac{5}{2}^-]_1(2179)$ $[\Delta\frac{5}{2}^-]_2(2187)$ $[\Delta\frac{5}{2}^-]_3(2210)$ $[\Delta\frac{5}{2}^-]_4(2290)$	$[\Delta\frac{5}{2}^-]_1(2152)$ $[\Delta\frac{5}{2}^-]_2(2179)$ $[\Delta\frac{5}{2}^-]_3(2230)$ $[\Delta\frac{5}{2}^-]_4(2247)$
$\Delta(2200)$	G_{37}	$\frac{7}{2}^-$	*	2120–2360	$[\Delta\frac{7}{2}^-]_1(2181)$ $[\Delta\frac{7}{2}^-]_2(2239)$	$[\Delta\frac{7}{2}^-]_1(2182)$ $[\Delta\frac{7}{2}^-]_2(2220)$
$\Delta(2400)$	G_{39}	$\frac{9}{2}^-$	**	2100–2518	$[\Delta\frac{9}{2}^-]_1(2280)$	$[\Delta\frac{9}{2}^-]_1(2207)$

force in these sectors. Thus, quite in contrast to the N sector we do not find a similar selective lowering for the $\Delta\frac{3}{2}^+(1600,***)$. Models which use the OGE interaction [6], have similar problems to account for this resonance [18]. In other phenomenological approaches [39,40] the low position of the $\Delta\frac{3}{2}^+(1600,***)$ is explained due to a flavor-dependent Goldstone-boson exchange interaction. It thus seems worthwhile to comment on the experimental situation of this somewhat puzzling resonance: Its position is extracted from tedious analyses of mostly older $\pi N \to \pi N$ scattering data. The different analyses often do not agree, but even exhibit very large discrepancies with a big range of possible values. The mass range quoted by the Particle Data Group [38] for this state is 1550 to 1700 MeV. In our opinion it is astonishing that the Particle Data Group [38] has given this state a three-star rating although the various analyses are not in good agreement. Thus, despite a three-star rating, the current experimental evidence concerning the position of $\Delta\frac{3}{2}^+(1600,***)$ is in our opinion not compulsory but rather unclear. Hence it becomes questionable if our calculated mass value of 1810 MeV for this resonance really constitutes a serious discrepancy, especially in view of more recent analyses [41, 42] that predict the resonance position at the upper end of this range at about 1700 MeV. In this respect we hope that with the new generation of experimental facilities and the corresponding new efforts in baryon spectroscopy, the

situation for this state will soon be clarified. In agreement with other (non-relativistic or "relativized") constituent quark models our framework predicts two further states with $J^\pi = \frac{3}{2}^+$ in the $2\hbar\omega$ shell. The state predicted at 1950 MeV in model $\mathcal{A}$ matches the observed three-star state $\Delta\frac{3}{2}^+(1920,***)$ within its uncertainties. The other state, whose mass value is predicted at 1871 MeV lies near this mass range. In model $\mathcal{B}$ all three states are clustered in the mass range of the $\Delta\frac{3}{2}^+(1920,***)$. In the spin-$(5/2^+)$ sector two states are predicted within the $2\hbar\omega$ band, as required by the experimental findings. The positions of the well-established four-star resonance $\Delta\frac{5}{2}^+(1905,****)$ and the two-star state $\Delta\frac{5}{2}^+(2000,**)$ and accordingly also their mass difference are fairly well described by the predictions at 1897 MeV and 1985 MeV in model $\mathcal{A}$. Again the situation is better than in model $\mathcal{B}$, which cannot reproduce this splitting due its minimal relativistic spin-orbit effects. But we should not attach too much importance to the $\Delta\frac{5}{2}^+(2000,**)$, which has only a two-star rating and moreover reveals big uncertainties in its determined mass position. In the sector $J^\pi = \frac{7}{2}^+$ the well-established four-star resonance $\Delta\frac{7}{2}^+(1950,****)$ is the only state seen in this mass range of the F_{37} partial wave, compatible with our prediction. The position of this state, which is a member of the positive-parity Δ Regge trajectory discussed previously, is exactly reproduced by the prediction at 1956 MeV in model $\mathcal{A}$, whereas model $\mathcal{B}$, which yields the mass value 1912 MeV, slightly underestimates this position.

5.3.4 States of the $3\hbar\omega$ band

Apart from the puzzling, low-lying $\Delta\frac{3}{2}^+(1600,***)$ resonance discussed previously, the present experimental Δ spectrum also shows a curious structure in the negative-parity sector, namely the three resonances $\Delta\frac{1}{2}^-(1900,**)$, $\Delta\frac{3}{2}^-(1940,*)$ and $\Delta\frac{5}{2}^-(1930,***)$ around 1900 MeV, which are nearly degenerate with the states of the positive-parity $2\hbar\omega$ shell. Taking these states seriously within a constituent quark model, they have to be naturally assigned to the $3\hbar\omega$ band, since the two states predicted in the $1\hbar\omega$ shell could already be uniquely assigned to the well-established resonances $\Delta\frac{1}{2}^-(1620,****)$ and $\Delta\frac{1}{2}^-(1700,****)$. As can be seen in figs. 3 and 4, neither model $\mathcal{A}$ nor model $\mathcal{B}$ can account for these rather low-lying states. In both models the rich structure of states assigned to the $3\hbar\omega$ shell is spread around 2200 to 2300 MeV, which agrees with the center of gravity of the other one- and two-star resonances observed in the $3\hbar\omega$ band; see also table 5, where the predicted masses for all Δ states in the $3\hbar\omega$ band are given explicitly. The only state of the $3\hbar\omega$ band that can be uniquely assigned to an experimentally observed resonance is the single state in the $\Delta\frac{9}{2}^-$ sector at 2280 MeV in model $\mathcal{A}$ and at 2207 MeV in $\mathcal{B}$: the predicted positions agree within the very big range of possible values of the single two-star resonance $\Delta\frac{9}{2}^-(2400,**)$ seen in the G_{39} partial wave. All other negative-parity resonances observed in this mass region have only a one-star rating. Their quite big ranges of possible values agree with the positions of several $3\hbar\omega$ states predicted by both models.

The lowest $3\hbar\omega$ states calculated in our models lie at about 2100 MeV, rather far above the masses of the three conspicuously low-lying states. Several other constituent quark models also cannot account for this puzzling structure (*e.g.*, models with OGE forces [6,18]): in general quark model predictions for the masses of these states are consistently too high by about 150–250 MeV. As in the case of the $\Delta\frac{3}{2}^+(1600,***)$, a comment concerning the experimental status of these mysterious resonances is necessary at this stage: Also here, the experimental situation is rather unclear and unsatisfactory. The existence of the one-star $\Delta\frac{3}{2}^-(1940,*)$ resonance anyway is questionable and concerning the two-star $\Delta\frac{1}{2}^-(1900,**)$ resonance it is worth emphasizing that in the 1998 edition of the *Review of Particle Physics* [43] this resonance has already been downgraded from three stars to two due to its weak signal in speed plots. Moreover, it should be mentioned that $\Delta\frac{3}{2}^-(1940,*)$ and $\Delta\frac{1}{2}^-(1900,**)$ have not been seen in various partial-wave analyses of $\pi N \to \pi N$ scattering data [44]. Furthermore, additional corrections to the existing partial-wave solutions due to additional new data from recently measured spin rotation parameters in $\pi^+ p$ elastic scattering at (ITEP)-PNPI [45] indicate that the signal of the $\Delta\frac{3}{2}^-(1940,*)$ resonance even completely disappears (see [44,46] and references therein). Concerning the three-star resonance $\Delta\frac{5}{2}^-(1930,***)$ the Particle Data Group [38] states that various analyses are not in good agreement. Due to this quite unclear experimental situation, we again do not pay too much attention to this puzzling structure when evaluating the quality of our confinement mechanisms. But we hope that also in this case the situation will soon be clarified by the new experimental investigations in baryon spectroscopy. Let us emphasize that the confirmation of these resonances would strongly disfavor our model as well as several other models [18].

5.3.5 Beyond the $3\hbar\omega$ band

The high mass part of the experimental Δ spectrum is still hardly explored. Explicit mass values for some of the states in model $\mathcal{A}$ and $\mathcal{B}$ assigned to the $4\hbar\omega$, $5\hbar\omega$ and $6\hbar\omega$ shell, are summarized in tables 6, 7 and 8, respectively.

In the positive-parity $4\hbar\omega$ band three resonances with spins $J^\pi = \frac{7}{2}^+$, $\frac{9}{2}^+$ and $\frac{11}{2}^+$ are found experimentally. In the $\Delta\frac{11}{2}^+$ sector this is the well-established four-star resonance $\Delta\frac{11}{2}^+(2420,****)$ which belongs to the positive-parity Regge trajectory discussed before. Both models predict a single $\Delta\frac{11}{2}^+$ state in the $4\hbar\omega$ shell which can be uniquely assigned to $\Delta\frac{11}{2}^+(2420,****)$. The position at 2442 MeV in model $\mathcal{A}$ and at 2388 MeV in model $\mathcal{B}$ nicely agrees within the errors of the empirically determined position. The big ranges of possible values of the observed

Table 6. Calculated positions of the positive-parity Δ states in the $4\hbar\omega$ shell with $J \geq \frac{7}{2}$ in comparison to the corresponding experimental mass values taken from [38]. Notation as in table 3.

Experimental state [38]	PW	J^π	Rating	Mass range [MeV] [38]	Model state in model $\mathcal{A}$	Model state in model $\mathcal{B}$
$\Delta(2390)$	F_{37}	$\frac{7}{2}^+$	*	2250–2485	$[\Delta\frac{7}{2}^+]_2(2339)$	$[\Delta\frac{7}{2}^+]_2(2400)$
					$[\Delta\frac{7}{2}^+]_3(2364)$	$[\Delta\frac{7}{2}^+]_3(2402)$
					$[\Delta\frac{7}{2}^+]_4(2421)$	$[\Delta\frac{7}{2}^+]_4(2424)$
					$[\Delta\frac{7}{2}^+]_5(2464)$	$[\Delta\frac{7}{2}^+]_5(2463)$
					$[\Delta\frac{7}{2}^+]_6(2506)$	$[\Delta\frac{7}{2}^+]_6(2477)$
					$[\Delta\frac{7}{2}^+]_7(2546)$	$[\Delta\frac{7}{2}^+]_7(2491)$
$\Delta(2300)$	H_{39}	$\frac{9}{2}^+$	**	2137–2550	$[\Delta\frac{9}{2}^+]_1(2393)$	$[\Delta\frac{9}{2}^+]_1(2392)$
					$[\Delta\frac{9}{2}^+]_2(2455)$	$[\Delta\frac{9}{2}^+]_2(2411)$
					$[\Delta\frac{9}{2}^+]_3(2509)$	$[\Delta\frac{9}{2}^+]_3(2460)$
$\Delta(2420)$	$H_{3\,11}$	$\frac{11}{2}^+$	****	2300–2500	$[\Delta\frac{11}{2}^+]_1(2442)$	$[\Delta\frac{11}{2}^+]_1(2388)$

Table 7. Calculated positions of the negative-parity Δ states in the $5\hbar\omega$ shell with $J \geq \frac{11}{2}$ in comparison to the corresponding experimental mass values taken from [38]. Notation as in table 3.

Experimental state [38]	PW	J^π	Rating	Mass range [MeV] [38]	Model state in model $\mathcal{A}$	Model state in model $\mathcal{B}$
	$I_{3\,11}$	$\frac{11}{2}^-$			$[\Delta\frac{11}{2}^-]_1(2608)$	$[\Delta\frac{11}{2}^-]_1(2599)$
					$[\Delta\frac{11}{2}^-]_2(2653)$	$[\Delta\frac{11}{2}^-]_2(2615)$
					$[\Delta\frac{11}{2}^-]_3(2719)$	$[\Delta\frac{11}{2}^-]_3(2663)$
					$[\Delta\frac{11}{2}^-]_4(2761)$	$[\Delta\frac{11}{2}^-]_4(2676)$
$\Delta(2750)$	$I_{3\,13}$	$\frac{13}{2}^-$	**	2550-2874	$[\Delta\frac{13}{2}^-]_1(2685)$	$[\Delta\frac{13}{2}^-]_1(2604)$

Table 8. Calculated positions of the positive-parity Δ states in the $6\hbar\omega$ shell with $J \geq \frac{13}{2}$ in comparison to the corresponding experimental mass values taken from [38]. Notation as in table 3.

Experimental state [38]	PW	J^π	Rating	Mass range [MeV] [38]	Model state in model $\mathcal{A}$	Model state in model $\mathcal{B}$
	$K_{3\,13}$	$\frac{13}{2}^+$			$[\Delta\frac{13}{2}^+]_1(2784)$	$[\Delta\frac{13}{2}^+]_1(2773)$
					$[\Delta\frac{13}{2}^+]_2(2830)$	$[\Delta\frac{13}{2}^+]_2(2786)$
					$[\Delta\frac{13}{2}^+]_3(2869)$	$[\Delta\frac{13}{2}^+]_3(2820)$
					$[\Delta\frac{13}{2}^+]_4(2922)$	$[\Delta\frac{13}{2}^+]_4(2863)$
$\Delta(2950)$	$K_{3\,15}$	$\frac{15}{2}^+$	**	2750–3090	$[\Delta\frac{15}{2}^+]_1(2824)$	$[\Delta\frac{15}{2}^+]_1(2769)$
					$[\Delta\frac{15}{2}^+]_2(2952)$	$[\Delta\frac{15}{2}^+]_2(2848)$

resonances in $\Delta\frac{7}{2}^+$ and $\Delta\frac{9}{2}^+$ agree with several states predicted in both models (see table 6).

In the energy region of the negative-parity $5\hbar\omega$ band only the resonance $\Delta\frac{13}{2}^-(2750, **)$ with a two-star rating has been observed in the $I_{3\,13}$ partial wave. Both models predict a single $\Delta\frac{13}{2}^-$ state (belonging to the $5\hbar\omega$ shell) at 2685 MeV in model $\mathcal{A}$ and at 2604 MeV in model $\mathcal{B}$, compatible with this single observed state. In the $\Delta\frac{11}{2}^-$ sector no resonance has been seen so far; the predicted states of model $\mathcal{A}$ and model $\mathcal{B}$ in this sector are given in table 7.

Finally, the highest observed excitation of the light-baryon spectrum, *i.e.* the two-star resonance $\Delta\frac{15}{2}^+(2950, **)$, which belongs to the positive-parity Regge trajectory, is the only observed state of the $6\hbar\omega$ shell. Both models predict in the $\Delta\frac{15}{2}^+$ sector two states whose positions at 2824 and 2952 MeV in model $\mathcal{A}$ and at 2769 and 2848 MeV in model $\mathcal{B}$ are within the uncertainty range of the $\Delta\frac{15}{2}^+(2950, **)$ (see table 8).

5.4 Summary for the Δ spectrum

To summarize our discussion of the Δ spectrum, we have presented the results for two different confinement models, which essentially differ only in the Dirac structure of their linearly rising part. In both models this part consists of a combination of a scalar and a time-like vector part. In model $\mathcal{B}$ this combination is such that relativistic spin-orbit forces of both parts almost cancel, whereas the combination in model $\mathcal{A}$ produces spin-orbit forces which are small enough to be still compatible with experimental findings.

Once the Dirac structures are fixed, we obtain in both models a quite good description of the complete Δ spectrum up to highest orbital excitations $J \leq \frac{15}{2}$. This is

achieved by adjusting only three (!) parameters: the non-strange quark mass m_n, the confinement offset-parameter a and the slope b, see table 1.

- Both models yield excellent Regge trajectories with the correct phenomenological characteristic $M^2 \propto J$ and the right slope, indicating that baryons with increasingly large separations of the quarks are well described. This feature strongly supports our string-like ansatz for confinement.
- In both variants $\mathcal{A}$ and $\mathcal{B}$, the resulting positions of the even- and odd-parity shell structures agree fairly well with the centroids of the experimentally observed band structures.
- Note that all of the seven well-established resonances of the Δ spectrum which have a four-star rating [38] are very well described in both confinement models.
- The results of the confinement models $\mathcal{A}$ and $\mathcal{B}$ mainly differ in the intra-band splittings. Due to the minimization of spin-orbit effects, model $\mathcal{B}$ shows hardly any splitting and the different states in each shell are nearly degenerate. Model $\mathcal{A}$, however, shows moderate intra-band splittings due to rather small relativistic spin-orbit effects. These splittings, *e.g.* in the $2\hbar\omega$ band, even tend to agree with experimentally observed structures as far as they actually can be disentangled from the rather large experimental uncertainties.

Thus we have shown that the major, well-established structures of the complete Δ-resonance spectrum in fact can satisfactorily be reproduced by proper choices of the confinement potential alone, *i.e.* without any need of an additional residual interaction in this flavor sector. This is quite in the spirit of our model which uses the instanton-induced interaction as residual force. Moreover, it is worthy to emphasize once more the economical simplicity of our model: with the spinorial Dirac structure of the confinement kernel fixed, the bulk of all structures is parameterized by three parameters only!

However, some puzzling structures of the Δ spectrum, such as the low-lying resonance $\Delta\frac{3}{2}^+(1600,***)$ in the positive $2\hbar\omega$ band, as well as the states $\Delta\frac{1}{2}^-(1900,**)$, $\Delta\frac{3}{2}^-(1940,*)$ and $\Delta\frac{5}{2}^-(1930,***)$ assigned to the negative-parity $3\hbar\omega$ band do not fit in. Despite the three-star rating of $\Delta\frac{3}{2}^+(1600,***)$ and $\Delta\frac{5}{2}^-(1930,***)$, we have the impression that the currently available experimental evidence for these structures from πN-phase shift analysis is not very convincing. Therefore, a verification of the positions of these resonances in reactions complementary to $\pi - N$ scattering, such as the electro-production of mesons off nucleons, is highly desirable to decide if the lack of these structures in our models (and more generally in all other quark models) really reflects a serious discrepancy.

Unfortunately, the present data basis of the other states, which also is extracted almost entirely from partial-wave analyses of older $\pi N \to \pi N$ total, elastic and charge exchange scattering data, is partly of rather limited quality and hence does not allow to favor one of the models at this stage. Hence, both models $\mathcal{A}$ and $\mathcal{B}$ are of almost the same quality in describing the present experimental situation of the Δ spectrum.

6 The hyperfine structure of the light ground-state baryons

In the foregoing section, we focused on the role of the confinement force alone. We considered the Δ spectrum which is not influenced by 't Hooft's force and thus we could fix in each model the three parameters a, b and m_n to get a satisfactory description of the whole Δ spectrum.

In order to fix models $\mathcal{A}$ and $\mathcal{B}$ for those strange baryons that are likewise not influenced by 't Hooft's force either, we still have to determine the strange constituent quark mass m_s. This is done by the positions of the other (strangeness $S^* \neq 0$) spin-(3/2) decuplet ground states, *i.e.* the hyperons $\Sigma^*(1385)$, $\Xi^*(1583)$ and $\Omega(1672)$. In this respect, the heavier strange quark mass $m_s > m_n$ then leads to the pattern of approximately equally spaced distances between decuplet ground states differing by $\Delta S^* = 1$. Then all parameters in table 1 apart from those of the 't Hooft interaction are fixed for both models. This is a proper starting point for analyzing the effect of 't Hooft's instanton-induced interaction on the remaining states, when turning on the 't Hooft couplings $g_{nn} > 0$ and $g_{ns} > 0$.

We will start this discussion with the spin-(1/2) octet ground states $N(939)$, $\Lambda(1116)$, $\Sigma(1193)$ and $\Xi(1318)$: In this respect, the first prominent feature of the baryon spectrum the instanton-induced interaction has to account for is generating the hyperfine structure of the ground states. In the present approach this means the lowering of the octet ground states relative to the unaffected decuplet ground states, in order to realize the mass differences $\Delta - N$, $\Sigma^* - \Sigma$, $\Xi^* - \Xi$ and $\Sigma - \Lambda$. As in non-relativistic quark models, the confinement potentials of models $\mathcal{A}$ and $\mathcal{B}$ cannot describe this splitting and, without a residual interaction, the octet and decuplet states with the same strangeness content are nearly degenerate.

In earlier (mostly non-relativistic) attempts, as initially suggested by De Rujula, Georgy and Glashow [47] and subsequently applied by Isgur *et al.* and others [36, 37, 6], this structure was explained quantitatively by the short-range spin-spin hyperfine part (Fermi contact term) of the Fermi-Breit interaction due to perturbative one-gluon exchange. Despite the success in describing the ground-state hyperfine structure by this spin-dependent contact interaction, there remain a lot of objections, for instance the spin-orbit problem connected with additional strong spin-orbit forces of the Fermi-Breit interaction or inconsistently large values of the strong-coupling constant α_s. As mentioned before this calls into question the justification for applying perturbative one-gluon exchange at least for light quarks. The most convincing argument against one-gluon exchange and in favor of the non-perturbative and explicitly flavor-dependent instanton-induced interaction is that the latter provides a natural solution of the π-η-η' puzzle, as well as an explanation

of the η-η' mixing in the mesonic sector, see for instance [8]. In leading order the OGE, however, is flavor independent and thus yields degenerate π and η mesons in clear contradiction to experiment. Moreover, the instanton force does not have a (phenomenologically unwanted) large spin-orbit part.

Ground-state baryon mass splittings with the alternative instanton-induced interactions have been first explored in a simple model by Shuryak and Rosner [48] and also by Dorokhov and Kochelev in a bag-like model (for a review see [49]). A first, more extensive study of the baryon (and meson) spectra in the framework of a nonrelativistic quark model[4] using a string-based confining interaction and instanton-induced interactions was made by Blask *et al.* [15,50]. Both attempts have shown that 't Hooft's interaction (which explains the ρ-π, K^*-K and π-η-η' mass splittings in the mesonic sector), also provides an appropriate description of the spin splittings in the octet and decuplet which is at least as good as that from the short-range spin-spin hyperfine part of the Fermi-Breit interaction.

6.1 Naive considerations

For the further discussion it is instructive to illustrate first in a simple (naive) non-relativistic first-order perturbative calculation, how the octet-decuplet mass splittings are generated in principle. Therefore, consider the nonrelativistic limit of the (unregularized) 't Hooft interaction (in lowest order $(\frac{p}{m})^0$ of a $(\frac{p}{m})$-expansion) leading for color antitriplet quark pairs to a spin-flavor–dependent pairing force

$$V^{\rm NR}_{\text{'t Hooft}}(\mathbf{x}_1-\mathbf{x}_2) := -4\mathcal{P}^{\mathcal{S}}_{S_{12}=0}\otimes\left(g_{nn}\,\mathcal{P}^{\mathcal{F}}_{\mathcal{A}}(nn)+g_{ns}\,\mathcal{P}^{\mathcal{F}}_{\mathcal{A}}(ns)\right)\delta^{(3)}(\mathbf{x}_1-\mathbf{x}_2), \quad (27)$$

where $\mathcal{P}^{\mathcal{S}}_{S_{12}=0} := \frac{1}{4}(\mathbb{1}\otimes\mathbb{1}-\boldsymbol{\sigma}\cdot\otimes\,\boldsymbol{\sigma})$ is the projector on quark pairs with trivial spin $S_{12}=0$, and $\mathcal{P}^{\mathcal{F}}_{\mathcal{A}}(nn)$ and $\mathcal{P}^{\mathcal{F}}_{\mathcal{A}}(ns)$ denote the flavor projectors on antisymmetric non-strange (nn) and non-strange–strange (ns) quark pairs, respectively. For simplicity we assume the normalized wave functions $|B_{\mathbf{8}}\rangle$ of all octet ground states $B_{\mathbf{8}} = N$, Λ, Σ and Ξ with total spin and parity $J^\pi = \frac{1}{2}^+$ to be given approximately by the S_3-invariant **56**-plet states

$$|B_{\mathbf{8}}\rangle \simeq |\psi^{L=0\,+}_{\mathcal{S}}\rangle\otimes\frac{1}{\sqrt{2}}\left[|\chi^{\frac{1}{2}}_{\mathcal{M}_{\mathcal{S}}}\rangle\otimes|\phi^{B_{\mathbf{8}}}_{\mathcal{M}_{\mathcal{S}}}\rangle+|\chi^{\frac{1}{2}}_{\mathcal{M}_{\mathcal{A}}}\rangle\otimes|\phi^{B_{\mathbf{8}}}_{\mathcal{M}_{\mathcal{A}}}\rangle\right], \quad (28)$$

where the totally symmetric S-wave ground-state function $|\psi^{L=0\,+}_{\mathcal{S}}\rangle$ in coordinate space is assumed to be the same for all states, *i.e.* distortions of the wave functions due to the heavier strange quark are ignored. $|\chi^{1/2}_{\mathcal{M}_{\mathcal{S}/\mathcal{A}}}\rangle$ denotes the mixed symmetric/antisymmetric spin-(1/2) wave function and $|\phi^{B_{\mathbf{8}}}_{\mathcal{M}_{\mathcal{S}/\mathcal{A}}}\rangle$ the mixed symmetric/antisymmetric flavor octet wave functions. Accordingly, we assume the wave functions $|B_{\mathbf{10}}\rangle$ of all decuplet ground states $B_{\mathbf{10}} = \Delta$, Σ^*, Ξ^* and Ω with total spin and parity $J^\pi = \frac{3}{2}^+$ to be given approximately by the S_3-invariant **56**-plet states

$$|B_{\mathbf{10}}\rangle \simeq |\psi^{L=0\,+}_{\mathcal{S}}\rangle\otimes|\chi^{\frac{3}{2}}_{\mathcal{S}}\rangle\otimes|\phi^{B_{\mathbf{10}}}_{\mathcal{S}}\rangle, \quad (29)$$

where $\chi^{3/2}_{\mathcal{S}}$ denotes the totally symmetric spin-(3/2) wave function and $|\phi^{B_{\mathbf{10}}}_{\mathcal{S}}\rangle$ the totally symmetric flavor decuplet wave functions. Without 't Hooft's force, the octet and decuplet states with the same strangeness content are degenerate. Due to its spin-flavor projector structure, the pairing force causes no shifts of the masses of decuplet baryons

$$\langle\Delta|V^{\rm NR}_{\text{'t Hooft}}\otimes\mathbb{1}|\Delta\rangle = \langle\Sigma^*|V^{\rm NR}_{\text{'t Hooft}}\otimes\mathbb{1}|\Sigma^*\rangle = \langle\Xi^*|V^{\rm NR}_{\text{'t Hooft}}\otimes\mathbb{1}|\Xi^*\rangle = \langle\Omega|V^{\rm NR}_{\text{'t Hooft}}\otimes\mathbb{1}|\Omega\rangle = 0, \quad (30)$$

but it shifts the octet states downward as they contain spin-singlet, S-wave, flavor antisymmetric quark pairs ("scalar diquarks"). In this simplified picture a first order perturbative calculation yields the following decuplet-octet mass splittings:

$$\begin{aligned}
&M_\Delta - M_N\ (\simeq 300\ \text{MeV}) \simeq \\
&-3\,\langle N|\,V^{\rm NR}_{\text{'t Hooft}}\otimes\mathbb{1}\,|N\rangle = C\,g_{nn},\\
&M_{\Sigma^*} - M_\Lambda\ (\simeq 270\ \text{MeV}) \simeq \\
&-3\,\langle\Lambda|\,V^{\rm NR}_{\text{'t Hooft}}\otimes\mathbb{1}\,|\Lambda\rangle = C\,\left(\tfrac{2}{3}\,g_{nn}+\tfrac{1}{3}\,g_{ns}\right),\\
&M_{\Sigma^*} - M_\Sigma\ (\simeq 200\ \text{MeV}) \simeq \\
&-3\,\langle\Sigma|\,V^{\rm NR}_{\text{'t Hooft}}\otimes\mathbb{1}\,|\Sigma\rangle = C\,g_{ns},\\
&M_{\Xi^*} - M_\Xi\ (\simeq 200\ \text{MeV}) \simeq \\
&-3\,\langle\Xi|\,V^{\rm NR}_{\text{'t Hooft}}\otimes\mathbb{1}\,|\Xi\rangle = C\,g_{ns},
\end{aligned} \quad (31)$$

where $C := 6\ \langle\psi^{L=0\,+}_{\mathcal{S}}|\delta^{(3)}(\mathbf{x_1}-\mathbf{x_2})|\psi^{L=0\,+}_{\mathcal{S}}\rangle > 0$ is a constant factor which is the same for all mass splittings. Here we have indicated roughly the experimental values in parentheses. Let us discuss in this naive model the implications of the particular flavor dependence for the baryon ground-state spectrum as sketched schematically in fig. 5:

- The equally spaced mass differences of about 150 MeV between the decuplet states are due to their different strange quark content and the explicit $SU(3)$ breaking caused by the heavier strange quark; without residual interaction octet and decuplet states of the same strangeness are degenerate (see A in fig. 5).
- The nucleon contains only a non-strange scalar diquark and hence the downward mass shift relative to the Δ is proportional to the coupling $g_{nn} > 0$ (see B in fig. 5).
- In a similar way the equally big downward mass shifts of Σ and Ξ relative to Σ^* and Ξ^*, respectively, are proportional to the strength $g_{ns} > 0$, since both these octet states contain a scalar non-strange–strange diquark only (see C in fig. 5).
- The Λ-hyperon, however, contains both types of diquarks, where the scalar non-strange diquark content

[4] We should mention here that this model is regained just in the non-relativistic limit of our fully covariant models $\mathcal{A}$ and $\mathcal{B}$.

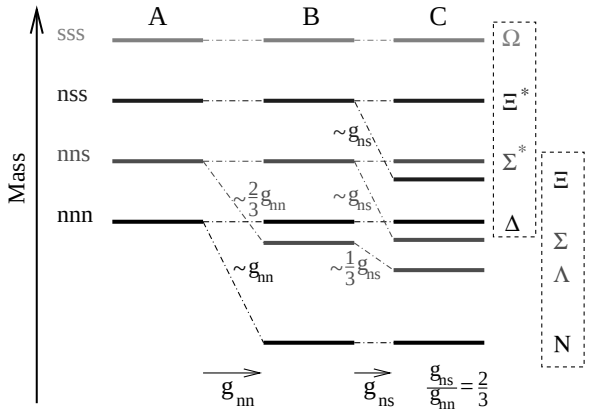

Fig. 5. Schematic mass spectra of the baryon ground states (due to a naive non-relativistic first-order perturbation theory, see text) with (A) no residual interaction, (B) the pairing force between non-strange quarks and (C) in addition the pairing force between a non-strange and a strange quark.

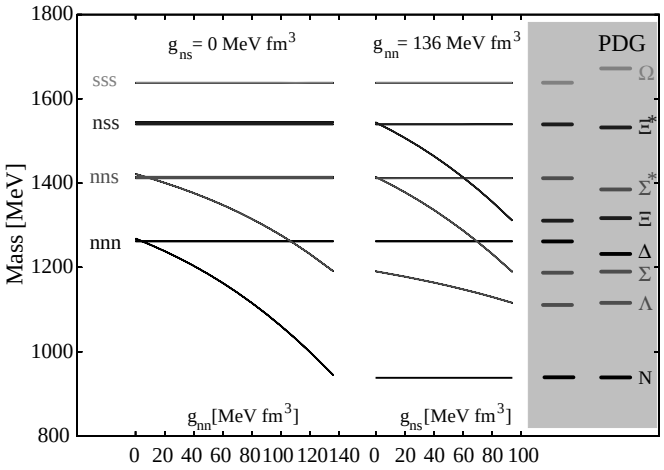

Fig. 6. Generating the hyperfine structure of the octet and decuplet ground-state baryons by the instanton force in model $\mathcal{A}$. The last column headed with "PDG" shows for comparison the experimental ground-state positions [38]. For a detailed explanation see text.

is twice that of the scalar non-strange–strange diquark content. This implies: concerning the non-strange coupling g_{nn} the mass shift of Λ is a factor 2/3 weaker than the nucleon mass shift and the lowering of the Λ mass due to the non-strange–strange coupling is only 1/3 of the corresponding lowering of Σ and Ξ, respectively (see B and C in fig. 5). In particular, we find the $\Sigma - \Lambda$ mass splitting to be given by the difference of the couplings g_{nn} and g_{ns}:

$$M_\Sigma - M_\Lambda \,(\simeq 70 \text{ MeV}) \simeq C\, \tfrac{2}{3}\,(g_{nn} - g_{ns})\,. \qquad (32)$$

Note that in the limit $g_{nn} = g_{ns}$ the 't Hooft interaction becomes flavor $SU(3)$ symmetric, such that the decuplet-octet mass splittings are then all the same. In particular, the $\Sigma - \Lambda$ mass difference then vanishes. Consequently, the correct description of the phenomenological value and sign of the $\Sigma - \Lambda$ mass difference within this simplified model requires the non-strange coupling g_{nn} to be bigger than the non-strange–strange coupling g_{ns}, thus implying a ratio $g_{ns}/g_{nn} < 1$. Using eqs. (31) and (32), the explicit flavor dependence of the pairing force leads to the simple relations

$$\frac{M_\Sigma - M_\Lambda}{M_\Delta - M_N} = \frac{2}{3}\left(1 - \frac{g_{ns}}{g_{nn}}\right)$$

$$\text{and} \qquad \frac{M_{\Sigma^*} - M_\Sigma}{M_\Delta - M_N} = \frac{M_{\Xi^*} - M_\Xi}{M_\Delta - M_N} = \frac{g_{ns}}{g_{nn}} \qquad (33)$$

between the $\Delta - N$ mass splitting and the splittings $\Sigma - \Lambda$, $\Sigma^* - \Sigma$ and $\Xi^* - \Xi$, respectively. This implies that all three relative mass differences have to be described by just one parameter, namely the ratio $g_{ns}/g_{nn} < 1$. Relating the experimental estimates of the $\Sigma - \Lambda$ splitting ($\simeq 70$ MeV) to the $\Delta - N$ mass difference ($\simeq 300$ MeV) due to the first equation yields a ratio of about $g_{ns}/g_{nn} \simeq 2/3$. This is consistent with the same ratio $g_{ns}/g_{nn} = 2/3$ that we get from the second relation by comparing the unequal mass shifts $\Sigma^* - \Sigma$, $\Xi^* - \Xi$ ($\simeq 200$ MeV) and $\Delta - N$ ($\simeq 300$ MeV). Consequently the instanton-induced, flavor-dependent pairing force indeed provides a consistent explanation of the ground-state pattern even in this crude naive model. As illustrated schematically in the last column C of fig. 5 the choice of the ratio $g_{ns}/g_{nn} = 2/3$ can indeed account for the correct level ordering of octet and decuplet ground states in accordance with the experimental findings: $M_N < M_\Lambda < M_\Sigma < M_\Delta < M_\Xi < M_{\Sigma^*} < M_{\Xi^*} < M_\Omega$.

Finally we want to add a remark here concerning the ratio $g_{ns}/g_{nn} < 1$. The fact that the instanton-induced attraction is weaker between a strange and a non-strange quark than between two non-strange quarks, is exactly what one anticipates from the normal ordering of the original three-flavor 't Hooft vertex (see sect. 3): The effective coupling g_{nn} results from a Wick contraction of the strange quark fields with the heavier effective strange quark mass, whereas g_{ns} is obtained by a contraction of a non-strange quark field with the lighter effective non-strange quark mass, thus in fact yielding $g_{ns} < g_{nn}$ as required by the phenomenology of the hyperfine structure (see eq. (21)).

6.2 Generating the hyperfine splittings in models $\mathcal{A}$ and $\mathcal{B}$

Now let us examine the instanton-induced hyperfine splittings with the full relativistic dynamics of our covariant Salpeter models. The influence of 't Hooft's force on the ground-state baryons in model $\mathcal{A}$ and model $\mathcal{B}$ is shown in figs. 6 and 7, respectively.

Without any residual interaction, *i.e.* $g_{nn} = 0$ and $g_{ns} = 0$, all ground states are bound from the flavor-independent three-body confinement potential only.

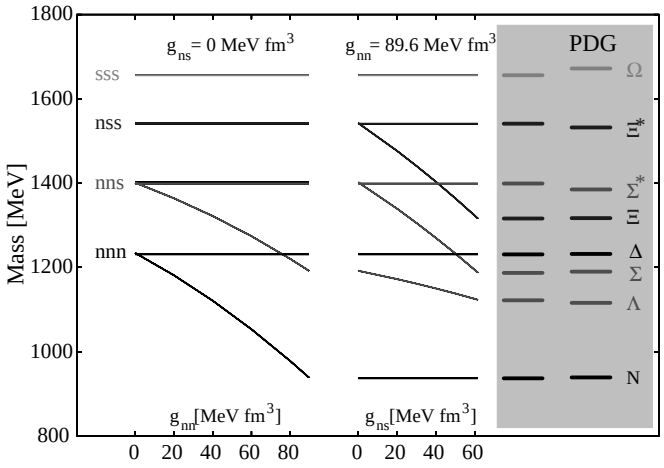

Fig. 7. Generation of the hyperfine structure of the octet and decuplet ground-state baryons by the instanton force in model $\mathcal{B}$. In the last column headed with "PDG" the experimental ground-state positions [38] are shown for comparison. For a detailed explanation see text.

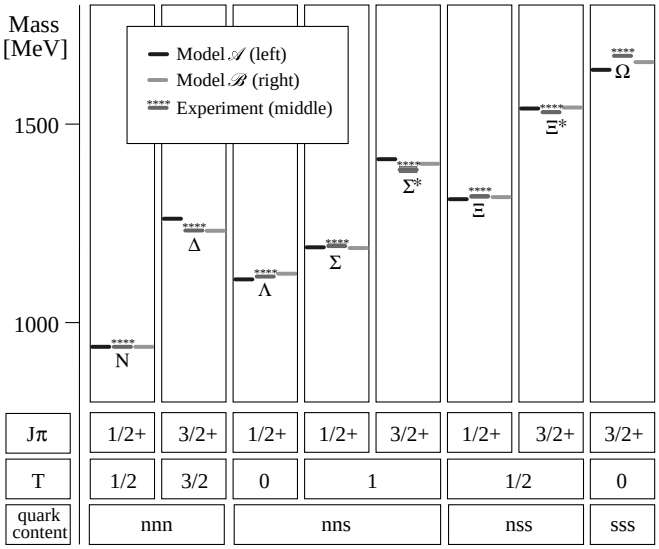

Fig. 8. The resulting spin-(1/2) octet and spin-(3/2) decuplet ground-state baryons calculated in model $\mathcal{A}$ (on the left in each column) and model $\mathcal{B}$ (on the right in each column) in comparison to experimental findings [38] (middle of each column). The explicit mass values are given in table 9.

Therefore, the octet ground states indeed are nearly degenerate to the corresponding decuplet ground states with the same number of strange quarks. Henceforth, the decuplet ground states remain unaffected by 't Hooft's force. The decuplet masses calculated in models $\mathcal{A}$ and $\mathcal{B}$ with the confinement parameters and quark masses given in table 1 are explicitly shown in the upper part of table 9. As discussed in the previous section, the position of the Δ-resonance in model $\mathcal{A}$ turns out to be slightly too high compared to the experimental value. The same also applies to Σ^*, whereas Ω comes out to be roughly 30 MeV too low compared to the observed position; consequently the mass gaps between states of different strangeness content become slightly smaller with increasing strangeness. Nevertheless, the agreement with the experimentally observed positions is still satisfactory; see also fig. 8. In model $\mathcal{B}$ the position of the Δ-resonance matches the experimental value exactly and the deviations of the remaining decuplet states to the corresponding observed positions are smaller than in model $\mathcal{A}$. Hence, the approximate equal mass gaps due to the flavor $SU(3)$ breaking are well described in model $\mathcal{B}$. Altogether the positions of the decuplet ground states are slightly better described in model $\mathcal{B}$ than in model $\mathcal{A}$; see also fig. 8 for a direct comparison of both models and experimental data.

Now let us investigate the effect of 't Hooft's force on the octet ground states in both models. First we consider the dependence on the non-strange coupling $g_{nn} > 0$ with the non-strange–strange coupling still kept fixed at $g_{ns} = 0$. This is shown by the mass curves in the left part of figs. 6 and 7. Due to the non-strange scalar diquark content of the nucleon, increasing the non-strange coupling g_{nn} lowers the nucleon mass M_N to its experimental value $M_N = 939$ MeV, thus generating the $\Delta - N$ mass splitting; this fixes the coupling g_{nn} in model $\mathcal{A}$ and model $\mathcal{B}$ to the values given in table 1. At the same time, the coupling of quark pairs to trivial spin and flavor leads also within the Λ to an attractive correlation of a scalar pair of non-strange quarks thus yielding a lowering of the Λ mass, which is not yet sufficient to match the corresponding experimental resonance position. The remaining mass shift of about 70 MeV in both models is expected just to come from the additional attractive correlation of the scalar non-strange–strange diquark. Note that in model $\mathcal{A}$ as well as in model $\mathcal{B}$ the mass shift of Λ is indeed about 70% weaker than that of the nucleon, in qualitative agreement with the factor 2/3 resulting from the static $SU(6)$ spin-flavor matrix element of 't Hooft's force as discussed previously in the naive model (compare also with column B of fig. 5). Of course, the two other octet states Σ and Ξ remained unaffected so far, as they do not contain quark pairs with trivial isospin (nn-diquark).

We now turn to the g_{ns} dependence of the ground-state spectrum as shown by the mass curves in the right part of figs. 6 and 7. With g_{nn} fixed to reproduce the $\Delta - N$ splitting in both models, an increasing coupling g_{ns} to the scalar, flavor-antisymmetric non-strange–strange diquarks has to lower the calculated masses of the hyperons Λ, Σ and Ξ in such a way that they simultaneously fit the corresponding experimentally observed resonance positions, thus generating the correct $\Sigma - \Lambda$, $\Sigma^* - \Sigma$ and $\Xi^* - \Xi$ mass splittings. This fixes the value of g_{ns} in both models. As shown in figs. 7 and 6, the dependence of the Λ, Σ and Ξ masses on the non-strange–strange coupling g_{ns} exhibits again a qualitatively similar behavior as in the naive model discussed previously (see for comparison column C of fig. 5): with increasing coupling g_{ns}, the masses of Σ and Ξ show almost the same downward shift, whereas the additional weaker mass shift of Λ amounts only to 35% and 32% in model $\mathcal{A}$ and model $\mathcal{B}$, respectively. This

Table 9. Calculated decuplet (upper part) and octet (lower part) ground-state baryons in the models $\mathcal{A}$ and $\mathcal{B}$ compared to experimental values [38]. Notation for model states as in table 3. For a graphical presentation see fig. 8.

Ground state	J^π	Experimental Mass [MeV] [38]	Model ground state in model $\mathcal{A}$	Model ground state in model $\mathcal{B}$
Δ	$\frac{3}{2}^+$	1232	$[\Delta\frac{3}{2}^+]_1(1260)$	$[\Delta\frac{3}{2}^+]_1(1231)$
Σ^*	$\frac{3}{2}^+$	1385	$[\Sigma\frac{3}{2}^+]_1(1411)$	$[\Sigma\frac{3}{2}^+]_1(1399)$
Ξ^*	$\frac{3}{2}^+$	1530	$[\Xi\frac{3}{2}^+]_1(1539)$	$[\Xi\frac{3}{2}^+]_1(1541)$
Ω	$\frac{3}{2}^+$	1672	$[\Omega\frac{3}{2}^+]_1(1636)$	$[\Omega\frac{3}{2}^+]_1(1656)$
N	$\frac{1}{2}^+$	939	$[N\frac{1}{2}^+]_1(939)$	$[N\frac{1}{2}^+]_1(939)$
Λ	$\frac{1}{2}^+$	1116	$[\Lambda\frac{1}{2}^+]_1(1108)$	$[\Lambda\frac{1}{2}^+]_1(1123)$
Σ	$\frac{1}{2}^+$	1193	$[\Sigma\frac{1}{2}^+]_1(1190)$	$[\Sigma\frac{1}{2}^+]_1(1188)$
Ξ	$\frac{1}{2}^+$	1318	$[\Xi\frac{1}{2}^+]_1(1310)$	$[\Xi\frac{1}{2}^+]_1(1316)$

Table 10. The hyperfine splittings between decuplet and octet ground-state baryons in the models $\mathcal{A}$ and $\mathcal{B}$ compared to experimental values.

Hyperfine splitting	Calculation of model $\mathcal{A}$ [MeV]	Calculation of model $\mathcal{B}$ [MeV]	Experiment [MeV]
$\Delta - N$	321	292	293
$\Sigma^* - \Lambda$	303	276	269
$\Sigma^* - \Sigma$	221	211	192
$\Xi^* - \Xi$	229	225	212
$\Sigma - \Lambda$	82	65	75

approximately agrees with the factor 1/3 of the previous naive estimate. Finally, with the fixed values for g_{ns} given in table 1, both models can indeed account remarkably well for the hyperon mass splittings and provide their mass positions in very good agreement with experiment. The resulting masses for the octet states are summarized in the lower part of table 9 and can be compared with the corresponding experimental values of the Particle Data Group [38].

Altogether, both models $\mathcal{A}$ and $\mathcal{B}$ are of the same good quality in describing the experimentally observed positions of the octet ground-state baryons N, Λ, Σ and Ξ. Also the level ordering of the octet and decuplet states is reproduced in accordance with experimental findings, as displayed in the last two columns of figs. 7 and 6. For a direct comparison of the results of models $\mathcal{A}$ and $\mathcal{B}$ (and the experimental data) see fig. 8.

The values of the hyperfine splittings $\Delta - N$, $\Sigma^* - \Lambda$, $\Sigma^* - \Sigma$, $\Xi^* - \Xi$ and $\Sigma - \Lambda$ calculated in both models are explicitly given in table 10. The absolute values of the ground-state splittings can be nicely reproduced. Here the predictions of model $\mathcal{B}$ are slightly better than of model $\mathcal{A}$, where all splittings turn out to be slightly too big. The small discrepancies in model $\mathcal{A}$ can be traced back to the decuplet states, whose calculated absolute positions came out to be slightly too high in model $\mathcal{A}$, as discussed before.

Finally, we want to comment on the values of the 't Hooft couplings g_{nn} and g_{ns} which have been adjusted to the experimental octet ground-state positions. The two model variants $\mathcal{A}$ and $\mathcal{B}$ mainly differ in the form assumed for the spinorial Dirac structure of the linearly rising part of the three-body confinement potential, or more precisely in the way how the scalar and the time-like vector part are combined. In particular, both versions yield the same non-relativistic limit. Although we are using for both models the same value $\lambda = 0.4$ fm for the effective range of the regularized instanton-induced interaction, the absolute values for the 't Hooft couplings g_{nn} and g_{ns} differ significantly: the couplings in model $\mathcal{A}$ are about 50% larger than in model $\mathcal{B}$ indicating a dependence of the action of 't Hooft's force on the structure of the confinement potential. Nevertheless, the ratio of the two couplings g_{nn} and g_{ns} turns out to be the same. Both models yield the ratio $g_{ns}/g_{nn} = 0.69$ which again is in qualitative accordance with the crude phenomenological estimate $g_{ns}/g_{nn} = 2/3$ from the previous naive consideration. Moreover, we should give a comment concerning the special choice for the effective range $\lambda = 0.4$ fm of the regularized instanton-induced four-fermion interaction. We note that there is some freedom to choose the value for λ. While a choice smaller than ~ 0.3 fm spoils the agreement with experiment (and moreover is also much more expensive to handle numerically), for arbitrary values $\lambda > 0.3$ fm the couplings g_{nn} and g_{ns} can always be adjusted such that an equally good result for the hyperfine ground splittings can be achieved. Recall from sect. 3 that 't Hooft's force describes the interaction of quark pairs via instantons up to a critical extension ρ_c which is required to cure the infrared problem. Thus, we expect the effective range λ of 't Hooft's force roughly to correspond to the critical instanton size ρ_c. The value for ρ_c (and thus also λ) should not be larger than ~ 0.5 fm to

be still within the scope of the two-loop approximation of the ρ-dependent running coupling constant (15). Hence, a reasonable value λ is somewhere in between 0.3 and 0.5 fm and we choose $\lambda = 0.4$ fm.

6.3 Summary for the hyperfine structure of ground states

In summary, the use of 't Hooft's residual instanton-induced interaction within our covariant framework provides in both confinement models $\mathcal{A}$ and $\mathcal{B}$ (with parameters being fixed to reproduce the linear Δ Regge trajectory) a good and consistent description of the decuplet and octet ground-state baryons (see fig. 8 for a comprehensive presentation of our results). It turns out that also with the fully relativistic dynamics the $\Delta - N$, $\Sigma^* - \Sigma - \Lambda$ and $\Xi^* - \Xi$ hyperfine splittings arise due to the attractive correlation of quark pairs with trivial spin and antisymmetric flavor to "scalar diquarks" in qualitatively the same manner as one already expects from a naive static, non-relativistic picture. The phenomenology of the hyperfine splittings requires a ratio $g_{ns}/g_{nn} < 1$ of the 't Hooft couplings which is compatible with the expectation from instanton physics. Our result is at least as satisfactory as other attempts (see, *e.g.*, refs. [6,18] and the discussion in appendix A) that explain the hyperfine structure by the short-range spin-spin hyperfine part of the one-gluon exchange.

Now all parameters of our model variants $\mathcal{A}$ and $\mathcal{B}$ are fixed to the values given in table 1. Calculations of all other resonance masses are parameter-free and thus constitute true predictions. In particular, we can investigate next, to what extent the instanton force can also account for the features of the non-strange and strange *excited* baryons. Therefore, we now turn to a detailed discussion of the complete excited N-baryon spectrum and especially analyze how instanton effects shape its characteristic structures. As already mentioned, the predictions for the strange excited baryons will be discussed in a separate paper [26].

7 The nucleon spectrum

We now turn to the investigation of the complete spectrum of nucleon resonances with isospin $T = \frac{1}{2}$ and strangeness $S^* = 0$, where now in addition to the confinement force also the influence of the instanton-induced interaction in general plays an essential role even for the excited states.

7.1 Remarks — Implications of 't Hooft's force and the experimental situation

Let us begin this discussion with some general remarks concerning the action of 't Hooft's force in the nucleon sector. The influence of the instanton force on the nucleon states is related to the content of quark pairs with trivial spin and isospin. The positive and negative energy components of the Salpeter amplitude $\Phi^N_{J^\pi}$ describing an excited flavor-octet nucleon state with spin and parity J^π are obtained by the embedding map (see ref. [1])

$$\Phi^N_{J^\pi} \;=\; T^{+++}\varphi^N_{J^\pi} \;+\; T^{---}\varphi^N_{J^{-\pi}} \tag{34}$$

of totally S_3-symmetric Pauli spinors $\varphi^N_{J^\pi}$ and $\varphi^N_{J^{-\pi}}$ which generally can be decomposed into the following four different spin-flavor $SU(6)$-configurations:

$$\begin{aligned}|\varphi^N_{J^\pm}\rangle = {} & |N\ J^\pm,\ {}^2 8[56]\rangle \;+\; |N\ J^\pm,\ {}^2 8[70]\rangle \\ & + |N\ J^\pm,\ {}^4 8[70]\rangle \;+\; |N\ J^\pm,\ {}^2 8[20]\rangle,\end{aligned} \tag{35}$$

with

$$\begin{aligned}
&|NJ^\pm,{}^2\,8[56]\rangle := \\
&\sum_L \left[|\psi^{L\pm}_{\mathcal{S}}\rangle \otimes \frac{1}{\sqrt{2}} \left(|\chi^{\frac{1}{2}}_{\mathcal{M}_\mathcal{A}}\rangle \otimes |\phi^N_{\mathcal{M}_\mathcal{A}}\rangle + |\chi^{\frac{1}{2}}_{\mathcal{M}_\mathcal{S}}\rangle \otimes |\phi^N_{\mathcal{M}_\mathcal{S}}\rangle \right) \right]^J, \\
&|NJ^\pm,{}^2\,8[70]\rangle := \\
&\sum_L \left[\frac{1}{2} |\psi^{L\pm}_{\mathcal{M}_\mathcal{A}}\rangle \otimes \left(|\chi^{\frac{1}{2}}_{\mathcal{M}_\mathcal{A}}\rangle \otimes |\phi^N_{\mathcal{M}_\mathcal{S}}\rangle + |\chi^{\frac{1}{2}}_{\mathcal{M}_\mathcal{S}}\rangle \otimes |\phi^N_{\mathcal{M}_\mathcal{A}}\rangle \right) \right. \\
&\qquad \left. + \frac{1}{2} |\psi^{L\pm}_{\mathcal{M}_\mathcal{S}}\rangle \otimes \left(|\chi^{\frac{1}{2}}_{\mathcal{M}_\mathcal{A}}\rangle \otimes |\phi^N_{\mathcal{M}_\mathcal{A}}\rangle - |\chi^{\frac{1}{2}}_{\mathcal{M}_\mathcal{S}}\rangle \otimes |\phi^N_{\mathcal{M}_\mathcal{S}}\rangle \right) \right]^J, \\
&|NJ^\pm,{}^4\,8[70]\rangle := \\
&\sum_L \left[\frac{1}{\sqrt{2}} \left(|\psi^{L\pm}_{\mathcal{M}_\mathcal{A}}\rangle \otimes |\chi^{\frac{3}{2}}_{\mathcal{S}}\rangle \otimes |\phi^N_{\mathcal{M}_\mathcal{A}}\rangle \right. \right. \\
&\qquad \left. \left. - |\psi^{L\pm}_{\mathcal{M}_\mathcal{S}}\rangle \otimes |\chi^{\frac{3}{2}}_{\mathcal{S}}\rangle \otimes |\phi^N_{\mathcal{M}_\mathcal{S}}\rangle \right) \right]^J, \\
&|NJ^\pm,{}^2\,8[20]\rangle := \\
&\sum_L \left[|\psi^{L\pm}_{\mathcal{A}}\rangle \otimes \frac{1}{\sqrt{2}} \left(|\chi^{\frac{1}{2}}_{\mathcal{M}_\mathcal{A}}\rangle \otimes |\phi^N_{\mathcal{M}_\mathcal{S}}\rangle - |\chi^{\frac{1}{2}}_{\mathcal{M}_\mathcal{S}}\rangle \otimes |\phi^N_{\mathcal{M}_\mathcal{A}}\rangle \right) \right]^J.
\end{aligned} \tag{36}$$

Here $\psi^{L\,\pm}_{R_L}$, $\chi^S_{R_S}$ and $\phi^N_{R_F}$ are the spatial, spin and flavor wave functions with definite S_3-symmetries $R_L, R_S, R_F \in \{\mathcal{S}, \mathcal{M}_\mathcal{S}, \mathcal{M}_\mathcal{A}, \mathcal{A}\}$. The sum runs over possible orbital angular momenta L that can be coupled with the internal spin S to the total spin J as denoted by the brackets $[\ldots]^J$. Due to the strong selection rule of the instanton-induced interaction, its action on the different states of the nucleon spectrum is qualitatively understandable from a simplified picture, in which one disregards the negative energy component and the relativistic effects from the embedding map of the Salpeter amplitudes (corresponding to the non-relativistic limit). Then we expect all those resonances, which in the pure confinement case ($g_{nn} = 0$) are dominantly ${}^4 8[70]$ and ${}^2 8[20]$, to be hardly influenced by 't Hooft's force. Consequently, these resonances should be determined mainly by the confining kernel alone, similar to the resonances in the Δ spectrum. For ${}^4 8[70]$ states in eq. (36) this selection rule is apparent from the total

symmetry of the spin-function $\chi_{\mathcal{S}}^{3/2}$. The $^2 8[20]$ states possess a totally antisymmetric spatial wave function, which is not affected by a point-like interaction. Moreover its spin-flavor wave function, which decomposes into mixed symmetric spin functions $\chi_{\mathcal{M}_\mathcal{S}}^{1/2}$ and mixed antisymmetric flavor functions $\phi_{\mathcal{M}_\mathcal{A}}^{N}$ and vice versa, never contains quark pairs with trivial spin and trivial flavor simultaneously. However, resonances which are dominantly $^2 8[56]$, like, *e.g.*, the nucleon ground state, are expected to exhibit quite strong effects induced by the instanton force. Furthermore, also the resonances which mainly consist of $^2 8[70]$ states should be affected by the 't Hooft interaction. Finally, it should be noted that 't Hooft's force in general mixes $^2 8[56]$ and $^2 8[70]$ configurations. From these simple non-relativistic considerations we thus expect that the majority of states is described by the confinement force alone, while 't Hooft's force acts in a selective manner on a particular limited set of states.

However, one has to be careful with such naive non-relativistic considerations. Due to our fully covariant Salpeter approach, relativistic effects might become essential in two ways:

1. From the outset (without instanton force), the initial mixing of the four different spin-flavor $SU(6)$ configurations (36) in (35), especially for the excited states, can strongly depend on the relativistic (spin-orbit) effects that emerge from the chosen confinement Dirac structure in connection with the embedding map (34) of the Salpeter amplitudes. In particular, distinct Dirac structures cause different initial intra-band splittings and level orderings. Consequently, the influence of the instanton-induced interaction on the excited nucleon spectrum may be different in our two model variants. As we will see in the following discussion, models $\mathcal{A}$ and $\mathcal{B}$ indeed show substantial differences concerning the effects of 't Hooft's force in the excited spectra, in contrast to the description of the ground-state hyperfine structure, where 't Hooft's force in both models works equally well. This dependence of the effects of the instanton force on the confinement mechanism in fact is a purely relativistic effect, since the expressions for the confinement kernels of both models lead to the same non-relativistic limit and thus in this limit also to the same results.
2. Furthermore, the fully relativistic treatment of 't Hooft's force within our covariant Salpeter approach leads already by itself to differences in the effects of this interaction as compared to a non-relativistic treatment. On the one hand the action on the Pauli amplitudes (36) is modified due to the embedding map for the Salpeter amplitudes and on the other hand the fully relativistic version of the instanton-induced interaction causes effects that are *a priori* absent in the non-relativistic limit. In particular, it also has repulsive components, unlike its non-relativistic version. In this respect, we should remark here that the projector structure of 't Hooft's interaction kernel actually decomposes into two different parts. On the one hand there is the projector onto *scalar diquarks* with trivial spin and antisymmetric flavor. This is the dominant attractive part, which survives in the non-relativistic limit. It is responsible for the strong attraction of diquarks in the octet ground-state baryons leading to the correct octet-decuplet ground-state splittings as discussed in the previous subsection. But, on the other hand, there is also a projector onto the orthogonal *pseudo-scalar diquarks* with trivial spin and antisymmetric flavor. In this channel the instanton force is repulsive. This part of the instanton force completely vanishes in the non-relativistic limit.

These issues in fact emphasize the importance of describing baryons in a fully relativistic framework and accordingly it is interesting to study to what extent our covariant approach leads to improvements in the description of the excited-state spectrum as compared to its non-relativistic version described earlier in [15,50]. Moreover, the different action of 't Hooft's force in combination with the two different confinement Dirac structures of models $\mathcal{A}$ and $\mathcal{B}$ will offer an additional, indirect criterion to decide which version provides a more realistic confinement force.

In the following discussion we will present a detailed investigation of instanton-induced effects on the excited spectrum of the nucleon resonances in both models (subsect. 7.3). In subsect. 7.2 we shall start by comparing the complete presently known empirical N^* spectrum with our final resulting resonance positions obtained with the coupling g_{nn} adjusted in the previous section to reproduce the experimentally measured position $M_N = 939$ MeV of the nucleon ground state. In this respect, the most striking experimental features of the nucleon spectrum, that a realistic quark model should account for, are [38]:

- The low position of four states in the positive-parity $2\hbar\omega$ band, which lie quite isolated from the other states of this shell around 2000 MeV and which form a striking pattern: The most prominent member of this structure is the well-established lowest isoscalar/scalar excitation, the famous Roper resonance $N\frac{1}{2}^+(1440,****)$ that appears even below the first excitations of the nucleon in the negative-parity $1\hbar\omega$ band. The puzzling low position of this particular resonance has been extensively discussed in the literature as the so-called *Roper problem* [37,39,40,51]. Furthermore, there are three other well-established states $N\frac{1}{2}^+(1710,***)$, $N\frac{3}{2}^+(1720,****)$ and $N\frac{5}{2}^+(1680,****)$ which are approximately degenerate at around 1700 MeV.
- The hyperfine structure of five observed three- and four-star states assigned to the negative-parity $1\hbar\omega$ shell, *i.e.* the mass splitting between the two groups of almost degenerate states $N\frac{1}{2}^-(1650,****)$ – $N\frac{3}{2}^-(1700,***)$ – $N\frac{5}{2}^-(1675,****)$ and $N\frac{1}{2}^-(1535,****)$ – $N\frac{3}{2}^-(1520,***)$.
- The overlap of alternating even- and odd-parity bands and accordingly the striking appearance of approximate "parity doublets": The overlapping negative-parity $1\hbar\omega$ and positive-parity $2\hbar\omega$ shells reveal the parity doublets

$N\frac{1}{2}^+(1710,***)$ – $N\frac{1}{2}^-(1650,****)$,
$N\frac{3}{2}^+(1720,****)$ – $N\frac{3}{2}^-(1700,***)$,
$N\frac{5}{2}^+(1680,****)$ – $N\frac{5}{2}^-(1675,****)$.

In the higher mass region we find, *e.g.*, the approximate doublets

$N\frac{7}{2}^+(1990,**)$ – $N\frac{7}{2}^-(2190,****)$,
$N\frac{9}{2}^+(2220,****)$ – $N\frac{9}{2}^-(2250,****)$.

The splittings within the parity partners are mostly within the experimental uncertainties.

Another aspect, which is currently of high interest, is the question of the so-called "*missing resonances*", *i.e.* states that appear in quark models but which have not been seen in πN partial-wave analyses. As already observed in the Δ sector, our Salpeter equation-based quark model (and constituent quark models for baryons in general) predicts a much richer resonance spectrum of states than has been observed so far in scattering experiments. Most of the resonance parameters of the N^* and Δ states listed in the *Review of Particle Properties* [38] stem largely from partial-wave analyses of mostly older $\pi N \to \pi N$ scattering data. Fortunately, the newly established experimental electron and photon facilities at CEBAF, ELSA, *etc.*, make it possible to investigate additional mechanisms of nucleon resonance excitations with photons with considerably improved experimental accuracy. Assuming that the "missing" states couple only weakly to the formation channels in $N\pi$ scattering [52,18] and thus escape from experimental observation, the investigation of these new complementary formation channels should lead to the discovery of some of these "missing" states in the near future. Indeed, in the sector of nucleon resonances considered here, there are already indications of three new states around 1900 MeV obtained from recent studies of photo-induced reactions with the SAPHIR detector at the ELSA electron accelerator in Bonn [53,54]. These allow a first glimpse of the high-mass spectrum of N^*-resonances:

– η' photoproduction: A fit to the SAPHIR total and differential cross-sections for the η' photoproduction obtained from the reaction chain $\gamma p \to p\eta' \to p\pi^+\pi^-\eta \to p\pi^+\pi^-\pi^+\pi^-\pi^0$ has been made [55] assuming resonance dominance and taking only S- and P-wave multipoles into account. The data indicate a coherent resonant production of two $p\eta'$ partial waves, S_{11} and P_{11}. The extracted resonance parameters are

partial wave	J^π	resonance position M [MeV]	decay width Γ [MeV]
S_{11}	$\frac{1}{2}^-$	$1897 \pm 50^{+30}_{-2}$	$396 \pm 115^{+35}_{-45}$
P_{11}	$\frac{1}{2}^+$	$1986 \pm 26^{+10}_{-30}$	$296 \pm 100^{+60}_{-10}$

– $\gamma p \to K^+\Lambda$: Recent measurements of the $\gamma p \to K^+\Lambda$ total cross-sections from SAPHIR [56] indicate for the first time a broad structure around 1900 MeV. This structure could not be resolved before due to the low quality of the old data. An analysis of these new and associated differential cross-section and recoil-polarization data in the framework of an isobar model [57] suggests the existence of a broad D_{13} state, where the choice of a D_{13} state is based on the agreement with quark-model predictions [58,59]. The fitted resonance parameters are:

partial wave	J^π	resonance position M [MeV]	decay width Γ [MeV]
D_{13}	$\frac{3}{2}^-$	1895	372

The discovery of "missing" states and the measurement of their resonance positions with high accuracy provides a convincing test for the quality and the predictive power of various constituent quark models in order to distinguish between realistic and less realistic quark models for the description of baryon masses. In this respect, it is interesting if and how these indications for these three new states fit into our models $\mathcal{A}$ and $\mathcal{B}$.

Before we begin our discussion organized according to the phenomenological issues of the excited N^* spectrum listed, it is worthwhile to remark once more that there is no freedom[5] left to fit the excited nucleon states. With the five parameters a, b, m_n and g_{nn}, λ fixed from the Δ spectrum and the $\Delta - N$ splitting, all the excited resonances of the N^* spectrum are now true predictions. In the subsequent subsect. 7.3 we will then illustrate in some more detail how instanton-induced effects due to 't Hooft's quark-quark interaction are in fact responsible for the phenomenology of the N^* spectrum.

7.2 Discussion of the complete N spectrum

Figures 9 and 10 show the resulting positions of the positive- and negative-parity nucleon resonances with total spins up to $J = \frac{13}{2}$ obtained in model $\mathcal{A}$ and $\mathcal{B}$, respectively. These are compared with the experimentally observed positions of all presently known resonances of each status taken from the Particle Data Group [38]. Again, the resonances in each column are classified by the total spin J and the parity π, where left in each column the results for at most ten excitations in model $\mathcal{A}$ or $\mathcal{B}$ are shown. In comparison the experimental positions [38] are displayed on the right in each column with the uncertainties of the resonance positions indicated by the shaded boxes and the rating of each resonance denoted by the corresponding number of stars and a different shading of the error box. In addition we also display the determined resonance positions of the three new states that have been recently discovered by the SAPHIR collaboration [55–57, 53,54]. These states are indicated by the symbol "S".

In the following, we turn to a shell-by-shell discussion of the complete nucleon spectrum. According to their assignment to a particular shell, we additionally summa-

[5] In principle there is freedom to choose a different effective range λ of the regularized 't Hooft interaction along with a new adjusted coupling g_{nn} to readjust the correct $N - \Delta$ mass difference. However, within the range of possible values λ, which are consistent with a reasonable description of the ground-state baryons, the structure of the excited nucleon spectrum shows only a fairly weak sensitivity to the choice of λ.

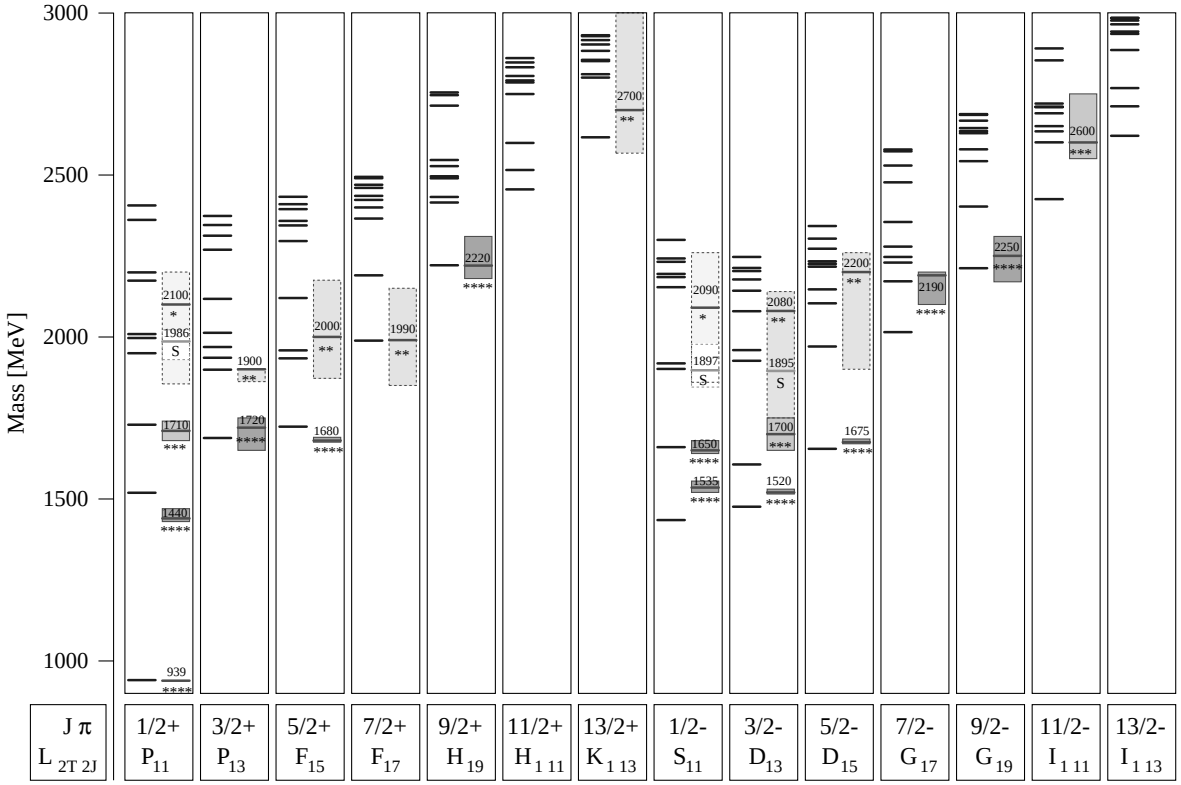

Fig. 9. The calculated positive- and negative-parity *N-resonance spectrum* (isospin $T = \frac{1}{2}$ and strangeness $S^* = 0$) in *model* $\mathcal{A}$ (left part of each column) in comparison to the experimental spectrum taken from Particle Data Group [38] (right part of each column). The resonances are classified by the total spin J and parity π. The experimental resonance position is indicated by a bar, the corresponding uncertainty by the shaded box, which is darker the better a resonance is established; the status of each resonance is additionally indicated by stars. The states labeled by "S" belong to new SAPHIR results [55–57, 53, 54], see text.

rized the explicit positions of the excited model states in tables 11, 12, 14, 15, 16 and 17.

7.2.1 States of the $2\hbar\omega$ band

Let us begin our discussion with the intra-band structure of the positive-parity $2\hbar\omega$ band including states with spins $J^\pi = \frac{1}{2}^+$, $\frac{3}{2}^+$, $\frac{5}{2}^+$ and $\frac{7}{2}^+$. The predicted positions of states belonging to this shell and their assignments to observed resonances due to a comparison with the phenomenological mass values are given explicitly in table 11.

Indeed we find in the $\frac{1}{2}^+$, $\frac{3}{2}^+$ and $\frac{5}{2}^+$ sectors for both models $\mathcal{A}$ and $\mathcal{B}$ a selective lowering of exactly four states, well separated from the remaining bulk of states which is centered around 2000 MeV. As we will illustrate in the next subsect. 7.3, this is indeed a consequence of the strongly attractive action of the instanton-induced residual interaction in these dominantly $^2 8[56, +]$ or $^2 8[70, +]$ states.

Concerning these states, let us first focus on the results of model $\mathcal{A}$. Figure 9 impressively shows that in model $\mathcal{A}$ these four separated states fit rather well into the experimentally observed pattern of splittings, thus yielding a unique one-to-one correspondence between our model states and the observed resonances. In particular, we can account for the puzzling low position of the Roper resonance $N\frac{1}{2}^+(1440, ****)$: the calculated position at 1518 MeV is only 78 MeV too high compared to the phenomenologically determined mass value. The discrepancy to the upper edge of the uncertainty range even amounts to only 48 MeV. We should note here that more recent analyses [41, 42] even determine a slightly higher Roper resonance position at 1462 ± 80 MeV and 1479 ± 80 MeV, respectively. We also obtain a very satisfactory description of the other three states that are grouped around 1700 MeV: in the $N\frac{1}{2}^+$ sector the second radial excitation after the Roper state predicted at 1729 MeV fits exactly into the uncertainty range of the $N\frac{1}{2}^+(1710, ***)$. The same is the case in the $N\frac{3}{2}^+$ sector, where the first excitation predicted at 1688 MeV nicely agrees with the well-established four-star state $N\frac{3}{2}^+(1720, ****)$. In the $N\frac{5}{2}^+$ sector our prediction for the first excited state at 1723 MeV slightly overestimates the observed position of the $N\frac{5}{2}^+(1680, ****)$. We would like to mention that a selective lowering of these states is also found in a non-relativistic treatment, see [15, 50]. However these calculations could only qualitatively describe these splittings: the Roper resonance and the other three positive-parity

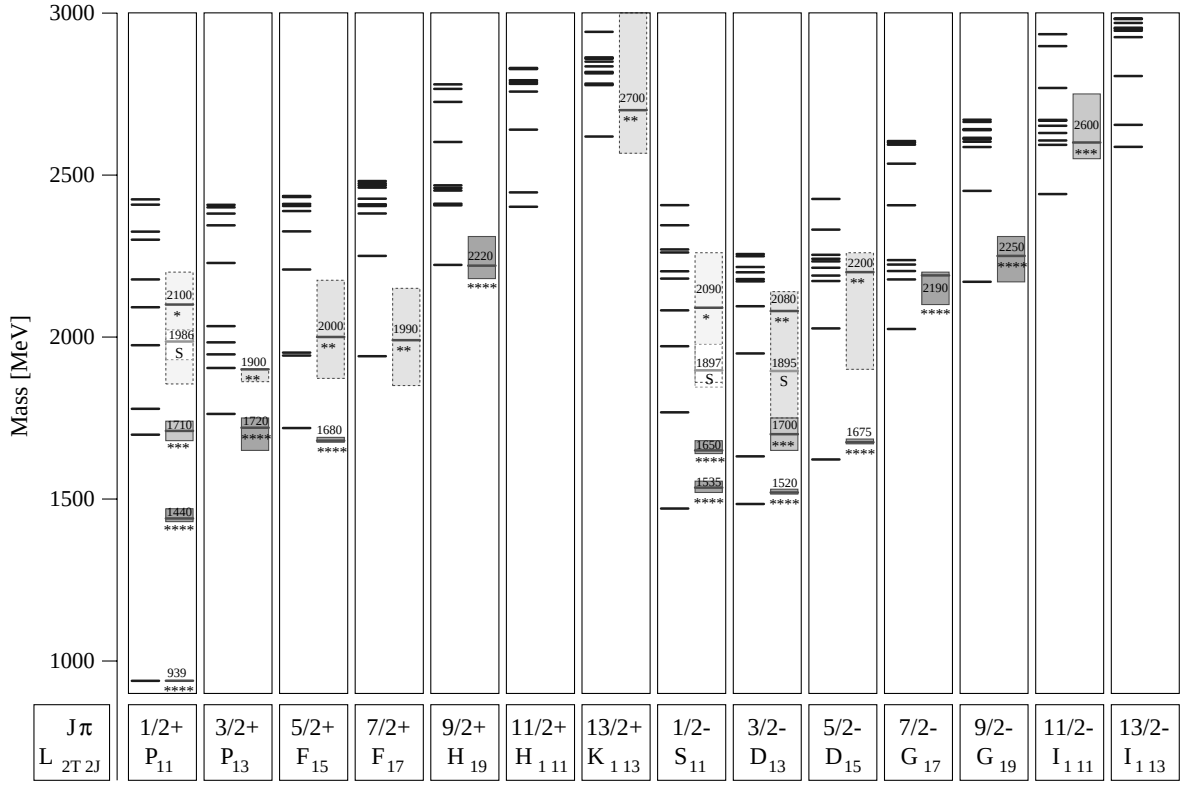

Fig. 10. The calculated positive- and negative-parity *N-resonance spectrum* (isospin $T = \frac{1}{2}$ and strangeness $S^* = 0$) in *model* $\mathcal{B}$ (left part of each column) in comparison to the experimental spectrum taken from Particle Data Group [38] (right part of each column). The resonances are classified by the total spin J and parity π. See also caption to fig. 9.

Table 11. Calculated positions of nucleon states assigned to the positive-parity $2\hbar\omega$ shell in comparison to the corresponding experimental mass values taken from [38]. Notation as introduced in the caption of table 3. The resonance $P_{11}(1986)$ denoted by "SAPHIR" (in the column "Rating") corresponds to the new η' photoproduction result from the SAPHIR collaboration [55].

Experimental state [38]	PW	J^π	Rating	Mass range [MeV] [38]	Model state in model $\mathcal{A}$	Model state in model $\mathcal{B}$
$N(1440)$	P_{11}	$\frac{1}{2}^+$	****	1430–1470	$[N\frac{1}{2}^+]_2(1518)$	$[N\frac{1}{2}^+]_2(1698)$
$N(1710)$	P_{11}	$\frac{1}{2}^+$	***	1680–1740	$[N\frac{1}{2}^+]_3(1729)$	$[N\frac{1}{2}^+]_3(1778)$
					$[N\frac{1}{2}^+]_4(1950)$	
$P_{11}(1986)$	P_{11}	$\frac{1}{2}^+$	SAPHIR	1930-2022	$[N\frac{1}{2}^+]_5(1996)$	$[N\frac{1}{2}^+]_4(1974)$
					$[N\frac{1}{2}^+]_6(2009)^\dagger$	
$N(2100)$	P_{11}	$\frac{1}{2}^+$	*	1855–2200		$[N\frac{1}{2}^+]_5(2092)$
$N(1720)$	P_{13}	$\frac{3}{2}^+$	****	1650–1750	$[N\frac{3}{2}^+]_1(1688)$	$[N\frac{3}{2}^+]_1(1762)$
$N(1900)$	P_{13}	$\frac{3}{2}^+$	**	1862–1900	$[N\frac{3}{2}^+]_2(1899)$	$[N\frac{3}{2}^+]_2(1904)$
					$[N\frac{3}{2}^+]_3(1936)$	$[N\frac{3}{2}^+]_3(1946)$
					$[N\frac{3}{2}^+]_4(1969)$	$[N\frac{3}{2}^+]_4(1983)$
					$[N\frac{3}{2}^+]_5(2013)$	$[N\frac{3}{2}^+]_5(2033)$
$N(1680)$	F_{15}	$\frac{5}{2}^+$	****	1675–1690	$[N\frac{5}{2}^+]_1(1723)$	$[N\frac{5}{2}^+]_1(1718)$
$N(2000)$	F_{15}	$\frac{5}{2}^+$	**	1872-2175	$[N\frac{5}{2}^+]_2(1934)$	$[N\frac{5}{2}^+]_2(1943)$
					$[N\frac{5}{2}^+]_3(1959)$	$[N\frac{5}{2}^+]_3(1952)$
$N(1990)$	F_{17}	$\frac{7}{2}^+$	**	1850–2150	$[N\frac{7}{2}^+]_1(1989)$	$[N\frac{7}{2}^+]_1(1941)$

† The predicted state $[N\frac{1}{2}^+]_6(2009)$ in model $\mathcal{A}$ actually belongs to the $4\hbar\omega$ shell but is lowered into the region of the $2\hbar\omega$ band due to the instanton force, see fig. 15 in subsect. 7.3.

excited states tend to be too massive by about 200–250 MeV. In this respect, we thus find the predictions of our fully covariant model $\mathcal{A}$ being of considerably better quality, emphasizing the necessity of a fully relativistic framework to describe this striking structure quantitatively. Looking at fig. 10, the corresponding predictions for these four states in model $\mathcal{B}$ confirm this statement: even though model $\mathcal{B}$ has the same non-relativistic limit as model $\mathcal{A}$, the fully relativistic treatment within our Salpeter framework yields a totally different result. Although we likewise observe in the $N\frac{1}{2}^+$, $N\frac{3}{2}^+$ and $N\frac{5}{2}^+$ sectors a separation of four states from the rest of the $2\hbar\omega$ band, model $\mathcal{B}$ obviously strongly fails in the description of the low position of the Roper resonance. Instead, we find in the $N\frac{1}{2}^+$ sector two slightly split states at 1698 MeV and 1778 MeV that lie near the experimentally observed resonance $N\frac{1}{2}^+(1710,***)$. On the other hand, the predictions of the two other resonances in the $N\frac{3}{2}^+$ and $N\frac{5}{2}^+$ sectors reproduce the states $N\frac{3}{2}^+(1720,****)$ and $N\frac{5}{2}^+(1680,****)$ rather satisfactorily. It is worth noting that the difference to model $\mathcal{A}$ concerning the Roper resonance is caused by a quite different influence of the instanton-induced interaction within the confinement versions $\mathcal{A}$ and $\mathcal{B}$. It has its origin in the different mixing of the spin-flavor $SU(6)$ contributions (36) to the embedded Pauli spinors and moreover in a different level ordering within the intra-band structure. This originates from various relativistic effects that are induced by the two confinement Dirac structures of model $\mathcal{A}$ and $\mathcal{B}$. Also these features shall be clarified in some more detail in the course of the next subsect. 7.3. Here let us note that this striking difference between the two models concerning the Roper resonance strongly supports model $\mathcal{A}$ to provide the more realistic confinement version in combination with 't Hooft's force as residual interaction.

As already mentioned, apart from these four separated, low-lying resonances, the remaining bulk of states predicted in the $2\hbar\omega$ shell is clustered around 2 GeV. In both models their mean mass corresponds nicely with the ranges of possible values of the three two-star states $N\frac{3}{2}^+(1900,**)$, $N\frac{5}{2}^+(2000,**)$ and $N\frac{7}{2}^+(1990,**)$ observed in this resonance region. Obviously, both models predict a substantial number of "missing" states in this region and thus the assignment of our model states to observed resonances by a comparison of the masses alone is in general not unique. Let us discuss the situation in each spin sector from $\frac{1}{2}^+$ to $\frac{7}{2}^+$ in turn:

In the $N\frac{7}{2}^+$ sector the assignment is still unambiguous: both models predict only a single state in accordance with the single resonance $N\frac{7}{2}^+(1990,**)$ seen in this mass range for the F_{17} partial wave. The predicted mass values at 1989 MeV in model $\mathcal{A}$ and at 1941 MeV in model $\mathcal{B}$ both agree with the observed position of this two-star resonance. Moreover, it is interesting to note that the Salpeter amplitude of this first excited $N\frac{7}{2}^+$ state exhibits an almost pure $^4 8[70]$ configuration ($> 99\%$) in both models and by no means is influenced by 't Hooft's force. Hence, this state is determined by the confinement potential alone. In the $N\frac{5}{2}^+$ sector there are predictions of two further nearly degenerate states in this higher resonance region at 1934 and 1959 MeV in model $\mathcal{A}$ and at 1943 and 1952 MeV in model $\mathcal{B}$. The calculated masses correspond rather well to the $N\frac{5}{2}^+(2000,**)$. In the $N\frac{3}{2}^+$ sector we find even a group of four other states in the $2\hbar\omega$ band which all lie in the range between ~ 1900 and ~ 2000 MeV. In both models, the first of these states (predicted at 1899 MeV in $\mathcal{A}$ and at 1904 MeV in $\mathcal{B}$) fits close to the reported position of the resonance $N\frac{3}{2}^+(1900,**)$. Thus, the gap of roughly 200 MeV between the resonances $N\frac{3}{2}^+(1720,****)$ and $N\frac{3}{2}^+(1900,**)$ is fairly well reproduced in both models and none of the three remaining "missing" states of this shell lies in between this gap as partly predicted in other quark models, as, *e.g.*, in the collective quark model of Bijker, Iachello and Leviatan [60, 61], which is based on a spectrum-generating algebra. In the $N\frac{1}{2}^+$ sector, the results of model $\mathcal{A}$ and $\mathcal{B}$ again differ significantly. In (the less realistic) model $\mathcal{B}$, the two remaining states that complete the $2\hbar\omega$ shell in this sector, are predicted at 1974 MeV and 2092 MeV. The first state agrees fairly well with the position of the new discovered resonance $P_{11}(1986)$ extracted by a recent analysis of η' photoproduction at the SAPHIR detector [55]. The second state fits the average value of the weakly established one-star resonance $N\frac{1}{2}^+(2100,*)$. Model $\mathcal{A}$, however, predicts a cluster of three close states at 1950 MeV, 1996 MeV and 2009 MeV. We should note that the first two predictions correspond to two (of four) remaining states that one usually expects to be assigned to the $2\hbar\omega$ shell. The third one is lowered from the $4\hbar\omega$ band into this resonance region due to a strong attraction of the instanton force for this state (for an illustration see fig. 15 in the next subsect. 7.3). All three predicted masses nicely fit within the uncertainty range of the recently discovered "SAPHIR resonance" $P_{11}(1986)$, which overlaps with the quite large error range of the one-star $N\frac{1}{2}^+(2100,*)$. To decide which of these three model states has to be assigned to this new resonance due to possible different couplings of these states to the $N\eta'$ decay channel would require the calculation of quasi-two-body decays of baryons into different meson-baryon final states within our covariant Bethe-Salpeter framework. Unfortunately this information is not yet available but it will be a principal objective of our investigations in the near future. For the moment it is interesting to emphasize that, similar to the $N\frac{3}{2}^+$ sector, there are no predicted "missing" states in between the new "SAPHIR resonance" $P_{11}(1986)$ and the established $N\frac{1}{2}^+(1710,***)$ resonance. Also here, our model $\mathcal{A}$ differs significantly from other constituent quark models [6,60,61]. In this respect, the possible discovery of new (so far "missing" and undiscovered) baryon states at CEBAF, ELSA and elsewhere just in this N^* resonance region is highly interesting and will provide an additional helpful

Table 12. Calculated positions of all nucleon states assigned to the negative-parity $1\hbar\omega$ shell in comparison to the corresponding experimental mass values taken from [38]. Notation as in table 3.

Experimental state [38]	PW	J^π	Rating	Mass range [MeV] [38]	Model state in model $\mathcal{A}$	Model state in model $\mathcal{B}$
$N(1535)$	S_{11}	$\frac{1}{2}^-$	****	1520–1555	$[N\frac{1}{2}^-]_1(1435)$	$[N\frac{1}{2}^-]_1(1470)$
$N(1650)$	S_{11}	$\frac{1}{2}^-$	****	1640–1680	$[N\frac{1}{2}^-]_2(1660)$	$[N\frac{1}{2}^-]_2(1767)$
$N(1520)$	D_{13}	$\frac{3}{2}^-$	****	1515–1530	$[N\frac{3}{2}^-]_1(1476)$	$[N\frac{3}{2}^-]_1(1485)$
$N(1700)$	D_{13}	$\frac{3}{2}^-$	***	1650–1750	$[N\frac{3}{2}^-]_2(1606)$	$[N\frac{3}{2}^-]_2(1631)$
$N(1675)$	D_{15}	$\frac{5}{2}^-$	****	1670–1685	$[N\frac{5}{2}^-]_1(1655)$	$[N\frac{5}{2}^-]_1(1622)$

criterion to distinguish between the different constituent quark models presently discussed in the literature [18].

7.2.2 States of the $1\hbar\omega$ band

We now turn to the description of those states which, in the language of the harmonic oscillator basis, belong to the negative-parity $1\hbar\omega$ band. Both models predict (as usual in constituent quark models for baryons) five states with spins $J^\pi = \frac{1}{2}^-$, $\frac{3}{2}^-$ and $\frac{5}{2}^-$ that can be uniquely identified with the five observed, well-established four- and three-star resonances listed in the baryon summary table of the Particle Data Group [38]. A comparison of the predicted masses with the corresponding empirical resonance positions is given in table 12.

In both models, the single $1\hbar\omega$ state predicted in the $N\frac{5}{2}^-$ sector is an approximately pure $^4 8[70]$ state ($> 99\%$). It thus remains totally unaffected by the instanton force similar to the first positive-parity excitation in the $N\frac{7}{2}^+$ sector. Hence also this state is determined by the three-quark confinement kernel alone. In model $\mathcal{A}$ this state is predicted at 1655 MeV, very close to the experimental position of the four-star resonance $N\frac{5}{2}^-(1675, ****)$. Model $\mathcal{B}$ slightly underestimates the empirical mass value by roughly 50 MeV. Also the mass splitting between the two resonances $N\frac{3}{2}^-(1520, ****)$ and $N\frac{3}{2}^-(1720, ***)$ in the $N\frac{3}{2}^-$ sector is equally well reproduced in both models. However, the calculated positions appear slightly too low compared to the two observed resonances in this sector. As already observed in the positive-parity $2\hbar\omega$ shell, the main difference between the two models again shows up in the sector with spin-(1/2): model $\mathcal{B}$, which already strongly failed in describing the low-lying Roper resonance, yields in the negative-parity $N\frac{1}{2}^-$ sector a much too large splitting of the two $1\hbar\omega$ states. The position of the four-star resonance $N\frac{1}{2}^-(1535, ****)$ is underestimated, while at the same time the calculated mass corresponding to $N\frac{1}{2}^-(1650, ****)$ appears much too high. Again, the situation is better described in model $\mathcal{A}$: although the position of the $N\frac{1}{2}^-(1535, ****)$ is still predicted 100 MeV too low, the predicted mass of the second excitation at 1660 MeV nicely agrees with the empirical resonance position of the $N\frac{1}{2}^-(1650, ****)$, even within its uncertainty range. Altogether, we thus obtain a rather well-predicted pattern of hyperfine splittings of the $1\hbar\omega$ band in model $\mathcal{A}$, which thus again is of better quality than in model $\mathcal{B}$. As already observed in the positive-parity sector, the differences between model $\mathcal{A}$ and model $\mathcal{B}$ have their origin in a different influence of the instanton-induced interaction. Again this can be traced back to a difference in relativistic effects that stem from the embedding map of the Salpeter amplitudes in combination with the two distinct confinement Dirac structures. For a more detailed discussion of this issue we again refer to subsect. 7.3.

7.2.3 Relative arrangement of the $2\hbar\omega$ and $1\hbar\omega$ bands — approximate parity doublets in the second resonance region

After discussing the individual hyperfine structures of the positive-parity $2\hbar\omega$ band and the negative-parity $1\hbar\omega$ band separately, let us now compare the relative positions of the positive and negative-parity states involved. We restrict this discussion to model $\mathcal{A}$, which so far led to consistently better results, especially in the sectors with spin $J = \frac{1}{2}$. Due to the selective lowering of a particular set of states of the $2\hbar\omega$ band relative to the other states, we can indeed reproduce the striking overlap of states of the two shells with opposite parity. The situation is displayed in fig. 11, where now in contrast to fig. 9 the states with the same total spin, but opposite parity are directly displayed side by side.

As discussed, model $\mathcal{A}$ nicely accounts for the low position of the Roper resonance. Unfortunately, due to the slightly too low predicted position of the first negative-parity $N\frac{1}{2}^-$ state, which still appears below the calculated position of the Roper resonance, the striking inversion of the ordering of positive- and negative-parity states in the spin-(1/2) sector cannot be achieved. On the other hand, figure 11 impressively demonstrates that our model $\mathcal{A}$ indeed reproduces the remarkable appearance of the lowest approximate "parity doublets" of the nucleon spectrum in the second resonance region around ~ 1700 MeV (shaded regions in fig. 11) remarkably well; see also table 13. Apart from the slightly too low calculated position of the $N\frac{3}{2}^-(1700, ***)$ even the experimentally observed splittings between the parity partners in general are fairly well described.

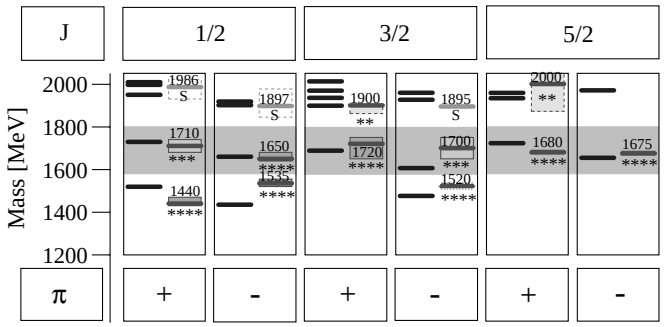

Fig. 11. Approximate parity doublets due to the overlap of the positive-parity $2\hbar\omega$ states and the negative-parity $1\hbar\omega$ states in the second resonance region around ~ 1700 MeV (shaded regions) as predicted in model $\mathcal{A}$. The left part in each column shows our calculation, which is compared with the experiment depicted in the right part. For each spin $J = \frac{1}{2}$, $\frac{3}{2}$ and $\frac{5}{2}$ the left column shows the even and the right column the odd parity. For an explicit illustration of how these doublet structures are generated by 't Hooft's instanton-induced interaction, see fig. 18 and the corresponding detailed discussion of instanton effects in subsect. 7.3.

Table 13. Approximate parity doublets in the second resonance region in model $\mathcal{A}$.

Approximate parity doublets around 1700 MeV	
"$2\hbar\omega$", $\pi = +$	"$1\hbar\omega$", $\pi = -$
$N\frac{1}{2}^+(1710, ***)$	$- N\frac{1}{2}^-(1650, ****)$
exp. : 1680–1740 MeV	1640–1680 MeV
model $\mathcal{A}$: 1729 MeV	1660 MeV
$N\frac{3}{2}^+(1720, ****)$	$- N\frac{3}{2}^-(1700, ***)$
exp. : 1650–1750 MeV	1650–1750 MeV
model $\mathcal{A}$: 1688 MeV	1606 MeV
$N\frac{5}{2}^+(1680, ****)$	$- N\frac{5}{2}^-(1675, ****)$
exp. : 1675–1690 MeV	1670–1685 MeV
model $\mathcal{A}$: 1723 MeV	1655 MeV

7.2.4 Beyond the $2\hbar\omega$ band

Finally let us have a look at the experimentally still rather poorly explored high-energy part of the nucleon spectrum, *i.e.* at the states that belong to the $3\hbar\omega$, $4\hbar\omega$, $5\hbar\omega$ and $6\hbar\omega$ bands with observed total spins up to $J = \frac{13}{2}$.

We start with the states of the $3\hbar\omega$ and $4\hbar\omega$ bands and their relative alignments. The predicted positions in both models for the lightest few states assigned to these shells are summarized and compared to the experimental mass values in table 14 and 15, respectively.

The Particle Data Group [38] lists all in all five negative-parity resonances in the energy region between roughly 2000 and 2300 MeV with $J^\pi = \frac{1}{2}^-$ to $\frac{9}{2}^-$. In the notation of the oscillator shell model these should be assigned to the $3\hbar\omega$ band: There are the well-established resonances of the four-star category, which are the lowest observed orbital excitations in the $N\frac{7}{2}^-$ and $N\frac{9}{2}^-$ sector (*i.e.* states of Regge-trajectory-type sequences), the $N\frac{7}{2}^-(2190, ****)$ and the $N\frac{9}{2}^-(2250, ****)$. Also there is in each of the lower spin sectors $J^\pi = \frac{1}{2}^-$, $\frac{3}{2}^-$ and $\frac{5}{2}^-$ some evidence for a radially excited resonance in this mass region. These are the weakly established one- and two-star resonances $N\frac{1}{2}^-(2090, *)$, $N\frac{3}{2}^-(2080, **)$ and $N\frac{5}{2}^-(2200, **)$ which have quite big uncertainties of several hundred MeVs. All these states form a shell structure with a mean mass of about 2200 MeV. Concerning the $N\frac{9}{2}^-(2250, ****)$ it is worth noting that the PDG quotes in the corresponding sector with the same total spin $J = \frac{9}{2}$ but with opposite positive parity the first excited resonance $N\frac{9}{2}^+(2220, ****)$ at almost the same mass value, *i.e.* nearly degenerate with the $N\frac{9}{2}^-(2250, ****)$. Due to its high spin $J = \frac{9}{2}$, this well-established four-star resonance in the positive-parity sector has to be a member of the $4\hbar\omega$ shell. The appearance of this approximate parity doublet $N\frac{9}{2}^+(2220, ****)$ – $N\frac{9}{2}^-(2250, ****)$ is a very striking feature in the high-energy part of the nucleon spectrum, and we should note here that (non-relativistic or "relativized") constituent quarks models which use one-gluon exchange as residual interaction [6] generally cannot account for this well-established structure.

In addition there are the new indications of resonant structures recently observed in the S_{11} and D_{13} partial waves of the photoproduction measurements of $\gamma p \to p\eta'$ and $\gamma p \to K^+\Lambda$ with the SAPHIR detector at ELSA in Bonn: the $S_{11}(1897)$ and $D_{13}(1895)$, which are labeled by the symbol "S" in figs. 9 and 10. Both states should belong to the $3\hbar\omega$ band, but their positions at about 1900 MeV are comparatively low, namely more than 200 MeV below the other observed states in the $3\hbar\omega$ shell quoted by the PDG. These new resonances are nearly degenerate with the upper part of the positive-parity $2\hbar\omega$ shell.

Before comparing these experimentally found structures with our predicted spectrum in this energy region in detail, it is instructive to discuss first the predicted intra-band structures of the $3\hbar\omega$ shell and the corresponding implications of the instanton force in general. As can be seen in figs. 9 and 10, in both models the bulk of states appears in a region between ~ 2100 and ~ 2300 MeV, which fairly well agrees with the range of possible mass values of the resonances presently stated by the PDG. The predicted spectrum of states in this shell is even richer than that of $2\hbar\omega$ band discussed before. Furthermore, in both models we again observe a particular set of states, which is selectively lowered relative to the rest of the states in the ~ 2200 MeV region. Consequently, also the $3\hbar\omega$ band splits into two well-separated parts, in a similar manner as observed in the $2\hbar\omega$ band: again, this lowering is due to the attractive action of the instanton-induced interaction in these states as will become more apparent by the more detailed investigation of these instanton-induced effects in the next subsection (see figs. 16 and 21 for an illustration of these effects in model $\mathcal{A}$ and model $\mathcal{B}$, respectively). The lowering of these particular $3\hbar\omega$ states occurs for the total spins $J^\pi = \frac{1}{2}^-$, $\frac{3}{2}^-$, $\frac{5}{2}^-$ and $\frac{7}{2}^-$ and is absent for the single state of this band predicted in the sector with spin

Table 14. Calculated positions for the lightest few negative-parity nucleon states in the $3\hbar\omega$ shell in comparison to the corresponding experimental mass values taken from [38]. Notation as in table 3. The resonances denoted by "SAPHIR" (in the column "Rating") corresponds to the new photoproduction results from the SAPHIR collaboration, see text.

Experimental state [38]	PW	J^π	Rating	Mass range [MeV] [38]	Model state in model $\mathcal{A}$	Model state in model $\mathcal{B}$
$S_{11}(1897)$	S_{11}	$\frac{1}{2}^-$	SAPHIR	1845–1977	$[N\frac{1}{2}^-]_3(1901)$ $[N\frac{1}{2}^-]_4(1918)$	$[N\frac{1}{2}^-]_3(1971)$
$N(2090)$	S_{11}	$\frac{1}{2}^-$	*	1860–2260	$[N\frac{1}{2}^-]_5(2153)$ $[N\frac{1}{2}^-]_6(2185)$ $[N\frac{1}{2}^-]_7(2194)$ $[N\frac{1}{2}^-]_8(2232)$ $[N\frac{1}{2}^-]_9(2242)$	$[N\frac{1}{2}^-]_4(2082)$ $[N\frac{1}{2}^-]_5(2180)$ $[N\frac{1}{2}^-]_6(2203)$ $[N\frac{1}{2}^-]_7(2261)$ $[N\frac{1}{2}^-]_8(2270)$ $[N\frac{1}{2}^-]_9(2345)$
$D_{13}(1895)$	D_{13}	$\frac{3}{2}^-$	SAPHIR	≈ 1895	$[N\frac{3}{2}^-]_3(1926)$ $[N\frac{3}{2}^-]_4(1959)$	$[N\frac{3}{2}^-]_3(1949)$
$N(2080)$	D_{13}	$\frac{3}{2}^-$	**	1750–2140	$[N\frac{3}{2}^-]_5(2079)$ $[N\frac{3}{2}^-]_6(2143)$ $[N\frac{3}{2}^-]_7(2177)$ $[N\frac{3}{2}^-]_8(2203)$ $[N\frac{3}{2}^-]_9(2213)$ $[N\frac{3}{2}^-]_{10}(2247)$	$[N\frac{3}{2}^-]_4(2095)$ $[N\frac{3}{2}^-]_5(2172)$ $[N\frac{3}{2}^-]_6(2179)$ $[N\frac{3}{2}^-]_7(2200)$ $[N\frac{3}{2}^-]_8(2216)$ $[N\frac{3}{2}^-]_9(2249)$ $[N\frac{3}{2}^-]_{10}(2256)$
$N(2200)$	D_{15}	$\frac{5}{2}^-$	**	1900–2260	$[N\frac{5}{2}^-]_2(1970)$ $[N\frac{5}{2}^-]_3(2104)$ $[N\frac{5}{2}^-]_4(2147)$ $[N\frac{5}{2}^-]_5(2217)$ $[N\frac{5}{2}^-]_6(2225)$ $[N\frac{5}{2}^-]_7(2233)$ $[N\frac{5}{2}^-]_8(2272)$ $[N\frac{5}{2}^-]_9(2303)$	$[N\frac{5}{2}^-]_2(2026)$ $[N\frac{5}{2}^-]_3(2173)$ $[N\frac{5}{2}^-]_4(2189)$ $[N\frac{5}{2}^-]_5(2213)$ $[N\frac{5}{2}^-]_6(2233)$ $[N\frac{5}{2}^-]_7(2241)$ $[N\frac{5}{2}^-]_8(2254)$ $[N\frac{5}{2}^-]_9(2331)$
$N(2190)$	G_{17}	$\frac{7}{2}^-$	****	2100–2200	$[N\frac{7}{2}^-]_1(2015)$ $[N\frac{7}{2}^-]_2(2171)$ $[N\frac{7}{2}^-]_3(2229)$ $[N\frac{7}{2}^-]_4(2247)$ $[N\frac{7}{2}^-]_5(2279)$	$[N\frac{7}{2}^-]_1(2024)$ $[N\frac{7}{2}^-]_2(2177)$ $[N\frac{7}{2}^-]_3(2203)$ $[N\frac{7}{2}^-]_4(2223)$ $[N\frac{7}{2}^-]_5(2237)$
$N(2250)$	G_{19}	$\frac{9}{2}^-$	****	2170–2310	$[N\frac{9}{2}^-]_1(2212)$	$[N\frac{9}{2}^-]_1(2170)$

$J = \frac{9}{2}^-$. It is worth mentioning here that the Salpeter amplitudes of all these states in fact commonly exhibit a strong mixture of dominant $^2 8[56]$ and $^2 8[70]$ configurations. The shift due to 't Hooft's force hence leads to a structure, which then lies in a region between roughly 1900 and 2000 MeV in model $\mathcal{A}$ and around 2000 MeV in model $\mathcal{B}$. This substructure lies fairly well in between the other members of the $3\hbar\omega$ shell and the upper part of the $1\hbar\omega$ shell and hence it overlaps with the upper part of the positive-parity $2\hbar\omega$ band. The arrangement of the $3\hbar\omega$ and $2\hbar\omega$ bands is quite similar to that of the $2\hbar\omega$ and $1\hbar\omega$ shells, leading there to the appearance of approximate parity doublets discussed above. In fact, similar predicted alignments even appear between the higher alternating even- and odd-parity bands, *e.g.* between the lowest states of the $4\hbar\omega$ band and the upper part of the $3\hbar\omega$ band.

Now let us discuss in detail to what extent these predicted intra-band structures along with the corresponding positioning of the alternating even- and odd-parity bands (*i.e.* $4\hbar\omega \leftrightarrow 3\hbar\omega$ and $2\hbar\omega \leftrightarrow 3\hbar\omega$) are indeed realized in the empirical nucleon mass spectrum. In the

Table 15. Calculated positions for the lightest few positive-parity nucleon states in the $4\hbar\omega$ shell in comparison to the corresponding experimental mass values taken from [38]. Notation as in table 3.

Experimental state [38]	PW	J^π	Rating	Mass range [MeV] [38]	Model state in model $\mathcal{A}$	Model state in model $\mathcal{B}$
					$[N\frac{1}{2}^+]_6(2009)$	
$N(2100)$	P_{11}	$\frac{1}{2}^+$	*	1850–2200	$[N\frac{1}{2}^+]_7(2174)$	$[N\frac{1}{2}^+]_6(2177)$
					$[N\frac{1}{2}^+]_8(2199)$	
					$[N\frac{1}{2}^+]_9(2361)$	$[N\frac{1}{2}^+]_7(2300)$
						$[N\frac{1}{2}^+]_8(2325)$
						$[N\frac{1}{2}^+]_9(2408)$
	P_{13}	$\frac{3}{2}^+$			$[N\frac{3}{2}^+]_6(2117)$	$[N\frac{3}{2}^+]_6(2228)$
					$[N\frac{3}{2}^+]_7(2269)$	$[N\frac{3}{2}^+]_7(2345)$
					$[N\frac{3}{2}^+]_8(2312)$	$[N\frac{3}{2}^+]_8(2381)$
	F_{15}	$\frac{5}{2}^+$			$[N\frac{5}{2}^+]_4(2120)$	$[N\frac{5}{2}^+]_4(2208)$
					$[N\frac{5}{2}^+]_5(2296)$	$[N\frac{5}{2}^+]_5(2326)$
					$[N\frac{5}{2}^+]_6(2344)$	$[N\frac{5}{2}^+]_6(2389)$
	F_{17}	$\frac{7}{2}^+$			$[N\frac{7}{2}^+]_2(2190)$	$[N\frac{7}{2}^+]_2(2250)$
					$[N\frac{7}{2}^+]_3(2365)$	$[N\frac{7}{2}^+]_3(2381)$
					$[N\frac{7}{2}^+]_4(2399)$	$[N\frac{7}{2}^+]_4(2404)$
$N(2220)$	H_{19}	$\frac{9}{2}^+$	****	2180–2310	$[N\frac{9}{2}^+]_1(2221)$	$[N\frac{9}{2}^+]_1(2221)$
					$[N\frac{9}{2}^+]_2(2415)$	$[N\frac{9}{2}^+]_2(2406)$
					$[N\frac{9}{2}^+]_3(2432)$	$[N\frac{9}{2}^+]_3(2411)$
	$H_{1\,11}$	$\frac{11}{2}^+$			$[N\frac{11}{2}^+]_1(2455)$	$[N\frac{11}{2}^+]_1(2402)$
					$[N\frac{11}{2}^+]_2(2515)$	$[N\frac{11}{2}^+]_2(2446)$

$N\frac{9}{2}^-$ sector both models predict only a single state belonging to the upper part of the $3\hbar\omega$ shell, which is the lowest excitation in this sector. The calculated masses at 2212 MeV and 2170 MeV in model $\mathcal{A}$ and model $\mathcal{B}$, respectively, match the single observed four-star resonance $N\frac{9}{2}^-(2250, ****)$ in the G_{19} partial wave quite well. Similar to the lowest predicted states in the $N\frac{7}{2}^+$ and $N\frac{5}{2}^-$ sector, also this state shows an almost pure $^4 8[70]$ configuration and thus remains totally unaffected by the instanton-induced interaction. In the corresponding $N\frac{9}{2}^+$ sector with the same spin but with opposite positive parity both models indeed can even account for the low position of the $N\frac{9}{2}^+(2220)$. Both predict for this state the same mass value of 2221 MeV. Consequently, our two alternative models can reproduce the striking parity-doublet structure $N\frac{9}{2}^+(2220, ****)$–$N\frac{9}{2}^-(2250, ****)$ in excellent agreement with the well-established experimental findings; see also fig. 12. In this respect we should mention that in contrast to the negative-parity $3\hbar\omega$ state this positive-parity $4\hbar\omega$ state is strongly influenced by 't Hooft's force, since in both models its spin-flavor part is dominantly a $^2 8[56]$ configuration with an additional strong admixture of $^2 8[70]$. Consequently, this state is significantly lowered (together with a group of other states belonging to the $4\hbar\omega$ band). It is remarkable that the 't Hooft coupling g_{nn} (as fixed by the $\Delta - N$ splitting) is just the right size to produce this (almost degenerate) parity doublet.

In the $N\frac{7}{2}^-$ sector both model variants predict the first excitation roughly 170 MeV too light compared to the four-star resonance $N\frac{7}{2}^-(2190, ****)$: model $\mathcal{A}$ predicts this state at 2015 MeV and model $\mathcal{B}$ at 2024 MeV. In both models this state is strongly lowered by 't Hooft's force, since in both model variants the states contain a dominant $^2 8[70]$ configuration ($\sim 65\%$) with an additional quite strong admixture of a $^2 8[56]$ contribution ($\sim 32\%$). The second excited state in this sector, however, is hardly influenced by 't Hooft's force, since it is dominantly $^4 8[70]$ in both models. Thus, it appears in the upper part of the $3\hbar\omega$ band and matches the $N\frac{7}{2}^-(2190, ****)$ quite well: model $\mathcal{A}$ predicts the position at 2171 MeV and model $\mathcal{B}$ at 2177 MeV in nice agreement with the empirical mass value. It is quite interesting to speculate whether the too low predicted position of the first excitation is really a shortcoming of our model or if indeed the first excited resonance in $N\frac{7}{2}^-$ should appear below $N\frac{7}{2}^-(2190, ****)$ at about 2015 MeV. Let us discuss this alternative interpretation on the basis of our spectroscopic results in the $3\hbar\omega$ shell in general. We should mention that a collective model of baryon masses developed by Bijker, Iachello and Leviatan [60,61] shows a similar result in the $N\frac{7}{2}^-$ sector. But in this model the nucleon states of the $3\hbar\omega$ band seem in general to be predicted too light. In our models, however, this is not the case, since a comparatively low position is observed only for a group of altogether six

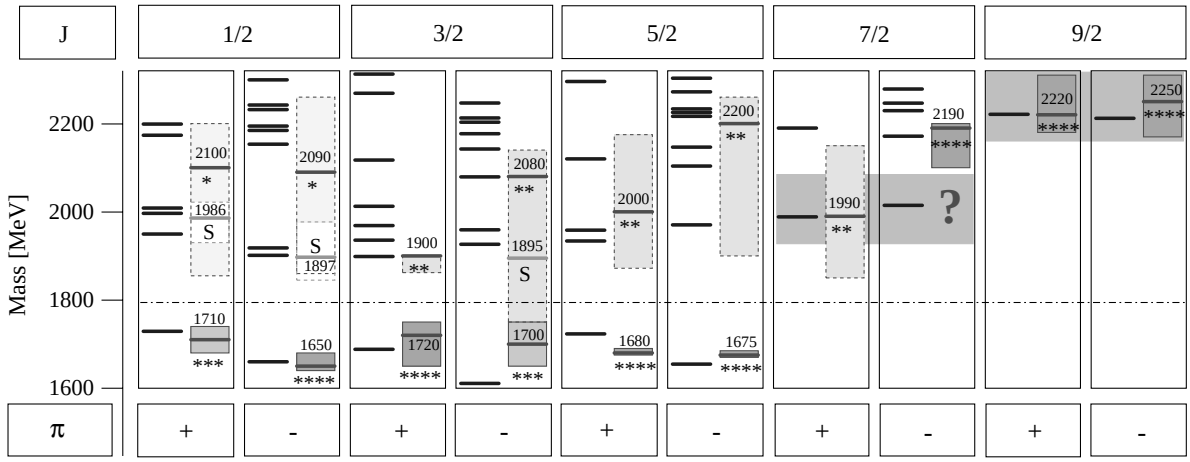

Fig. 12. Approximate parity doublets due to the overlap of the negative-parity $3\hbar\omega$ shell with the positive-parity $2\hbar\omega$ shell and $4\hbar\omega$ shell, respectively, as predicted in model $\mathcal{A}$. For an explicit illustration of how these doublet structures are generated due to 't Hooft's instanton-induced interaction see figs. 18 and 19 and the corresponding detailed discussion of instanton effects in subsect. 7.3.

Table 16. Calculated positions for the lightest few negative-parity nucleon states in the $5\hbar\omega$ shell with $J \geq \frac{9}{2}$ in comparison to the corresponding experimental mass values taken from [38]. Notation as in table 3.

Experimental state [38]	PW	J^π	Rating	Mass range [MeV] [38]	Model state in model $\mathcal{A}$	Model state in model $\mathcal{B}$
	G_{19}	$\frac{9}{2}^-$			$[N\frac{9}{2}^-]_2(2402)$	$[N\frac{9}{2}^-]_2(2451)$
					$[N\frac{9}{2}^-]_3(2542)$	$[N\frac{9}{2}^-]_3(2586)$
					$[N\frac{9}{2}^-]_4(2579)$	$[N\frac{9}{2}^-]_4(2602)$
					$[N\frac{11}{2}^-]_1(2425)$	$[N\frac{11}{2}^-]_1(2441)$
$N(2600)$	$I_{1\,11}$	$\frac{11}{2}^-$	***	2550–2750	$[N\frac{11}{2}^-]_2(2600)$	$[N\frac{11}{2}^-]_2(2593)$
					$[N\frac{11}{2}^-]_3(2634)$	$[N\frac{11}{2}^-]_3(2606)$
					$[N\frac{11}{2}^-]_4(2650)$	$[N\frac{11}{2}^-]_4(2629)$
	$I_{1\,13}$	$\frac{13}{2}^-$			$[N\frac{13}{2}^-]_1(2621)$	$[N\frac{13}{2}^-]_1(2587)$
					$[N\frac{13}{2}^-]_2(2712)$	$[N\frac{13}{2}^-]_2(2655)$

Table 17. Calculated positions for the lightest few positive-parity nucleon states in the $6\hbar\omega$ shell with $J \geq \frac{11}{2}$ in comparison to the corresponding experimental mass values taken from [38]. Notation as in table 3.

Experimental state [38]	PW	J^π	Rating	Mass range [MeV] [38]	Model state in model $\mathcal{A}$	Model state in model $\mathcal{B}$
	$H_{1\,11}$	$\frac{11}{2}^+$			$[N\frac{11}{2}^+]_3(2598)$	$[N\frac{11}{2}^+]_3(2640)$
					$[N\frac{11}{2}^+]_4(2749)$	$[N\frac{11}{2}^+]_4(2757)$
					$[N\frac{11}{2}^+]_5(2785)$	$[N\frac{11}{2}^+]_5(2781)$
$N(2700)$	$K_{1\,13}$	$\frac{13}{2}^+$	**	2567–3100	$[N\frac{13}{2}^+]_1(2616)$	$[N\frac{13}{2}^+]_1(2619)$
					$[N\frac{13}{2}^+]_2(2800)$	$[N\frac{13}{2}^+]_2(2777)$
					$[N\frac{13}{2}^+]_3(2811)$	$[N\frac{13}{2}^+]_3(2782)$

states of the $3\hbar\omega$ shell with spins J^π from $\frac{1}{2}^-$ to $\frac{7}{2}^-$. This group is lowered with respect to the other states of this shell due to the selective action of 't Hooft's force. The lowest excitation predicted in $N\frac{7}{2}^-$ is just the state with the highest spin $J = \frac{7}{2}$ in this group . Hence, concerning the rather low predicted position of the first excited $N\frac{7}{2}^-$ state, the question is how realistic this well-separated part of the $3\hbar\omega$ shell in fact is. In this respect, the analysis of the new SAPHIR data on η' and kaon photoproduction, which shows evidence for resonances in the S_{11} and D_{13} partial waves, respectively, is very fortunate. Indeed, the determined resonance positions strongly support this structure. Let us restrict this discussion to the more realistic model $\mathcal{A}$: the resonance position extracted from the S_{11} partial wave of $\gamma p \to p\eta'$ at 1897 MeV (with the error

range of 1845 MeV to 1977 MeV) excellently agrees with the two predicted $N\frac{1}{2}^-$ states of model $\mathcal{A}$ in this region at 1901 and 1918 MeV. Also the determined resonance position extracted from the D_{13} partial wave of $\gamma p \to K^+\Lambda$ at almost the same mass value of 1895 MeV (unfortunately there is no error assigned to this value) fairly agrees with the prediction of the two close lying $N\frac{3}{2}^-$ states in model $\mathcal{A}$ at 1926 and 1959 MeV. In the $N\frac{5}{2}^-$ our model $\mathcal{A}$ predicts a single low-lying state belonging to the same structure at 1970 MeV which still is "missing" and finally in the $N\frac{7}{2}^-$ sector we correspondingly have the low predicted state in question at 2015 MeV which indeed should appear far below the $N\frac{7}{2}^-(2190,****)$, if we take this instanton-induced structure seriously. An experimentally proven existence of such comparatively low-lying states in the $N\frac{5}{2}^-$ and $N\frac{7}{2}^-$ sector might become a sensitive test for our model $\mathcal{A}$ and especially for the residual 't Hooft interaction used in this model. In this respect, we should note here that the prediction of such well separated states in $N\frac{5}{2}^-$ and $N\frac{7}{2}^-$ seems to depend strongly on the residual quark-quark interaction employed: other quark models which use a different residual force (as for instance one-gluon exchange [6]) do not predict such states. Moreover, we should anticipate already here that the corresponding lowest Λ state in the $\Lambda\frac{7}{2}^-$ sector (see our subsequent paper [26]) is strongly lowered by the same instanton-induced effect and thus nicely explains the comparatively low position of the $\Lambda\frac{7}{2}^-(2100,****)$. Figure 12 shows the relative arrangements of parts of the negative-parity $3\hbar\omega$ band and parts of the positive-parity $2\hbar\omega$ and $4\hbar\omega$ bands in model $\mathcal{A}$. In contrast to fig. 9, the sectors with the same total spin J and opposite parity are now directly displayed side by side. In addition, also the mass region around 1700 MeV with the previously discussed approximate parity doublets of the $2\hbar\omega$ and $1\hbar\omega$ bands is shown for comparison. The figure nicely illustrates the relatively strong overlap of the predicted structures of the negative-parity $3\hbar\omega$ and the positive-parity $2\hbar\omega$ shell. Experimental evidence supporting this comes from the comparatively low positions of the newly discovered "SAPHIR resonances". The predicted overlap of the $3\hbar\omega$ and $4\hbar\omega$ shell nicely reproduces the observed parity doublet pattern in the $N\frac{9}{2}^\pm$ sectors. Referring back to our discussion of a possibly low-lying state in the $N\frac{7}{2}^-$ sector, it is very interesting that the lowest state calculated in this sector at 2015 MeV (in model $\mathcal{A}$) together with the experimentally observed lowest positive-parity excitation $N\frac{7}{2}^+(1990,**)$ ($\hat{=}$ 1988 MeV in model $\mathcal{A}$) fits much better into the scheme of approximate parity doublets than the lowest state observed, up to now the $N\frac{7}{2}^-(2190,****)$, does.

Finally, let us compare our results with the highest mass states of the experimental nucleon spectrum, *i.e.* the lowest excitations in the sectors $N\frac{11}{2}^-$ and $N\frac{13}{2}^+$ reported by the Particle Data Group [38]. These are the three- and two-star resonances $N\frac{11}{2}^-(2600,***)$ and $N\frac{13}{2}^+(2700,**)$, which in the notation of the oscillator model should belong to the negative-parity $5\hbar\omega$ and the positive-parity $6\hbar\omega$ shell, respectively. The positions predicted for the lightest few $5\hbar\omega$ and $6\hbar\omega$ states in both models are given in tables 16 and 17, respectively.

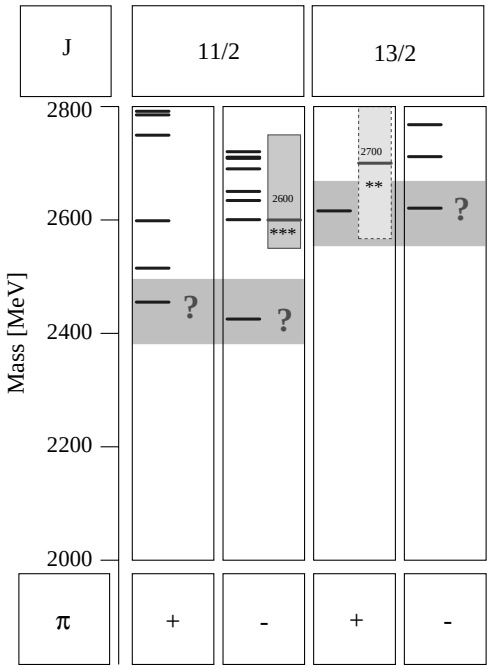

Fig. 13. Approximate parity doublets in $N\frac{11}{2}^\pm$ and $N\frac{13}{2}^\pm$ (in model $\mathcal{A}$).

In the $N\frac{11}{2}^-$ sector the situation is very similar to that found in the $N\frac{7}{2}^-$ sector. Again the lowest excitation is strongly influenced by 't Hooft's force and thus is strongly lowered relative to other states in this sector. Consequently, the first excited state is predicted roughly 160-175 MeV too low compared to the position of the resonance $N\frac{11}{2}^-(2600,***)$: model $\mathcal{A}$ predicts the first excitation at 2425 MeV and model $\mathcal{B}$ at 2441 MeV. The higher excitations, however, again fit nicely within the range of possible values of the $N\frac{11}{2}^-(2600,***)$ (see also table 16). Again, we can just speculate if this is a shortcoming of our models or if there is really a state below the $N\frac{11}{2}^-(2600,***)$. But once again it is quite interesting to note that the predicted first excitation in this sector forms an approximate parity doublet structure together with the first excitation predicted in the $N\frac{11}{2}^+$ sector which belongs to the positive-parity $4\hbar\omega$ band. Unfortunately, no resonance has been seen experimentally in $N\frac{11}{2}^+$ hitherto. Model $\mathcal{A}$ predicts the first excitation in $N\frac{11}{2}^+$ at 2455 MeV and model $\mathcal{B}$ at 2402 MeV (see also table 15). A graphical illustration of this approximate spin-11/2 parity doublet in model $\mathcal{A}$ is given in the left part of fig. 13.

The lowest excitation $N\frac{13}{2}^+(2700,**)$ observed in the $N\frac{13}{2}^+$ sector is the highest spin of a resonance in the nucleon sector measured at all. This resonance is the highest lying member of the positive-parity N Regge trajectory

Table 18. Position of states belonging to the positive-parity N Regge trajectory calculated in the models $\mathcal{A}$ and $\mathcal{B}$ in comparison to the experimental resonance positions [38]. For a graphical presentation see fig. 14.

Regge state	Rating	J^π	Experimental Mass [MeV] [38]	Mass [MeV] Model $\mathcal{A}$	Mass [MeV] Model $\mathcal{B}$
$N(939)$	****	$\frac{1}{2}^+$	939	939	939
$N(1680)$	****	$\frac{5}{2}^+$	1675–1690	1723	1718
$N(2220)$	****	$\frac{9}{2}^+$	2180–2310	2221	2221
$N(2700)$	**	$\frac{13}{2}^+$	2567–3100	2616	2619

(see discussion below). Due to a lowering by 't Hooft's force, both models predict the first excited state in the $N\frac{13}{2}^+$ sector well isolated, *i.e.* roughly 160-180 MeV below the other excited states. The predicted masses are close to the measured position and lie within the range of possible values for this two-star resonance: model $\mathcal{A}$ yields 2616 MeV and model $\mathcal{B}$ 2619 MeV (see also table 17). Again we find this lowest excited model state in $N\frac{13}{2}^+$ belonging to a parity doublet structure together with the corresponding lowest excitation in the sector $N\frac{13}{2}^-$ with the same spin but negative parity. This negative-parity state belongs to the $5\hbar\omega$ shell, and model $\mathcal{A}$ and model $\mathcal{B}$ predict the position at 2621 MeV and 2587 MeV, respectively (see also table 16). The right part of fig. 13 depicts this parity doublet structure in model $\mathcal{A}$. Unfortunately, the first excitation of $N\frac{13}{2}^-$ has not been discovered yet.

To summarize our investigations concerning the relative alignment of the alternating even- and odd-parity bands in the excited-nucleon spectrum, let us finally stress the most striking feature of our model that could be exposed in the course of this discussion and becomes immediately evident from figs. 12 and 13. It is the systematical occurrence of approximately degenerate states with the same spin and opposite parity. On the one hand our models nicely reproduce the approximate doublet structures which in fact are observed experimentally. On the other hand, these doublets also appear, where the present experimental situation either seems to deviate from such a parity doublet structure, or members of these doublets are "missing". In fact, we predict for really all the lowest excitations with spins from $J = \frac{5}{2}$ to $J = \frac{13}{2}$ such a pattern of approximate parity doublets. As already partly indicated in the previous discussion, this systematics originates from 't Hooft's force: the two members of the doublet belong to two adjacent shells with opposite parity and 't Hooft's force lowers one of these strongly, whereas the other one remains totally unaffected. In this way, both states become approximately degenerate in energy. For a more detailed discussion of this scenario in the context of a detailed investigation of instanton-induced effects, we refer to subsect. 7.3.

7.2.5 The positive-parity N Regge trajectory

Finally, let us conclude the discussion of the nucleon spectrum with the states $N\frac{1}{2}^+(939, ****)$, $N\frac{5}{2}^+(1680, ****)$, $N\frac{9}{2}^+(2220, ****)$ and $N\frac{13}{2}^+(2700, **)$ of the positive-parity N Regge trajectory, which belong to a sequence of three-quark states with increasing separations of the quarks. Figures 9 and 10 show that all states of the trajectory are fairly well described in both confinement models $\mathcal{A}$ and $\mathcal{B}$; see also table 18, in which the calculated positions of Regge states are explicitly summarized and compared to the experimental mass values. This result shows that the string-like, flavor-independent confinement force of both models (with parameters fixed to account for the positive-parity Δ trajectory up to highest orbital excitations) works equally well also for nucleon excitations with increasing quark separations. But here one should note the substantial difference to the states of the Δ Regge trajectory: in contrast to the Δ trajectory, all states of the N trajectory are quite strongly lowered due to the action of the instanton-induced force. The nucleon ground state $N(939)$ shows the largest downward mass shift and with increasing mass of the Regge states the mass shift decreases. In this respect it is very interesting to investigate to what extent 't Hooft's force actually influences the Regge behavior $M^2 \sim J$.

Figure 14 shows the Chew-Frautschi plot (M^2 *vs.* J) of the positive-parity N Regge trajectory obtained in model $\mathcal{A}$ and $\mathcal{B}$, respectively. To illustrate the influence of 't Hooft's instanton-induced interaction, we additionally displayed the trajectory as given by the confinement forces of models $\mathcal{A}$ and $\mathcal{B}$ alone. Thus, neglecting 't Hooft's force, both confinement variants yield the characteristic Regge behavior $M^2 \propto J$, as one would expect from the results for the Δ Regge trajectory discussed before. In particular, the slope is approximately the same as in the Δ sector. It is quite astonishing that the effect of the instanton force on the states of the trajectory indeed is such that it maintains the linear Regge characteristic $M^2 \propto J$ with almost the same slope, in nice agreement with phenomenology. Hence, adjusting the effective 't Hooft coupling g_{nn} to describe just the ground state (*i.e.* the $\Delta - N$ splitting) correctly, the whole model trajectory shows an equally large downward shift in the square of the baryon masses M^2 thus leading to an excellent quantitative agreement with the empirical linear N Regge trajectory. This non-trivial compatibility of the instanton-induced effects with the observed linear Regge characteristic in the nucleon spectrum is a quite remarkable and an interesting feature of 't Hooft's force. Moreover, figure 14 convincingly demonstrates once more that even in the highest mass regions of the nucleon spectrum, instanton-induced

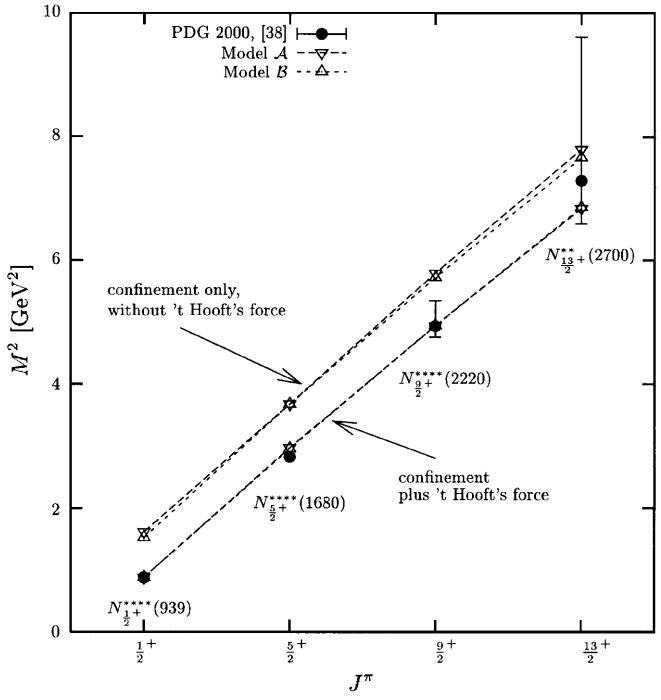

Fig. 14. Chew-Frautschi plot (M^2 *vs.* J) of the positive-parity N Regge trajectory $N\frac{1}{2}^+$, $N\frac{5}{2}^+$, $N\frac{9}{2}^+$, $N\frac{13}{2}^+$, ..., in the models $\mathcal{A}$ and $\mathcal{B}$ (lower curves) compared to experimental masses from the Particle Data Group (see [38]). The upper curves show the trajectories without influence of 't Hooft's instanton-induced interaction. Note the remarkable fact that both models exhibit the correct linear Regge characteristic $M^2 \sim J$ with almost the same slope in both cases, *i.e.* without and even with the contribution of the instanton force. Hence, adjusting the 't Hooft coupling g_{nn} to describe just the ground state correctly in both models, the whole model trajectory fits the empirical Regge behavior in excellent quantitative agreement. See table 18 for explicit values.

effects are crucial for the correct description of resonance positions.

7.3 A study of instanton effects in the excited-nucleon spectrum

So far we presented a detailed discussion of the predicted nucleon spectrum in both confinement models $\mathcal{A}$ and $\mathcal{B}$ with the strength of the instanton-induced interaction fixed to match the observed position of the nucleon ground state $N(939)$. We investigated the calculated structures of the single positive- and negative-parity shells and compared these to the hitherto observed experimental patterns. In fact, we found a remarkably good agreement between the predictions of our model version $\mathcal{A}$ and the empirical nucleon mass spectrum in the lower resonance regions as well as for the higher and highest mass regions including orbital excitations up to $J = \frac{13}{2}$ (Regge trajectory). In particular, all the striking hyperfine splittings within the intra-band structures and accordingly the arrangements between the alternating even- and odd-parity shells could be nicely reproduced in at least qualitative but mostly even in completely quantitative agreement with the experimental findings. In particular, we clearly reproduced in model $\mathcal{A}$

- the important downshift of the Roper resonance and three other low-lying states of the $2\hbar\omega$ shell around 1700 MeV,
- the hyperfine structure of the five states in the $1\hbar\omega$ band,
- the fine structure of the $3\hbar\omega$ band as far as it is indicated by the new SAPHIR photoproduction results,
- the approximate parity doublets due to partial overlapping of shells: $1\hbar\omega \leftrightarrow 2\hbar\omega$, $2\hbar\omega \leftrightarrow 3\hbar\omega$, $3\hbar\omega \leftrightarrow 4\hbar\omega$, $4\hbar\omega \leftrightarrow 5\hbar\omega$ and $5\hbar\omega \leftrightarrow 6\hbar\omega$.

In the discussion of the foregoing subsection we already mentioned that in our fully covariant model $\mathcal{A}$ all these striking features of the excited-nucleon spectrum arise due to 't Hooft's instanton-induced quark-quark interaction. To supplement this discussion, we shall now illustrate in some more detail that the effects of this residual interaction are in fact responsible for generating all these structures simultaneously. In this respect it is instructive to study how the 't Hooft interaction affects the energy levels when, starting from the case with confinement only, it is switched on and its strength is gradually increased. It is our aim to demonstrate in this way that prominent features of the spectrum like the $\Delta - N$ ground-state splitting and the conspicuous low position of the Roper resonance can be put along with all the other observed phenomena into a somewhat wider perspective, *i.e.* that instanton-induced effects indeed dominate the fine structure of the *whole* nucleon spectrum.

Another issue that has to be clarified in this context is the difference between the predictions of model $\mathcal{A}$ and model $\mathcal{B}$. Although model $\mathcal{B}$ could also account for most of the features discussed, it strongly failed concerning the low position of the Roper resonance in the $N\frac{1}{2}^+$ sector and moreover predicted a much too large splitting of the two lowest S_{11} resonances in the corresponding $N\frac{1}{2}^-$ sector with negative parity. As already mentioned, this indicates that the action of 't Hooft's force might strongly depend on the Dirac structures chosen for the three-body confinement kernel and on the corresponding relativistic effects induced in combination with the embedding map of the Salpeter amplitudes. Also this aspect shall be analyzed here in some more detail.

To study the effects of 't Hooft's force in model $\mathcal{A}$, we display the dependence of the nucleon masses on the effective 't Hooft coupling g_{nn} in figs. 15 and 16 for the positive and negative-parity sector, respectively. The corresponding results of model $\mathcal{B}$ are shown in fig. 21. In each sector with spin J and parity π the leftmost spectrum in each column shows the spectrum obtained with the three-body confinement kernel alone. The curves show the change of the spectrum as a function of the 't Hooft coupling g_{nn}: Starting from the case with confinement only the coupling is gradually increased and finally is fixed to reproduce the

$\Delta - N$ splitting (right spectrum in each column). The rightmost spectrum shows for comparison the experimental resonance positions as before.

7.3.1 Pure confinement spectra

Let us first consider the spectra in figs. 15, 16 and 21 as they are determined by the two different three-body confinement kernels alone, *i.e.* in the case $g_{nn} = 0$ (leftmost spectrum in each column): Without 't Hooft's force the linear confining interaction arranges the nucleon spectrum into a sequence of alternating even- and odd-parity shells. As one expects, the situation is quite similar to the spectrum of Δ-resonances. The states of these rather narrow bands are clustered around a common mean value, which, however, fairly agrees only with the upper parts of the rather widespread band structures observed experimentally.

In fact, some of these experimentally observed resonances even are already well described by single model states in both confinement versions. This, for instance, is the case for the three resonances $N\frac{5}{2}^-(1675, ****)$, $N\frac{7}{2}^+(1990, **)$ and $N\frac{9}{2}^-(2250, ****)$. These are single states with maximum total spin J in the $1\hbar\omega$, $2\hbar\omega$ and $3\hbar\omega$ shell, respectively. In general, in the naive oscillator shell model, the involved relative orbital angular momenta in the $N\hbar\omega$ shell can be maximally combined to a total orbital angular momentum $L_{\max} = N$. To achieve the maximal total spin $J_{\max}(N)$ in this shell, $L_{\max} = N$ has to be coupled with the symmetric $S = \frac{3}{2}$ internal spin-quartet function to get $J_{\max}(N) = N + \frac{3}{2}$. Thus, we find for the different $N\hbar\omega$ multiplets of the oscillator shell model the maximum total spins as displayed in table 19, where the corresponding states have internal spin $S = \frac{3}{2}$ and are just the lowest excited states in the sectors $J^\pi_{\max}(N)$.

Analyzing the spin-flavor $SU(6)$ configurations of the lowest excited states with spin and parity $J^\pi = \frac{5}{2}^-$, $\frac{7}{2}^+$, $\frac{9}{2}^-$, $\frac{11}{2}^+$ and $\frac{13}{2}^-$ in our models $\mathcal{A}$ and $\mathcal{B}$, we find that they indeed have in common to be almost pure $^4 8[70]$ configurations ($> 99\%$), see table 20. Consequently, due to the selection rules of 't Hooft's force, these states are expected to be hardly influenced by the residual interaction and thus indeed should be almost determined by the confining force alone. In fact, switching on 't Hooft's force, these states, *i.e.* their masses (as shown in figs. 15, 16 and 21) as well as their Salpeter amplitudes (table 20) are by no means affected with increasing strength $g_{nn} > 0$, in nice accordance with the observed resonances $N\frac{5}{2}^-(1675, ****)$, $N\frac{7}{2}^+(1990, **)$ and $N\frac{9}{2}^-(2250, ****)$ in these sectors. On the one hand, this result indicates that the confinement force, whose parameters have been fixed on the phenomenology of the Δ spectrum, works equally well also in the nucleon spectrum concerning the arrangement and positions of the shells. On the other hand, it shows that the strong selection rules of 't Hooft's interaction are really consistent with the phenomenology of these three particular nucleon resonances.

Table 19. Maximum total spins of states arising in the different oscillator shells.

Shell $N\hbar\omega$	$1\hbar\omega$	$2\hbar\omega$	$3\hbar\omega$	$4\hbar\omega$	$5\hbar\omega$	$6\hbar\omega$
$J^\pi_{\max}(N) = N + \frac{3}{2}$	$\frac{5}{2}^-$	$\frac{7}{2}^+$	$\frac{9}{2}^-$	$\frac{11}{2}^+$	$\frac{13}{2}^-$	$\frac{15}{2}^+$

Concerning the structures of the shells in the pure confinement spectrum, it should be noted that model $\mathcal{A}$ exhibits somewhat larger intra-band splittings than model $\mathcal{B}$, due to slightly bigger relativistic spin-orbit effects in model $\mathcal{A}$ (here compare to the discussion of the Δ spectrum). However, unlike the Δ spectrum, the multiplet structure of alternating positive and negative-parity bands is obviously strongly broken in the phenomenological nucleon spectrum, and the intra-band structures generated by the two different confinement kernels by no means can account for the quite large observed hyperfine splittings in the shells. This is most apparent from the experimentally rather well-established structure of the lower part of the $2\hbar\omega$ shell, where (in case of the low-lying Roper resonance) the deviations between the pure confinement spectra and the empirical mass spectrum are even of the same order of magnitude as the $\Delta - N$ ground-state splitting, which also cannot be accounted for in the case $g_{nn} = 0$. Similar large deviations are also found in higher mass regions, as *e.g.* in case of the $N\frac{9}{2}^+(2220, ****)$. Thus, apart from the $\Delta - N$ ground-state hyperfine splitting, also the shortcomings in the excited pure confinement spectrum strongly indicate missing residual spin-spin interactions in the nucleon sector.

Hence, the question arises to what extent 't Hooft's instanton-induced interaction, which already could nicely explain the octet-decuplet ground-state splittings, can *simultaneously* also account for the striking mass splittings observed in the excited-nucleon spectrum. That this is indeed the case in our model version $\mathcal{A}$ is already evident from the previous discussion of the complete nucleon spectrum but will now be even more convincingly demonstrated when, starting from the case with confinement only, the 't Hooft coupling g_{nn} is turned on and then is increased gradually until the model ground state fits the experimental position of $N\frac{1}{2}^+(939)$. In this respect let us first focus on the effects in the positive-parity spectrum of model $\mathcal{A}$ shown in fig. 15.

7.3.2 Instanton-induced effects in model $\mathcal{A}$ — positive-parity spectrum

In the $2\hbar\omega$ band one finds a selective lowering of exactly four states relative to the other states as required by the experimental findings and it is quite impressive how the instanton-induced effects even shape the pattern of these four model states to come into considerably good agreement with the observed (well-established) pattern at the value of the coupling, where the $\Delta - N$ splitting is reproduced. In addition to the graphical representation

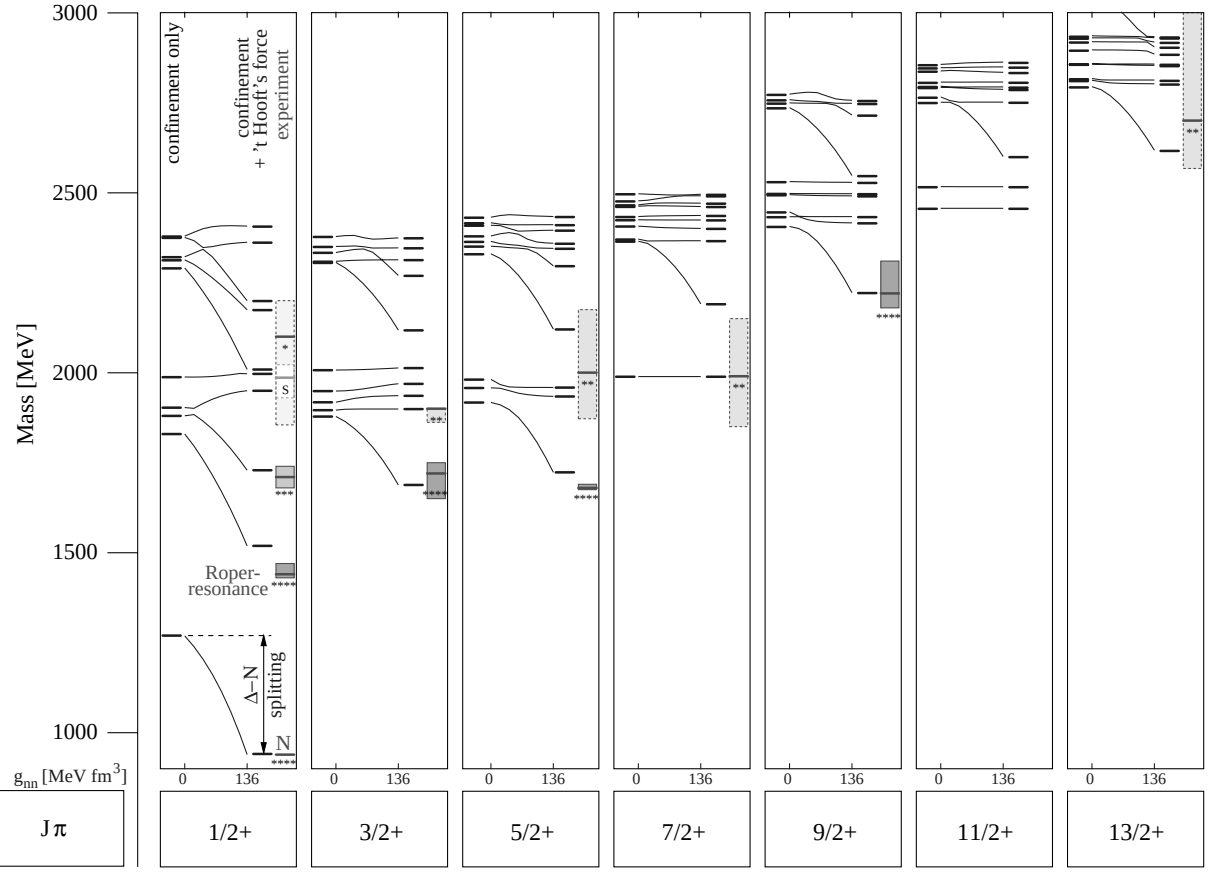

Fig. 15. The effect of the instanton-induced interaction on the positive-parity nucleon resonances in model $\mathcal{A}$. In each column the leftmost spectrum is determined by confinement alone. The curves illustrate the variation of the spectrum with increasing 't Hooft coupling g_{nn} which finally is fixed to reproduce the correct $N-\Delta$ splitting. As can be seen, the 't Hooft interaction can indeed account for essential structures (*e.g.*, the *Roper resonance*) of the experimental spectrum, which is shown on the right in each column.

of this effect in fig. 15, we demonstrate the influence of 't Hooft's force on the $2\hbar\omega$ states (in comparison to the ground state) also in table 21 by displaying the explicit mass values as well as the configuration mixing of these states for the cases without ($g_{nn}=0$ MeV fm^3) and with ($g_{nn}=136$ MeV fm^3) 't Hooft's force. In fact, one of the states in the ground-state sector $N\frac{1}{2}^+$, namely the lowest excitation in the pure confinement spectrum at 1830 MeV, is lowered even strongly enough (by the same amount of roughly 300 MeV like the ground state) to match almost the conspicuous low position of the Roper resonance $N\frac{1}{2}^+(1440,****)$. In this respect it is very interesting to note that, similar to the ground state, this state shows an almost pure ^{2}8[56] spin-flavor $SU(6)$ configuration in the case without 't Hooft interaction. But also when 't Hooft's force is switched on with a strength to bring the ground state roughly 300 MeV down to its experimental value, both the ground state and the Roper state still exhibit almost the same configuration mixing. The final configuration mixing of both states differs from the pure confinement case essentially by a 7-8% admixture of a ^{2}8[70] configuration. Thus, the behavior of the Roper state in model $\mathcal{A}$ under the influence 't Hooft's force is very similar to that of the ground state. The third excited $N\frac{1}{2}^+$ state of the pure confinement spectrum has a dominant ^{2}8[70] configuration. In comparison to the Roper state this state is only moderately lowered by 't Hooft's force by 175 MeV and hence becomes the second excited state matching nicely the position of the $N\frac{1}{2}^+(1710)$. Also each of the lowest states in the $N\frac{3}{2}^+$ and $N\frac{5}{2}^+$ sectors exhibits in the pure confinement case a dominant ^{2}8[56] configuration, however, with rather big admixtures of the other configuration. These states show a common downward shift of roughly 190 MeV somewhat smaller than the Roper resonance but quite similar to the second excitation in the $N\frac{1}{2}^+$ sector. Hence the equally big downward mass shift of all three states is just of the right size to reproduce the nearly degenerate structure of the three resonances $N\frac{1}{2}^+(1710,***)$, $N\frac{3}{2}^+(1720,****)$ and $N\frac{5}{2}^+(1680,****)$ around 1700 MeV.

Note however that the formation of such a well separated shell substructure, which is lowered relative to the bulk of the other states, is not just restricted to the $2\hbar\omega$ band but in general can be found also in the other even

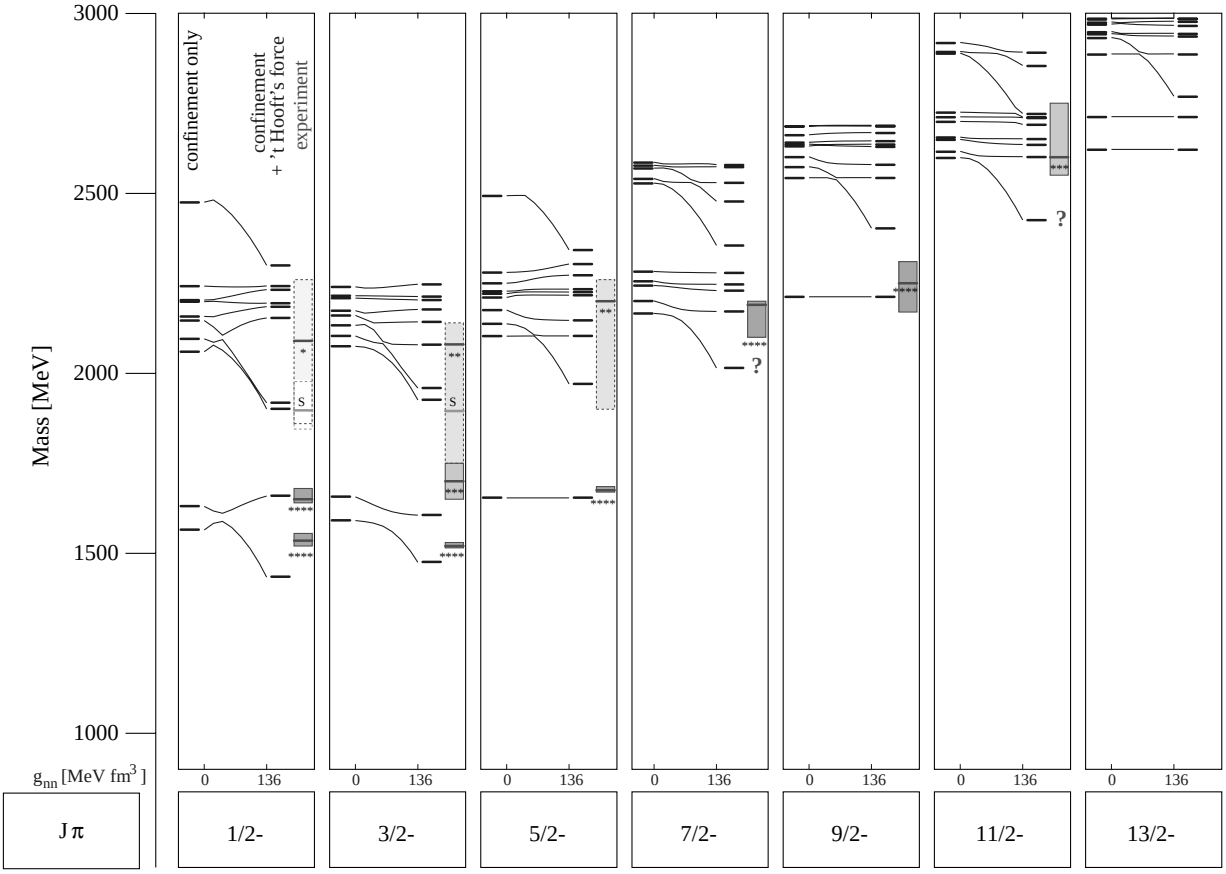

Fig. 16. Instanton-induced splittings of negative-parity nucleon states in model $\mathcal{A}$. In each column the leftmost spectrum is obtained with the confinement force alone. The curves show the change of the spectrum with increasing 't Hooft coupling g_{nn}. The right spectrum finally displays the spectrum with g_{nn} fixed to reproduce the right nucleon ground-state position at 939 MeV. For comparison the experimental resonance positions are displayed rightmost in each column.

parity shells. In the $4\hbar\omega$ and $6\hbar\omega$ band the downward shift of these structures amounts to roughly 180 MeV when g_{nn} is fixed by the correct ground-state position. Again the states of these well-separated sub-shells have dominant $^2 8[56]$ contributions (55%-70%) with additional (in general quite big) admixtures of $^2 8[70]$ configurations (30%-45%). In the $4\hbar\omega$ shell this downward shift is just the right size to achieve the correct description of the well-established Regge state $N\frac{9}{2}^+(2220, ****)$ and in the $6\hbar\omega$ shell the shift isolates the first excitation of the $N\frac{13}{2}^+$ sector, which is assigned to the Regge state $N\frac{13}{2}^+(2700, **)$. Notice that all excited members of the positive-parity N Regge trajectory, *i.e.* each of the lowest excitations in the $N\frac{5}{2}^+$, $N\frac{9}{2}^+$ and $N\frac{13}{2}^+$ sectors, belong to these sub-shells of the $2\hbar\omega$, $4\hbar\omega$ and $6\hbar\omega$ band, respectively, and remember the remarkable feature that their mass shifts, along with the lowering of the ground state, conform excellently with the observed linear Regge characteristic of the trajectory states $N\frac{1}{2}^+(939, ****)$, $N\frac{5}{2}^+(1680, ****)$, $N\frac{9}{2}^+(2220, ****)$ and $N\frac{13}{2}^+(2700, **)$ as discussed in the previous subsection (see fig. 14). In summary we thus find that along with the $\Delta - N$ ground-state splitting really *all* essential hyperfine structures of the positive-parity N^* spectrum, which the confinement kernel of model $\mathcal{A}$ alone cannot account for, are in fact consistently and simultaneously generated by the instanton-induced 't Hooft interaction. Apart from the success of 't Hooft's force in generating the hyperfine structure of ground-state baryons, these results thus give a further strong evidence for our conjecture that the instanton-induced short-distance interaction in fact might play the dominant role for the structure of the whole nucleon spectrum.

7.3.3 Instanton-induced effects in model $\mathcal{A}$ — negative-parity spectrum

We now turn to the instanton-induced effects in the negative-parity nucleon spectrum predicted by model $\mathcal{A}$. Figure 16 shows that the instanton force causes similar effects in the odd-parity $1\hbar\omega$, $3\hbar\omega$, $5\hbar\omega$ bands. Again, in each shell a multiplet of particular states shows a downward level shift of roughly 180–200 MeV, thus generating substructures of nearly degenerate states that are well separated from the rest of the shell. Analyzing the spin-flavor content of the corresponding Salpeter amplitudes, we find

Table 20. Masses and configuration mixing of states in each $N\hbar\omega$ shell with maximal total spin $J_{\max}(N) = N + \frac{3}{2}$ ($N = 1, \ldots, 5$, compare table 19). For each different contribution to the Salpeter amplitude the corresponding Salpeter norm is given in %. In each row the upper line shows the positive and the lower line the negative energy contribution. These states remain totally unaffected by 't Hooft's force, *i.e.* the values without and with 't Hooft's force (right) are exactly the same. See the text for a more detailed explanation.

Model $\mathcal{A}$:

Shell	$J^\pi_{\max}$	Exp. state ΔM [MeV]	Rating	Mass [MeV]	pos. neg.	^{2}8[56] ^{2}8[56]	^{2}8[70] ^{2}8[70]	^{4}8[70] ^{4}8[70]	^{2}8[20] ^{2}8[20]
$1\hbar\omega$	$\frac{5}{2}^-$	$N(1675)$ 1670-1685	****	1655	98.4	0.0	0.0	**98.4**	0.0
					1.6	0.1	0.3	1.0	0.2
$2\hbar\omega$	$\frac{7}{2}^+$	$N(1990)$ 1850-2150	**	1989	98.1	0.0	0.0	**98.1**	0.0
					1.9	0.2	0.2	1.4	0.2
$3\hbar\omega$	$\frac{9}{2}^-$	$N(2250)$ 2170-2310	****	2212	98.2	0.0	0.0	**98.2**	0.0
					1.8	0.1	0.3	1.2	0.2
$4\hbar\omega$	$\frac{11}{2}^+$	"missing"		2455	98.0	0.0	0.0	**97.9**	0.0
					2.0	0.2	0.2	1.5	0.2
		"missing"		2515	97.7	0.0	0.0	**97.7**	0.0
					2.3	0.1	0.4	1.8	0.1
$5\hbar\omega$	$\frac{13}{2}^-$	"missing"		2621	98.3	0.0	0.0	**98.3**	0.0
					1.7	0.0	0.3	1.2	0.2
		"missing"		2712	98.0	0.0	0.0	**98.0**	0.0
					2.0	0.2	0.1	1.6	0.2

Mass and configuration mixing with and without 't Hooft's force

Model $\mathcal{B}$:

Shell	$J^\pi_{\max}$	Exp. state ΔM [MeV]	Rating	Mass [MeV]	pos. neg.	^{2}8[56] ^{2}8[56]	^{2}8[70] ^{2}8[70]	^{4}8[70] ^{4}8[70]	^{2}8[20] ^{2}8[20]
$1\hbar\omega$	$\frac{5}{2}^-$	$N(1675)$ 1670-1685	****	1622	99.9	0.0	0.0	**99.9**	0.0
					0.1	0.0	0.0	0.1	0.0
$2\hbar\omega$	$\frac{7}{2}^+$	$N(1990)$ 1850-2150	**	1941	99.9	0.0	0.0	**99.9**	0.0
					0.1	0.0	0.0	0.1	0.0
$3\hbar\omega$	$\frac{9}{2}^-$	$N(2250)$ 2170-2310	****	2170	99.9	0.0	0.0	**99.9**	0.0
					0.1	0.0	0.0	0.1	0.0
$4\hbar\omega$	$\frac{11}{2}^+$	"missing"		2402	99.8	0.0	0.0	**99.8**	0.0
					0.2	0.0	0.0	0.1	0.0
		"missing"		2446	99.7	0.0	0.0	**99.7**	0.0
					0.3	0.0	0.0	0.2	0.0
$5\hbar\omega$	$\frac{13}{2}^-$	"missing"		2587	99.8	0.0	0.0	**99.8**	0.0
					0.2	0.0	0.0	0.2	0.0
		"missing"		2655	99.7	0.0	0.0	**99.7**	0.0
					0.3	0.0	0.0	0.3	0.0

Mass and configuration mixing with and without 't Hooft's force

that all these states have dominant contributions of ^{2}8[70] configurations with additional large admixtures of ^{2}8[56].

In the $1\hbar\omega$ band this mechanism generates the level splittings of the five experimentally well-established states. The single state of this shell in the $N\frac{5}{2}^-$ sector, which is almost a pure ^{4}8[70] configuration, remains totally unaffected, as previously mentioned. Note that moderate spin-orbit effects of the confinement kernel $\mathcal{A}$ already break the degeneracy of the states in the pure confinement spectrum and cause a slight mixture of the ^{2}8[70] and ^{4}8[70] configurations in the two states of the $N\frac{1}{2}^-$ and $N\frac{3}{2}^-$ sectors, respectively. In both sectors the mass splitting of ~ 65 MeV is such that the state with dominant ^{2}8[70] configuration lies above the state with dominant ^{4}8[70] configuration. The action of 't Hooft's force just reverses this initial level ordering and moreover causes a significant admixture of the ^{2}8[56] configuration (roughly 10%) to the lowest states in $N\frac{1}{2}^-$ and $N\frac{3}{2}^-$. This scenario is documented in table 22, where we displayed the masses as well as the explicit configuration mixings of the $1\hbar\omega$ states for the cases without and with 't Hooft's interaction. Note that in the $N\frac{1}{2}^-$ sector the relativistic

Table 21. Masses and configuration mixing for the nucleon ground state and the excited states of the positive-parity $2\hbar\omega$ shell without (left) and with (right) 't Hooft's force in model $\mathcal{A}$. For each contribution to the Salpeter amplitude the corresponding Salpeter norm is given in %. In each row the upper line shows the positive and the lower line the negative energy contributions. Dominant contributions are bold printed and underlined.

	Without 't Hooft's force						With 't Hooft's force					
J	Mass [MeV]	pos. neg.	^{2}8[56] ^{2}8[56]	^{2}8[70] ^{2}8[70]	^{4}8[70] ^{4}8[70]	^{2}8[20] ^{2}8[20]	Mass [MeV]	pos. neg.	^{2}8[56] ^{2}8[56]	^{2}8[70] ^{2}8[70]	^{4}8[70] ^{4}8[70]	^{2}8[20] ^{2}8[20]
$\frac{1}{2}$	1270	98.5	**98.5**	0.0	0.0	0.0	939	96.3	**90.4**	5.8	0.0	0.0
		1.5	0.3	0.6	0.5	0.0		3.7	1.3	1.8	0.6	0.0
	1830	98.2	**97.5**	0.4	0.2	0.1	1518	97.2	**90.8**	6.1	0.1	0.2
		1.8	0.4	0.7	0.7	0.0		2.8	0.8	1.3	0.6	0.0
	1880	97.9	0.0	13.7	**71.8**	12.4	1729	97.9	15.5	**81.4**	0.7	0.3
		2.1	0.0	0.3	1.8	0.0		2.1	0.6	0.8	0.6	0.1
	1903	98.1	0.6	**75.9**	19.4	2.2	1950	97.9	0.9	0.9	**88.6**	7.4
		1.9	0.4	0.7	0.8	0.1		2.1	0.0	0.2	1.8	0.1
	1988	97.7	0.1	8.4	6.4	**82.9**	1996	97.7	34.2	5.9	6.8	**50.8**
		2.3	0.0	0.8	1.0	0.5		2.3	0.2	0.6	1.3	0.3
$\frac{3}{2}$	1878	98.0	**53.0**	18.7	23.7	2.5	1688	97.0	**66.6**	29.9	0.5	0.1
		2.0	0.4	0.4	1.2	0.0		3.0	1.1	0.7	1.3	0.0
	1896	98.3	0.5	0.7	**93.7**	3.3	1899	98.1	0.2	0.1	**93.9**	4.0
		1.7	0.1	0.3	1.2	0.1		1.9	0.2	0.5	1.1	0.1
	1918	97.9	6.3	24.6	**67.0**	0.0	1936	97.8	6.5	14.6	**67.1**	9.7
		2.1	0.1	0.6	1.4	0.1		2.2	0.2	0.8	1.2	0.0
	1949	97.9	37.6	**44.0**	7.5	8.8	1969	98.1	20.2	**56.0**	21.6	0.3
		2.1	0.4	1.0	0.7	0.0		1.9	0.2	0.8	1.0	0.1
	2007	97.8	0.7	9.8	4.2	**83.0**	2013	97.8	0.8	1.1	12.9	**82.9**
		2.2	0.0	0.8	1.0	0.4		2.2	0.0	0.9	1.0	0.3
$\frac{5}{2}$	1917	98.0	**61.7**	2.8	33.5	0.0	1723	96.8	**65.9**	30.6	0.3	0.0
		2.0	0.8	0.6	0.5	0.1		3.2	1.0	1.2	0.9	0.2
	1957	97.9	20.8	20.8	**56.3**	0.0	1934	97.8	13.1	25.7	**59.0**	0.0
		2.1	0.2	0.7	0.6	0.6		2.2	1.1	0.6	0.5	0.0
	1981	98.0	15.5	**74.3**	8.1	0.0	1959	97.9	16.0	**43.3**	38.5	0.0
		2.0	0.6	0.4	0.7	0.3		2.1	0.3	0.6	0.5	0.8
$\frac{7}{2}$	1989	98.1	0.0	0.0	**98.1**	0.0	1989	98.1	0.0	0.0	**98.1**	0.0
		1.9	0.2	0.2	1.4	0.2		1.9	0.2	0.2	1.4	0.2

version of the instanton force acts repulsive on the dominantly ^{4}8[70] state due to the repulsive part of 't Hooft's force acting in the pseudoscalar diquark sector. In this way the position of $N\frac{1}{2}^-(1650)$ is nicely reproduced. Unfortunately, the lowering of the other state in this sector is slightly too strong, such that it shifts the first predicted excitation below the experimentally observed $N\frac{1}{2}^-(1535)$ and thus below the first predicted state with the opposite positive parity assigned to the Roper resonance. Nonetheless, the splitting between the upper multiplet $N\frac{1}{2}^-(1650)-N\frac{3}{2}^-(1700)-N\frac{5}{2}^-(1675)$ and the lower multiplet $N\frac{1}{2}^-(1535)-N\frac{3}{2}^-(1520)$ is, all in all, reasonably well reproduced in this manner.

In the $3\hbar\omega$ shell region the first evidences for new resonances in the $N\frac{1}{2}^-$ and $N\frac{3}{2}^-$ sectors around 1900 MeV from recent SAPHIR photoproduction results in the channels $p\gamma \to p\eta'$ and $p\gamma \to K\Lambda$, respectively, might indeed be interpreted as first experimental indications of such a comparatively low-lying structure of the $3\hbar\omega$ band: With g_{nn} adjusted to the nucleon ground state, 't Hooft's force separates two close states in both sectors whose positions then nicely agree with the resonance positions reported. As illustrated, also the lowest model excitations in the $N\frac{5}{2}^-$ and $N\frac{7}{2}^-$ sector belong to this well-separated structure. Presently, there is still no experimental evidence for such a comparatively low-lying state in the $N\frac{5}{2}^-$ sector. Concerning the first excited $N\frac{7}{2}^-$ state, we now see that just because of the downward shift of roughly 180 MeV, its predicted position turns out to be 170 MeV too light compared to the position of the first observed excitation in this sector, *i.e.* the four star state $N\frac{7}{2}^-(2190)$. However, the second excitation in $N\frac{7}{2}^-$ along with the other $3\hbar\omega$ states in this sector in fact is hardly influenced by the instanton force and thus fits the $N\frac{7}{2}^-(2190)$ quite well. Hence, the explanation of the comparatively low position of the two new SAPHIR resonances $S_{11}(1897)$ and $D_{13}(1895)$ as instanton-induced effect requires the confirmation of the two states in the $N\frac{5}{2}^-$ and $N\frac{7}{2}^-$ sectors at roughly 2 GeV even below the hitherto observed first excitation $N\frac{7}{2}^-(2190)$ in order to complete this predicted multiplet.

Table 22. Masses and configuration mixing for the states of the negative-parity $1\hbar\omega$ shell without (left) and with (right) 't Hooft's force in model $\mathcal{A}$. For each contribution to the Salpeter amplitude the corresponding Salpeter norm is given in %. In each row the upper line shows the positive and the lower line the negative energy contributions. Dominant contributions are bold printed and underlined.

	Without 't Hooft's force						With 't Hooft's force					
J	Mass [MeV]	pos. neg.	^{2}8[56] ^{2}8[56]	^{2}8[70] ^{2}8[70]	^{4}8[70] ^{4}8[70]	^{2}8[20] ^{2}8[20]	Mass [MeV]	pos. neg.	^{2}8[56] ^{2}8[56]	^{2}8[70] ^{2}8[70]	^{4}8[70] ^{4}8[70]	^{2}8[20] ^{2}8[20]
$\frac{1}{2}$	1566	98.3	0.0	18.1	**80.2**	0.0	1435	96.0	10.6	**83.2**	2.2	0.0
		1.7	0.0	0.1	1.1	0.5		4.0	2.4	0.8	0.1	0.6
	1631	98.1	0.0	**80.0**	18.1	0.0	1660	98.5	0.4	3.0	**94.6**	0.6
		1.9	0.7	0.4	0.5	0.4		1.5	0.1	0.0	1.2	0.2
$\frac{3}{2}$	1592	98.2	0.0	24.7	**73.5**	0.0	1476	97.3	9.0	**87.6**	0.7	0.0
		1.8	0.0	0.4	0.8	0.4		2.7	0.6	0.9	0.9	0.3
	1657	98.4	0.0	**73.6**	24.8	0.0	1606	98.2	0.5	0.5	**97.2**	0.0
		1.6	0.2	0.4	0.8	0.2		1.8	0.2	0.5	0.7	0.3
$\frac{5}{2}$	1655	98.4	0.0	0.0	**98.4**	0.0	1655	98.4	0.0	0.0	**98.4**	0.0
		1.6	0.1	0.3	1.0	0.1		1.6	0.1	0.3	1.0	0.2

The same effect as in the $N\frac{7}{2}^-$ sector can also be seen in the $N\frac{11}{2}^-$ sector where the lowest predicted excitation belongs to the strongly lowered multiplet structure of the $5\hbar\omega$ band. Again, the downward mass shift of roughly 190 MeV due to the instanton force brings the first calculated excitation in $N\frac{11}{2}^-$ about 175 MeV below the first observed excitation $N\frac{11}{2}^-(2600)$. But the second predicted state matches the $N\frac{11}{2}^-(2600)$ exactly, as it remains unaffected by 't Hooft's force. Hence, the residual 't Hooft interaction again leads to a state below the $N\frac{11}{2}^-(2600)$ at 2425 MeV, which is the state with the highest total spin in the lowered multiplet of the $5\hbar\omega$ shell. Note that the two lowest predicted states of $N\frac{7}{2}^-$ and $N\frac{11}{2}^-$ belong to the same negative-parity Regge trajectory and the lowering of the states of this trajectory is quite analogous to the lowering of the positive-parity trajectory discussed previously. There it was just this instanton-induced downward mass shift which brought all states of this trajectory simultaneously into excellent agreement with the experiment.

7.3.4 Explanation for approximate parity doublets

Finally, let us focus in the context of instanton effects (in model $\mathcal{A}$) on the appearance of more or less mass degenerate nucleon states of equal total spin and opposite parity. Comparing the illustrations of instanton-induced effects for the positive- and negative-parity nucleon spectrum in figs. 15 and 16, respectively, we find in fact a simple explicit foundation of the occurrence of near parity doublets in the excited N^* spectrum due to 't Hooft's force. In this respect let us consider the global arrangements of the band structures in the nucleon spectrum formed within the framework of our model: Without the instanton-induced interaction, the three-body confinement kernel alone arranges the nucleon spectrum into even- and odd-parity shells, where the odd-parity bands lie in between the even-parity bands (and vice versa).

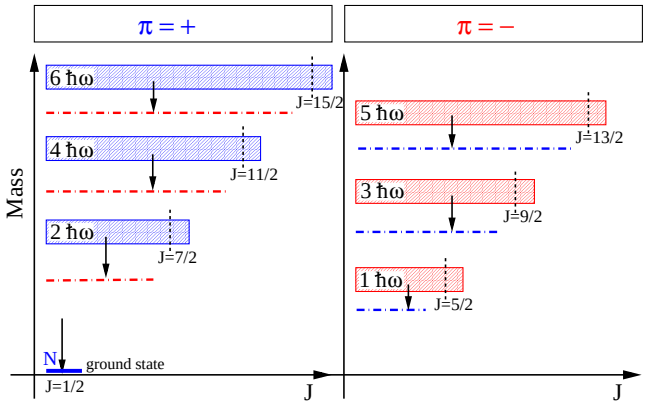

Fig. 17. Schematical illustration of the explanation for the appearance of approximate parity doublets in the nucleon spectrum due to instanton-induced effects in our relativistic Salpeter-equation–based model. For a detailed explanation see the text.

As demonstrated, the instanton-induced interaction then splits each of these shells into two well-separated parts due to its strong selection rules: the lower part, namely a particular subset of states, which are mixtures of dominantly ^{2}8[56] and ^{2}8[70] configurations, is significantly lowered with respect to the upper part, *i.e.* the remaining bulk of states which is hardly influenced by the residual interaction. This situation is schematically demonstrated in fig. 17.

Let us in general consider a $N\hbar\omega$ shell with $N \geq 2$ in the positive (N even) or negative (N odd) parity sector, respectively. When the 't Hooft coupling g_{nn} is adjusted to fit the nucleon ground state, the lowering of the shell substructure is such that it comes to lie approximately in between the unshifted parts of the adjacent $N\hbar\omega$ and $(N-2)\hbar\omega$ bands with the same parity. Accordingly it becomes positioned nearly degenerate with the corresponding unshifted part of the $(N-1)\hbar\omega$ shell with

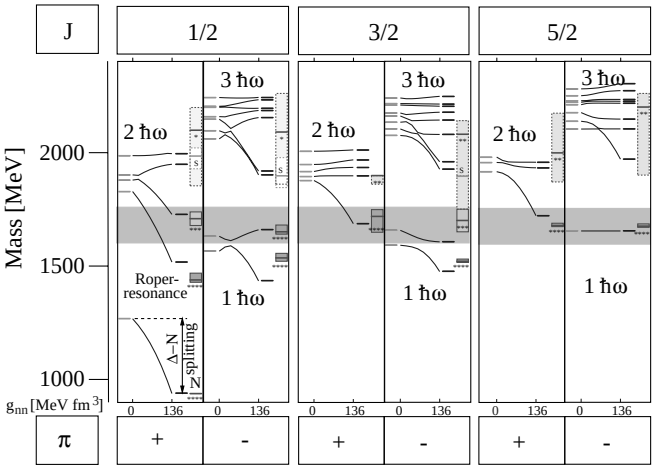

Fig. 18. Generation of approximate parity doublets due to the overlap of the positive-parity $2\hbar\omega$ and the negative-parity $1\hbar\omega$ shells induced by 't Hooft's force (in model $\mathcal{A}$).

the opposite parity. This nearly degenerate arrangement of the upper/lower part of a shell with the lower/upper part of a shell with opposite parity consequently leads to the near parity doublets in our model, which we already discussed in detail in the foregoing subsection (see figs. 11 and 12).

The positioning of the positive-parity $2\hbar\omega$ shell and the negative-parity $1\hbar\omega$ shell due to instanton effects, which leads to approximate doublets in the second resonance region of the excited-nucleon spectrum around 1700 MeV, is once more explicitly illustrated in fig. 18; we therefore combined the columns of fig. 15 (positive parity) and fig. 16 (negative parity) corresponding to the spins $J = \frac{1}{2}$, $\frac{3}{2}$ and $\frac{5}{2}$ in such a way that the sectors with same spin and opposite parity are directly displayed side by side. We thus see that in the framework of our covariant quark model $\mathcal{A}$ the instanton-induced effects indeed suggest a quite simple and appealing explanation for these experimentally observed approximate parity doublets in the second resonance region.

Moreover, this mechanism works even for the higher mass regions of the nucleon spectrum: The general arrangement of shell multiplets as indicated schematically in fig. 17 is most prominent for the lowest-lying[6] states of the sectors with J^π from $\frac{5}{2}^\pm$ to $\frac{13}{2}^\pm$ (Regge-trajectory-type states): From table 19 we see that the lowest states of the sectors $J^\pi = \frac{5}{2}^-$, $\frac{7}{2}^+$, $\frac{9}{2}^-$, $\frac{11}{2}^+$, and $\frac{13}{2}^-$ are just the states with maximum total spin $J_{\max}(N) = N + \frac{3}{2}$ of the $N\hbar\omega$ shells, with $N = 1$, 2, 3, 4, and 5. As discussed earlier these states are not influenced by 't Hooft's force since they necessarily contain a totally symmetric spin-quartet ($S = \frac{3}{2}$) wave function to achieve this maximal total spin. But in the corresponding sectors with the same total spin J but opposite parity we then always find exactly one state of the higher lying $N + 1$ band that is selectively lowered by 't Hooft's force and thus becomes the lowest excitation in this opposite-parity sector fairly isolated from the other states. The arrangement of these states in model $\mathcal{A}$ in comparison with the present experimental situation is shown in fig. 19, where again the sectors with the same spin and opposite parity are displayed side by side. It is quite astonishing that the strength g_{nn} as fixed on the ground state is just the right size to form in this way *systematically* patterns of approximate parity doublets for *all* lowest excitations in the sectors $J = \frac{5}{2}$ to $J = \frac{13}{2}$. In the $N\frac{5}{2}^\pm$ and $N\frac{9}{2}^\pm$ sectors this scenario is nicely confirmed by the well-established parity doublet structures $N\frac{5}{2}^+(1680, ****) - N\frac{5}{2}^-(1675, ****)$ and $N\frac{9}{2}^+(2220, ****) - N\frac{9}{2}^-(2250, ****)$, respectively. In the $N\frac{7}{2}$ sector, however, the present experimental findings of the lowest excitations seem to deviate from such a parity doubling structure due to the rather high measured resonance position of the $N\frac{7}{2}^-(2190, ****)$ with respect to the $N\frac{7}{2}^+(1990, **)$. Therefore, a new investigation of this situation and especially the presently stated position of the first $N\frac{7}{2}^-$ excitation is highly desirable. In fact, the interesting energy range around 2000 MeV is accessible by the new photo- and electro-production experiments, *e.g.* with the Crystal Barrel detector at ELSA (University of Bonn, Germany) or with the CLAS detector at CEBAF (Jefferson Lab, USA), so that an early clarification of the situation looks promising. But also an exploration of the higher spin states with $J = \frac{11}{2}$ and $J = \frac{13}{2}$ by future experiments on high baryon excitations is desirable. The verification of the position of the first excited $N\frac{11}{2}^-$ state, which presently differs significantly from our prediction, as well as the discovery of the still "missing" first (two) excitation(s) in the sectors $N\frac{11}{2}^+$ and $N\frac{13}{2}^-$ is essential to decide whether this striking feature of systematical parity doublets induced by instanton effects is indeed a realistic global structure exhibited also by the experimental nucleon spectrum.

To conclude this discussion of approximate parity doublets, it is worthwhile mentioning that a further test of this scenario for parity doublets based on instanton effects should be possible by the measurement of electromagnetic ($p\gamma^* \to N^*$) transition form factors into each member of the doublets shown in fig. 19. Such a measurement provides a deeper insight into the structure of the corresponding resonances. In this respect it is crucial that one member of each doublet, namely that which belongs to the maximum total spin $J_{\max}(N) = N + \frac{3}{2}$ of the corresponding $N\hbar\omega$ shell, is by no means influenced by 't Hooft's force whereas its partner with opposite parity is strongly affected by this residual interaction. Therefore, both members of the doublet have significantly different internal structures that should be manifest in systematically different shapes of the two corresponding magnetic multipole transition form factors: the member of each parity doublet affected by 't Hooft's force exhibits a rather strong scalar-diquark correlation and thus its structure

[6] Note that these states are rather isolated and furthermore experimentally the most simply (or even the only) accessible resonances especially of the higher oscillator shells.

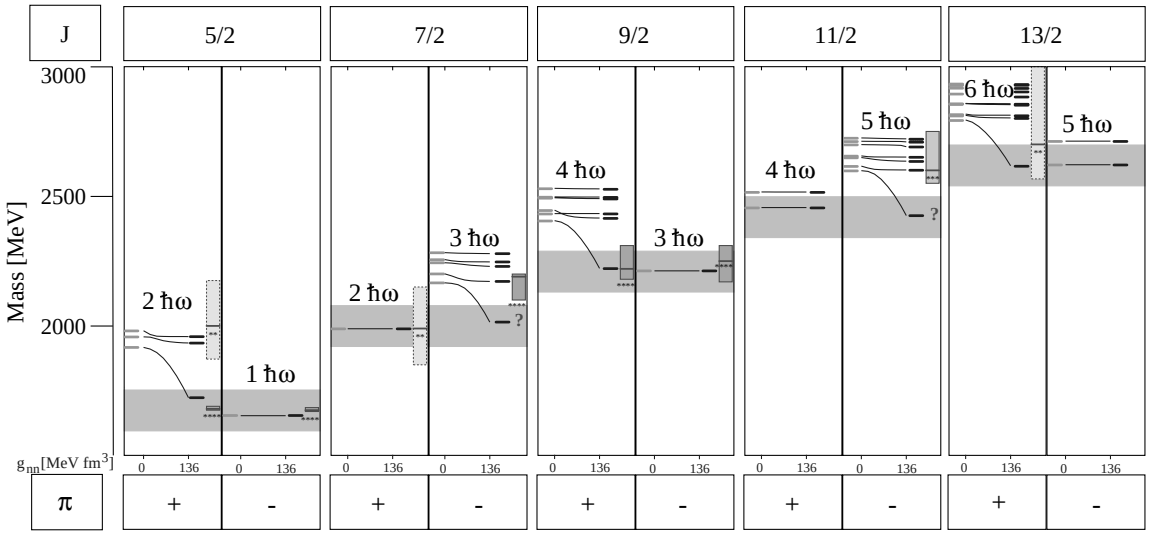

Fig. 19. Instanton-induced generation of approximate parity doublets of lowest lying states (Regge-trajectory–type states) in the sectors with J from $\frac{5}{2}$ to $\frac{13}{2}$ (in model $\mathcal{A}$).

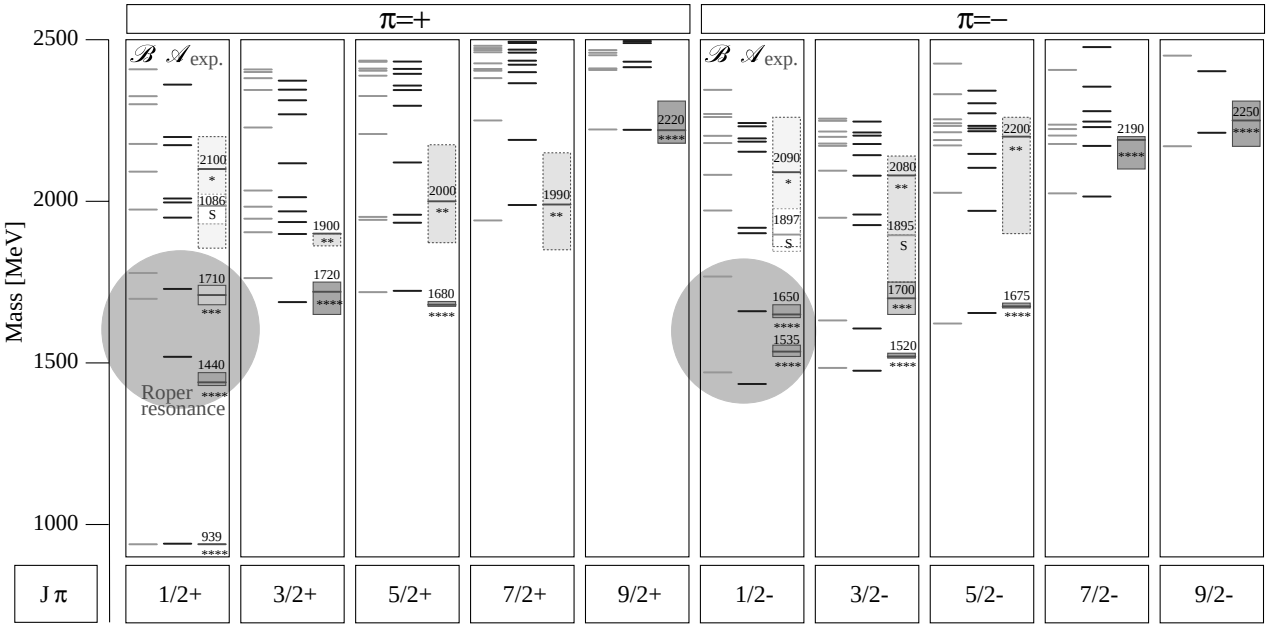

Fig. 20. Comparison of the N^* spectrum in model $\mathcal{A}$ (middle) and $\mathcal{B}$ (left); see text.

should be more compact, in comparison to its unaffected doublet partner whose structure is expected to be rather soft. Consequently for larger momentum transfers Q^2 the transition form factors $p\gamma^* \to N^*$ for the lowest excitation in $N^*\frac{5}{2}^-$, $N^*\frac{7}{2}^+$, $N^*\frac{9}{2}^-$, $N^*\frac{11}{2}^+$, and $N^*\frac{13}{2}^-$ should systematically decrease faster than those of opposite parity [62].

7.3.5 Instanton-induced effects in model $\mathcal{B}$ — differences to model $\mathcal{A}$

In our earlier discussion of the complete nucleon spectrum we found some significant differences between the models $\mathcal{A}$ and $\mathcal{B}$: although also model $\mathcal{B}$ is able to describe uniformly most of the structures of the excited N^* spectrum up to highest excitations similar to model $\mathcal{A}$ (*e.g.*, the positive-parity N-Regge trajectory), it strongly failed, in contrast to model $\mathcal{A}$, in describing one of the most prominent and interesting features of the nucleon spectrum, namely the Roper resonance in the $N\frac{1}{2}^+$ sector. Moreover, model $\mathcal{B}$ predicted a much too large hyperfine splitting between the first two $N\frac{1}{2}^-$ excitations in the $1\hbar\omega$ shell; see fig. 20, where the results of both models can be directly compared. Thus, apart from further rather small differences, the most distinct deviations between model $\mathcal{A}$

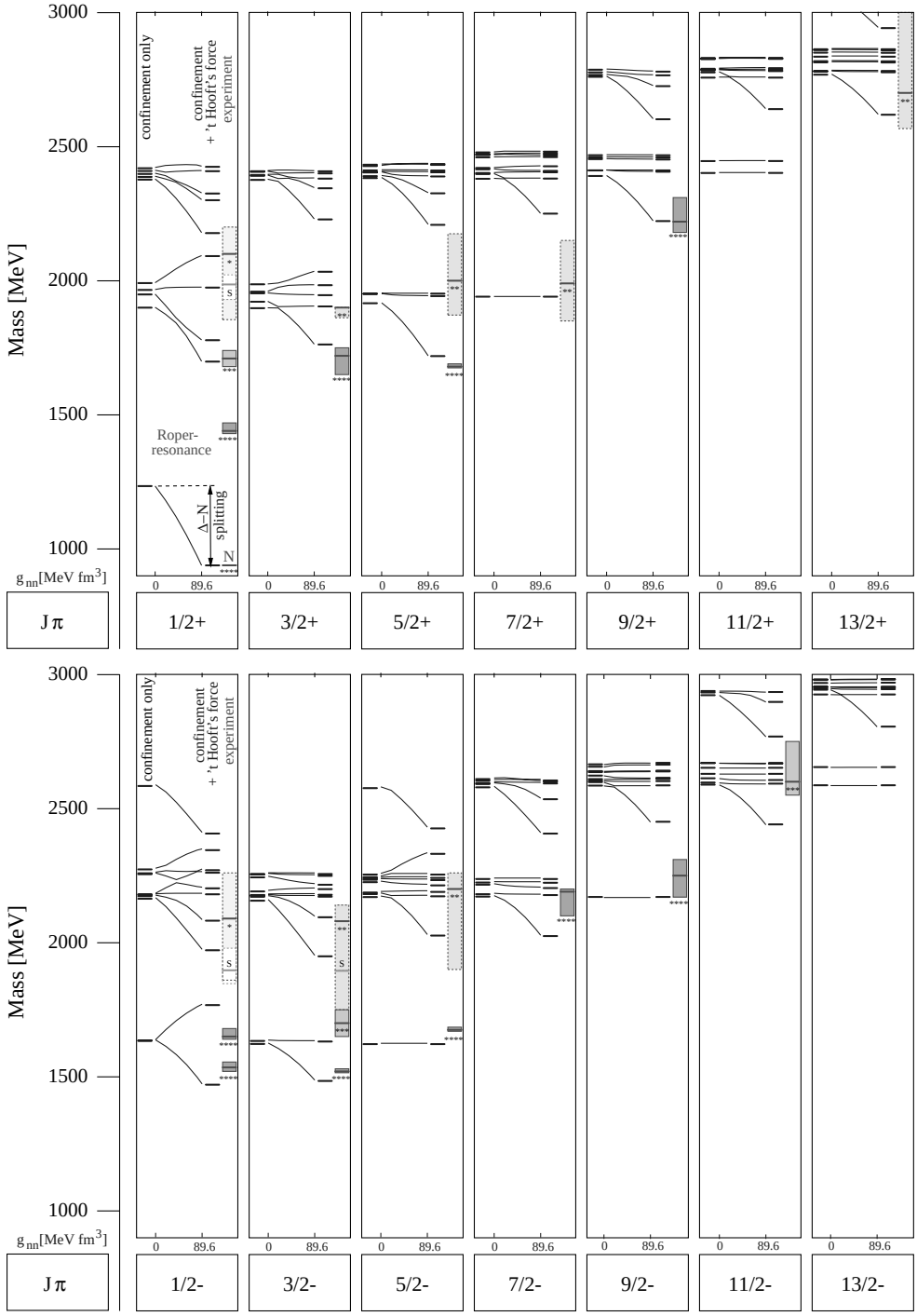

Fig. 21. Instanton-induced effects in the positive (above) and negative (below) parity nucleon spectrum of model $\mathcal{B}$. The figures show the variation of the N^* mass levels with increasing effective 't Hooft coupling g_{nn} analogous to figs. 15 and 16 corresponding to model $\mathcal{A}$. Note that in contrast to model $\mathcal{A}$ the residual 't Hooft interaction here cannot account for the Roper resonance $N\frac{1}{2}^+(1440)$ and moreover strongly fails in the description of $N\frac{1}{2}^-(1650)$!

and $\mathcal{B}$ show up in the sectors with total spin $J = \frac{1}{2}$. Since the equally good results of both models concerning the description of the complete presently known Δ spectrum did not allow to favor one of the two phenomenological confinement potentials, the quite different results concerning the Roper resonance provide a suitable indirect criterion that strongly supports version $\mathcal{A}$ to provide the more realistic confinement potential in combination with 't Hooft's force as residual interaction.

Studying now the effects of 't Hooft's force on the energy levels of the N^* spectrum in model $\mathcal{B}$ and comparing these with the corresponding results of model $\mathcal{A}$ presented

Table 23. Masses and configuration mixing for nucleon states of the negative-parity $1\hbar\omega$ shell without (left) and with (right) 't Hooft's force in model $\mathcal{B}$. For each contribution to the Salpeter amplitude the corresponding Salpeter norm is given in %. In each row the upper line shows the positive and the lower line the negative energy contributions. Dominant contributions are bold printed and underlined.

	Without 't Hooft's force						With 't Hooft's force					
J	Mass [MeV]	pos. neg.	^{2}8[56] ^{2}8[56]	^{2}8[70] ^{2}8[70]	^{4}8[70] ^{4}8[70]	^{2}8[20] ^{2}8[20]	Mass [MeV]	pos. neg.	^{2}8[56] ^{2}8[56]	^{2}8[70] ^{2}8[70]	^{4}8[70] ^{4}8[70]	^{2}8[20] ^{2}8[20]
$\frac{1}{2}$	1634	99.9	0.0	12.2	**87.7**	0.0	1470	99.7	6.1	**87.1**	6.5	0.0
		0.1	0.0	0.0	0.1	0.0		0.3	0.2	0.0	0.0	0.0
	1636	99.9	0.0	**87.6**	12.2	0.0	1767	99.9	1.7	6.2	**91.2**	0.9
		0.1	0.1	0.0	0.0	0.0		0.1	0.0	0.0	0.1	0.0
$\frac{3}{2}$	1623	99.9	0.0	**64.8**	35.1	0.0	1485	99.9	6.1	**90.7**	3.2	0.0
		0.1	0.0	0.0	0.0	0.0		0.1	0.0	0.0	0.0	0.0
	1634	99.9	0.0	35.1	**64.8**	0.0	1631	99.9	0.0	3.1	**96.7**	0.0
		0.1	0.0	0.0	0.0	0.0		0.1	0.0	0.0	0.0	0.0
$\frac{5}{2}$	1622	99.9	0.0	0.0	**99.9**	0.0	1622	99.9	0.0	0.0	**99.9**	0.0
		0.1	0.0	0.0	0.1	0.0		0.1	0.0	0.0	0.1	0.0

in the foregoing subsection, we want to show that the differences between the models indeed have their origin in a different influence of instanton-induced effects due to different relativistic effects of the confinement kernels in both models: In both models $\mathcal{A}$ and $\mathcal{B}$ the three-quark confinement kernel is provided with a combination of scalar ($\mathbb{1}\otimes\mathbb{1}\otimes\mathbb{1}$) and time-like vector ($\mathbb{1}\otimes\gamma^0\otimes\gamma^0+$ cycl. perm.) Dirac structures. Both versions just differ (apart from different model parameters) in the way how these two spinorial Dirac structures are combined in the linearly rising part of the confinement kernel. Since both models have the *same non-relativistic limit* and hence yield in this limit the same results, the large differences between model $\mathcal{A}$ and $\mathcal{B}$ concerning the Roper resonance in $N^*\frac{1}{2}^+$ and the hyperfine splittings of the $1\hbar\omega$ states in $N^*\frac{1}{2}^-$ in fact can be considered as pure relativistic effects in our Salpeter equation-based quark model. This shall be clarified more precisely in the course of this discussion.

In analogy to figs. 15 and 16 of model $\mathcal{A}$, fig. 21 shows the influence of 't Hooft's force on the energy levels of the excited positive- and negative-parity nucleon spectrum in model $\mathcal{B}$. Before analyzing in detail the differences to model $\mathcal{A}$ let us briefly discuss those effects that both models have in common. Considering globally the influence of 't Hooft's force on the N^* spectrum in model $\mathcal{B}$, we indeed find a lot of effects similar to those in model $\mathcal{A}$. In each shell we again find the systematics of well-separated multiplets of states which show dominant contributions of the $2^8[56]$ and $2^8[70]$ configurations or their mixtures. These shell substructures are rather strongly lowered relative to the majority of states in the corresponding bands that are hardly affected by 't Hooft's force. As in model $\mathcal{A}$, this systematics leads again to the occurrence of more or less mass degenerate states of equal spin and opposite parity. We do not want to discuss this aspect again in detail here and just remark that this instanton-induced mechanism of generating approximate parity doublets works slightly better in model $\mathcal{A}$. As before, the instanton interaction for several model states induces downward mass shifts again of the right size to reproduce the correct experimentally determined resonance positions, if the 't Hooft coupling g_{nn} is fixed such that the model ground state matches the experimental mass. In the positive-parity spectrum these are, for instance, the states assigned to the Regge trajectory, *i.e.* besides the ground state the three states $N\frac{5}{2}^+(1680,****)$, $N\frac{9}{2}^+(2220,****)$ and $N\frac{13}{2}^+(2700,**)$. In the negative-parity spectrum we again find the lowest predicted states in the $N\frac{7}{2}^-$ and $N\frac{11}{2}^-$ roughly 160–170 MeV below the observed first excitations $N\frac{7}{2}^-(2190)$ and $N\frac{11}{2}^-(2600)$ stated by the PDG [38]. This is caused in the same way as in model $\mathcal{A}$ just because of the strong downward mass shift of the first excited states in these sectors by roughly 150 MeV.

To investigate the most striking differences in the influence of 't Hooft's force compared to model $\mathcal{A}$, let us now have a closer look at the negative-parity $1\hbar\omega$ shell and the positive-parity $2\hbar\omega$ shell, where, as mentioned before, the biggest deviations show up in the $N\frac{1}{2}^\pm$ sectors. We start with the states of the $1\hbar\omega$ shell. For this discussion we also show the explicit masses and the configuration mixing of the $1\hbar\omega$ states for the cases without and with instanton force in table 23.

Again, the $N\frac{5}{2}^-$ state, which fits the $N\frac{5}{2}^-(1675,****)$ reasonably well, remains unaffected as in model $\mathcal{A}$. In the pure confinement case, *i.e.* $g_{nn}=0$, we find in model $\mathcal{B}$ that all $1\hbar\omega$ states are almost degenerate at roughly 1630 MeV; for explicit values see table 23. This is quite in contrast to model $\mathcal{A}$, where, due to moderate spin-orbit effects of the confinement kernel, the degeneracy of the $N\frac{1}{2}^-$ and $N\frac{3}{2}^-$ states was already lifted right from start and mass splittings showed up already in the pure confinement spectrum. This difference is due to the different combinations of the scalar and time-like vector Dirac structures in the linearly rising part of the three-body confinement kernels of model $\mathcal{A}$ and $\mathcal{B}$: While that of model

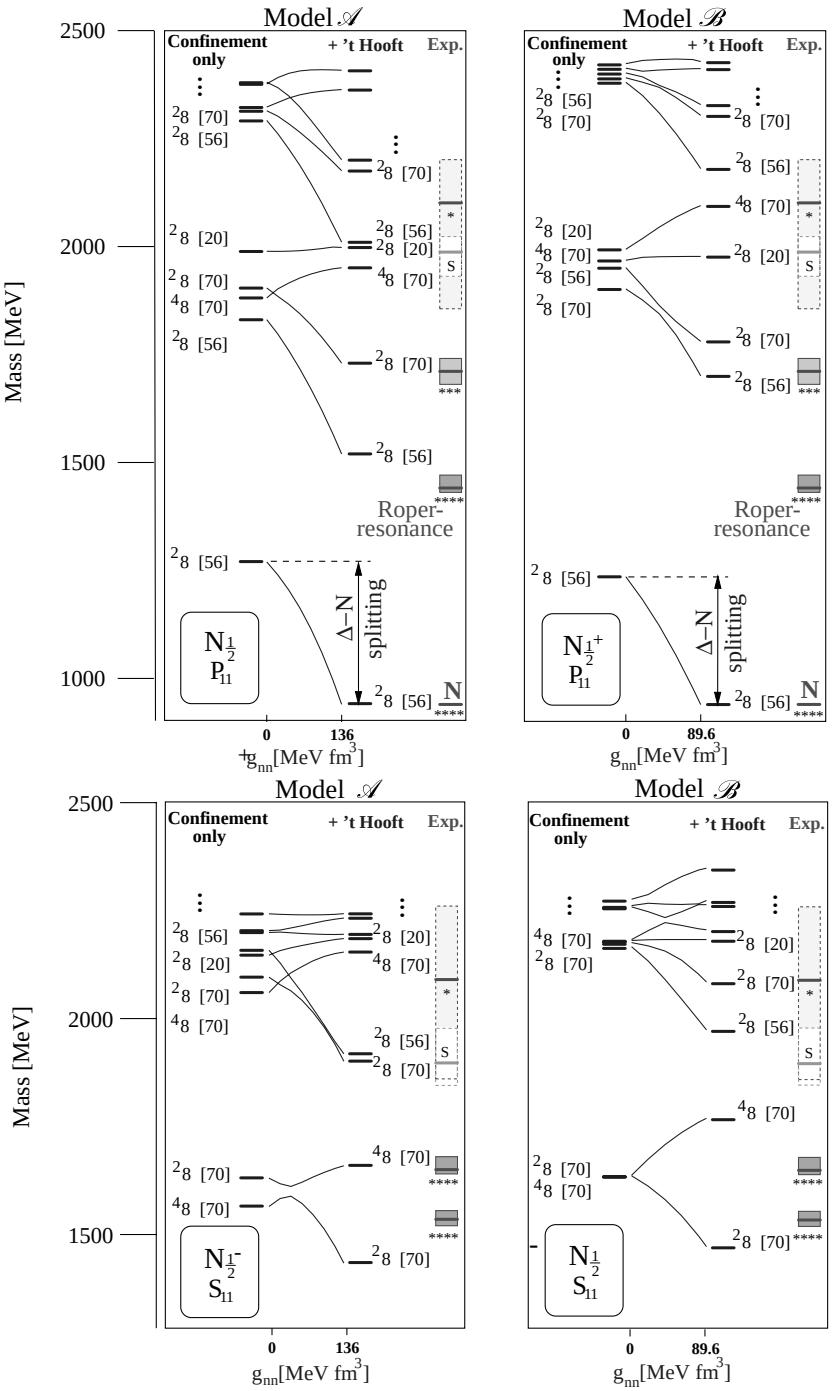

Fig. 22. Comparison of the different instanton-induced effects in model $\mathcal{A}$ (left) and model $\mathcal{B}$ (right) in the $J = \frac{1}{2}$ sector due to different spin-orbit effects of the two confinement versions. In both cases, each state is labeled by its dominant spin-flavor $SU(6)$ contribution, see tables 21, 24, 22 and 23. See the text for a detailed discussion and explanation.

$\mathcal{B}$ is chosen to really minimize relativistic spin-orbit effects owing to a cancellation of effects from the scalar and time-like vector part, the Dirac structure of model $\mathcal{A}$ exhibits moderate spin-orbit effects. This we illustrated already in the earlier discussion of the Δ spectrum. Let us analyze what these different relativistic effects imply for the effect of 't Hooft's force. Turning on 't Hooft's interaction ($g_{nn} > 0$) the degeneracy is lifted: In the $N\frac{3}{2}^-$ sector one of the two states, *i.e.* the state with dominant ^{2}8[70] configuration, shows a downward shift while the position of the other one, with the dominant ^{4}8[70] configurations, remains almost unchanged. Thus, the experimentally observed splitting between $N\frac{3}{2}^-(1700, ****)$ and

Table 24. Masses and configuration mixing for the nucleon ground state and the excited states of the positive-parity $2\hbar\omega$ shell without (left) and with (right) 't Hooft's force in model $\mathcal{B}$. For each contribution to the Salpeter amplitude the corresponding Salpeter norm is given in %. In each row the upper line shows the positive and the lower line the negative energy contributions. Dominant contributions are bold printed and underlined.

	Without 't Hooft's force						**With 't Hooft's force**					
J	Mass [MeV]	pos. neg.	^{2}8[56] ^{2}8[56]	^{2}8[70] ^{2}8[70]	^{4}8[70] ^{4}8[70]	^{2}8[20] ^{2}8[20]	Mass [MeV]	pos. neg.	^{2}8[56] ^{2}8[56]	^{2}8[70] ^{2}8[70]	^{4}8[70] ^{4}8[70]	^{2}8[20] ^{2}8[20]
$\frac{1}{2}$	1234	99.9	**99.9**	0.0	0.0	0.0	939	99.7	**96.1**	3.5	0.0	0.0
		0.1	0.0	0.1	0.0	0.0		0.3	0.1	0.2	0.1	0.0
	1900	99.9	0.2	**99.0**	0.0	0.7	1698	99.8	**73.5**	25.4	0.1	0.8
		0.1	0.0	0.0	0.0	0.0		0.2	0.1	0.1	0.1	0.0
	1949	99.9	**94.6**	0.1	3.9	1.2	1778	99.9	30.2	**69.1**	0.6	0.0
		0.1	0.0	0.1	0.1	0.0		0.1	0.0	0.1	0.0	0.0
	1966	99.9	4.6	0.1	**91.6**	3.6	1974	99.9	0.6	0.0	39.1	**60.2**
		0.1	0.0	0.0	0.1	0.0		0.1	0.0	0.0	0.1	0.0
	1991	99.9	0.4	0.7	4.5	**94.3**	2092	99.9	1.4	3.4	**59.1**	36.0
		0.1	0.0	0.1	0.0	0.0		0.1	0.0	0.0	0.1	0.0
$\frac{3}{2}$	1898	99.9	0.4	0.0	**99.1**	0.4	1762	99.9	**77.7**	20.6	0.7	0.9
		0.1	0.0	0.0	0.1	0.0		0.1	0.0	0.0	0.0	0.0
	1922	99.9	**98.0**	1.2	0.7	0.1	1904	99.9	1.0	1.2	**95.8**	2.0
		0.1	0.0	0.0	0.0	0.0		0.1	0.0	0.0	0.1	0.0
	1953	99.9	0.7	**85.1**	12.7	1.4	1946	99.9	15.6	**64.5**	8.9	10.9
		0.1	0.0	0.0	0.1	0.0		0.1	0.0	0.0	0.1	0.0
	1959	99.9	0.8	8.3	**78.5**	12.3	1983	99.9	0.4	1.3	39.8	**58.4**
		0.1	0.0	0.0	0.1	0.0		0.1	0.0	0.0	0.1	0.0
	1986	99.9	0.0	5.4	8.8	**85.7**	2033	99.9	3.0	15.0	**54.3**	27.6
		0.1	0.0	0.0	0.1	0.0		0.1	0.0	0.0	0.0	0.0
$\frac{5}{2}$	1916	99.9	**97.4**	1.3	1.2	0.0	1718	99.9	**65.1**	32.9	1.8	0.1
		0.1	0.0	0.0	0.0	0.0		0.1	0.0	0.0	0.0	0.0
	1951	99.9	2.4	**74.0**	23.6	0.0	1943	99.9	32.1	**67.4**	0.4	0.0
		0.1	0.0	0.0	0.0	0.0		0.1	0.0	0.0	0.0	0.0
	1952	99.9	0.2	24.6	**75.2**	0.0	1952	99.9	0.5	1.6	**97.8**	0.0
		0.1	0.0	0.0	0.0	0.0		0.1	0.0	0.0	0.0	0.0
$\frac{7}{2}$	1941	99.9	0.0	0.0	**99.9**	0.0	1941	99.9	0.0	0.0	**99.9**	0.0
		0.1	0.0	0.0	0.1	0.0		0.1	0.0	0.0	0.1	0.0

$N\frac{3}{2}^-(1520,***)$ is fairly well reproduced and of similar quality as in model $\mathcal{A}$. But now let us focus on the quite different effects in both models for the $N\frac{1}{2}^-$ XS sector. For the sake of a better comparison the results of both models in this sector are depicted together in the lower part of fig. 22. In model $\mathcal{B}$, the dominantly ^{2}8[70] state again shows a downward mass shift as in the $N\frac{3}{2}^-$ sector due to the attractive scalar-diquark correlation, but at the same time the repulsive part of the relativistic version of 't Hooft's force, that acts in the pseudo-scalar diquark sector (and is absent in the non-relativistic limit), very strongly shifts the state with the dominant ^{4}8[70] configuration upwards. Hence, the experimental position of $N\frac{1}{2}^-(1650,****)$ and thus the hyperfine splitting between $N\frac{1}{2}^-(1635,****)$ and $N\frac{1}{2}^-(1650,****)$ is largely overestimated, in contrast to model $\mathcal{A}$. There the situation is improved just because of the moderate relativistic effects of the confinement force. Recall that the mass splitting in the pure confinement case exhibits the reversed level ordering in model $\mathcal{A}$: the dominantly ^{4}8[70] state lies below the state with the dominant ^{2}8[70] configuration. Thus, in contrast to model $\mathcal{B}$, the increasing 't Hooft coupling g_{nn} leads in model $\mathcal{A}$ first to a level crossing cancelling the first confinement-induced splitting before a reversed level ordering is achieved. Hence the net effect is a weaker and thus improved hyperfine splitting in model $\mathcal{A}$ that agrees better with the experimental findings than in model $\mathcal{B}$.

We now turn to the instanton effects in the $2\hbar\omega$ shell that show up in model $\mathcal{B}$. For this discussion see also table 24, which shows the explicit mass values and configuration mixings of the states without and with 't Hooft interaction. In figure 21 again a lowering of exactly four states of this shell can be observed, when the 't Hooft coupling g_{nn} is gradually increased. In the $N\frac{1}{2}^+$ sector, however, the effect of 't Hooft's force obviously strongly fails in generating the low position of the Roper resonance, whereas in the $N\frac{3}{2}^+$ and $N\frac{5}{2}^+$ sectors the situation still is quite similar to model $\mathcal{A}$. Counting the $2\hbar\omega$ states in the non-relativistic oscillator model, we expect exactly one ^{2}8[56] state in both sectors $N\frac{3}{2}^+$ and $N\frac{5}{2}^+$. Accordingly, we find in our models one state in both sectors, whose

embedded Pauli spinors exhibit a dominant ^{2}8[56] contribution. These are lowered relative to the other states by 't Hooft's force, quite similarly in both models. Again, let us focus on the $N\frac{1}{2}^+$ sector, where the largest deviations from the experimental findings and from the results of model $\mathcal{A}$ become evident. For a more detailed investigation of the different instanton-induced effects the results of both models are depicted together in the upper part of fig. 22. The totally different results of model $\mathcal{A}$ and model $\mathcal{B}$ again can be traced back to different relativistic effects stemming from the confinement forces. As one expects from counting states in the non-relativistic oscillator model, we find in the pure confinement spectra of both models exactly four $N\frac{1}{2}^+$ states belonging to the $2\hbar\omega$ shell. Each of the four possible spin-flavor $SU(6)$ configurations ^{2}8[56], ^{2}8[70], ^{4}8[70] and ^{2}8[20] occurs and can be assigned to one of these states. Of course, in the pure confinement spectra of our Salpeter equation-based models $\mathcal{A}$ and $\mathcal{B}$ the degeneracy is lifted due to the anharmonicity of the linear confinement potential and still more importantly due to relativistic effects depending on the spinorial Dirac structure of the confining forces. Consequently, the two confinement versions induce different intra-band hyperfine structures of these states. Comparing the masses and the corresponding contributions of the spin-flavor $SU(6)$ configurations to the embedded Pauli spinors of the Salpeter amplitudes (see table 21 and 24) one finds, apart from the different pattern of mass splittings, a totally different level ordering and configuration mixing of the states in both models. In model $\mathcal{B}$ we find rather pure $SU(6)$ configurations ($>$ 91%) and a level ordering ^{2}8[70] $<^2$ 8[56] $<^4$ 8[70] $<^2$ 8[20] , whereas in model $\mathcal{A}$ we observe, apart from an almost pure ^{2}8[56] state, moderate admixtures ($\approx$ 20–30%) to the dominant configurations and, in particular, a different level ordering ^{2}8[56] $<^4$ 8[70] $<^2$ 8[70] $<^2$ 8[20] XS. From our considerations at the beginning of this section concerning the effect of 't Hooft's force on the different spin-flavor configurations, one expects a lowering of the two states with dominant ^{2}8[56] and ^{2}8[70] contributions, where the shift is strongest for the ^{2}8[56] state and rather moderate for the ^{2}8[70] state. In this respect, the crucial difference between the pure confinement spectra of the two models is that model $\mathcal{A}$ exhibits an ordering of the levels with the dominantly ^{2}8[56] state already below the dominantly ^{2}8[70] state, whereas in model $\mathcal{B}$ this order is reversed and the ^{2}8[56] state lies $\sim$ 120 MeV above the position in model $\mathcal{A}$. Consequently, we observe in model $\mathcal{A}$ this initial mass splitting being increased by a strong lowering of the ^{2}8[56] state of 312 MeV (very similar to the ground state) and a more moderate downward shift of the ^{2}8[70] state of 174 MeV thus very nicely reproducing the striking low position of the Roper resonance $N\frac{1}{2}^+(1440, ****)$ and the position of $N\frac{1}{2}^+(1710, ***)$. In model $\mathcal{B}$, however, the initial reversed ordering of these two states leads to a level crossing, which mixes the two configurations. Consequently the net effect of the residual interaction is weakened and thus neither the low position of the Roper resonance nor the splitting between the Roper resonance and the $N\frac{1}{2}^+(1710, ***)$ can be explained.

To summarize, our discussion convincingly demonstrates the importance of relativistic effects as they are present in our fully covariant framework based on the Salpeter equation. To generate prominent hyperfine structures in the N^* spectrum like the Roper resonance by 't Hooft's residual force, the interplay of the residual force and the confinement force due to relativistic effects of the confinement Dirac structure is very crucial. We have seen that two different confinement Dirac structures, which exhibit the same non-relativistic limit and work almost equally well for the description of the Δ spectrum and the spectrum of the light ground states, might cause a totally different behavior of particular excited N^* states under the influence of the residual 't Hooft interaction. The different results of both models concerning the Roper resonance thus strongly favor the confinement version of model $\mathcal{A}$ to be the more realistic confinement force in combination with 't Hooft's residual force.

Let us conclude this subsection by drawing the following general conclusions from this discussion:

- The very different effects of 't Hooft's residual force on the Roper state in two models that have the *same non-relativistic limit*, convincingly demonstrates the importance for describing baryons in a genuine *fully relativistic framework* in order to decide whether a possible choice for a residual interaction is a realistic candidate for explaining prominent hyperfine structures of the excited baryon spectrum.
- In particular, the effect of a residual interaction cannot be considered independently from a suitable assumption on the spinorial Dirac structure of the confinement force. This is often done by non-relativistic or "relativized" potential models which either completely neglect the resulting relativistic effects of the confinement Dirac structure by just using central confining potentials or which take only a part of the terms of the rather poorly converging ($|\mathbf{p_q}|/m_q \approx 1$) generalized Fermi-Breit expansion of the confinement force (and also of the residual interaction itself) into account. Relativistic effects of both, the residual force *and* the confinement force, must be consistently taken into account.
- From our point of view this implies that statements concerning the role of a special choice of the residual interaction for generating the hyperfine structures in the excited light-baryon spectrum, which are based on "relativized" or even non-relativistic potential models, are highly context dependent.

7.4 Summary for the nucleon spectrum

After this rather lengthy and detailed discussion of the excited-nucleon spectrum, which emphasized the role of 't Hooft's instanton-induced interaction for explaining all the various, striking features of the mass spectrum, it is worthwhile to summarize our main results and statements.

With the confinement parameters and the non-strange quark mass fixed by the phenomenology of the global Δ spectrum and the 't Hooft coupling g_{nn} chosen to fit the $\Delta - N$ splitting, we subsequently calculated the complete excited-nucleon mass spectrum. All states of the N^* spectrum thus were *real predictions* within the models $\mathcal{A}$ and $\mathcal{B}$.

In a first detailed investigation of the predicted structures in the positive- and negative-parity shells, we indeed found excellent agreement between the empirical nucleon mass spectrum and the predictions of our model $\mathcal{A}$. Both the lower resonance regions and the higher (and even highest) mass regions could be uniformly described:

- As in the Δ sector, we found an excellent description of the positive-parity Regge trajectory $N\frac{1}{2}^+(939)$, $N\frac{5}{2}^+(1680)$, $N\frac{9}{2}^+(2220)$, $N\frac{13}{2}^+(2700)$, ... up to highest orbital excitations $J = \frac{13}{2}$. In particular, the model yields the correct phenomenological characteristic $M^2 \propto J$ with the right slope of the trajectory. We pointed out that, similar to the ground state, all excited states of the trajectory likewise are lowered by 't Hooft's force showing the non-trivial property of the instanton-induced force to be compatible with the observed linear Regge characteristics.
- All striking hyperfine intra-band structures in the even- and odd-parity shells can be nicely reproduced in at least qualitative (but mostly even in completely quantitative) agreement with the hitherto established, experimentally observed patterns. As a particular nice feature of model $\mathcal{A}$ we found that it is able to explain the conspicuous low position of the Roper resonance $N\frac{1}{2}^+(1440)$ in the $2\hbar\omega$ band (Roper *problem*), *i.e.* the first scalar/isoscalar excitation of the nucleon. Apart from the Roper state, the model can also account for the positions of three other rather low-lying states of the positive-parity $2\hbar\omega$ band around 1700 MeV, *i.e.* the $N\frac{1}{2}^+(1710)$, $N\frac{3}{2}^+(1720)$ and $N\frac{5}{2}^+(1680)$. In the negative-parity $1\hbar\omega$ shell, the hyperfine splittings of the five experimentally observed states $N\frac{1}{2}^-(1535)$, $N\frac{3}{2}^-(1520)$, $N\frac{1}{2}^-(1650)$, $N\frac{3}{2}^-(1700)$ and $N\frac{5}{2}^-(1675)$ are reasonably well reproduced.
- Concerning the experimental indications for the three new resonances showing up around 1900 MeV in photoproduction experiments with the SAPHIR detector at ELSA in Bonn, we found that our model indeed predicts possible candidates of states in the corresponding sectors. These predicted states nicely match the determined resonance position of the $P_{11}(1986)$ in the $N\frac{1}{2}^+$ sector and also the comparatively low positions of the $S_{11}(1897)$ and $D_{13}(1895)$ in the negative-parity sectors $N\frac{1}{2}^-$ and $N\frac{3}{2}^-$, respectively.
- Comparing the relative arrangement of the different even- and odd-parity bands, we indeed found overlapping substructures of shells with positive and negative parity leading to the occurrence of more or less degenerate states with the same spin and opposite parity. Hence, our model is able to account for the striking observed pattern of approximate parity doublets in the excited-nucleon spectrum as, *e.g.*, $N\frac{1}{2}^+(1710) - N\frac{1}{2}^-(1650)$, $N\frac{3}{2}^+(1720) - N\frac{3}{2}^-(1700)$, $N\frac{5}{2}^+(1680) - N\frac{5}{2}^-(1675)$ and $N\frac{9}{2}^+(2220) - N\frac{9}{2}^-(2250)$.

The corresponding discussion of model $\mathcal{B}$ has shown that it works less well and, in particular, strongly fails in describing one of the most prominent features, namely the low position of the Roper resonance. Hence we favor model $\mathcal{A}$ as the more realistic model.

In the subsequent, second part of our discussion we then analyzed in some detail the instanton-induced effects in the excited-nucleon spectrum of model $\mathcal{A}$ in order to clarify to what extent 't Hooft's force actually is responsible for generating all these striking features of the N^* spectrum simultaneously. Starting from the case with confinement only, we investigated how 't Hooft's force affects the energy levels when its strength is gradually increased from zero until the correct $\Delta - N$ splitting is achieved. Due to the selection rules of 't Hooft's force we observed in each shell a systematic lowering of those states which exhibit a dominant $^2 8[56]$ or $^2 8[70]$ spin-flavor $SU(6)$ configuration. In fact, we found that really all the prominent features of the N^* spectrum like, *e.g*, the Roper resonance or the patterns of approximate parity doublets are simultaneously generated along with the $\Delta - N$ splitting in this way. Accordingly, we thus could convincingly demonstrate that the instanton-induced interaction indeed provides a consistent, systematic and uniform explanation not only for the ground-state splitting between the Δ and the nucleon, but really for all the observed phenomena of the complete N^* spectrum listed above. All prominent features of the nucleon spectrum can be remarkably well described in our fully relativistic model $\mathcal{A}$.

To understand the shortcomings of model $\mathcal{B}$ in the $J = \frac{1}{2}^\pm$ sectors, we finally analyzed the effects of 't Hooft's force also in model $\mathcal{B}$. Comparing the instanton-induced effects in both models in the $N\frac{1}{2}^+$ sector, we demonstrated that the failure of model $\mathcal{B}$ in describing the low position of the Roper resonance indeed is caused by a quite different influence of the instanton-induced interaction on the excited $N\frac{1}{2}^+$ states of the $2\hbar\omega$ shell. We found that the different instanton-induced effects have their origin in a different initial level ordering and a different initial configuration mixing of the embedded Pauli spinors in the pure confinement case. This is caused by the different relativistic effects that are induced by the two distinct confinement Dirac structures of both models in combination with the embedding map of the Salpeter amplitudes. Hence we found the interplay of the residual force with the relativistic effects of the confinement Dirac structure to be very crucial. This clearly shows the importance to describe the light baryons in a fully relativistic framework.

The discussion of the whole non-strange baryon mass spectrum is thus completed and we have shown that with our model version $\mathcal{A}$ a simultaneous, consistent description of the complete Δ and nucleon mass spectra can indeed be achieved with only five parameters.

8 Summary and conclusion

In this paper we have computed the non-strange baryon spectrum on the basis of the three-particle Bethe-Salpeter equation with instantaneous interactions kernels. More precisely we used a string-like three-body confinement force and a regularized version of 't Hooft's instanton-induced interaction. We could construct a more or less unique model concerning the best fit of the model parameters. The following points (concerning the favored model $\mathcal{A}$) are particularly remarkable in comparison with the non-relativistic or relativized calculations. Regge trajectories up to the highest observed angular momenta could be reproduced. The hyperfine structure of the mass spectrum and in particular the Roper resonance and the parity doublets found a natural explanation. The lowering of the Roper resonance was due to a specific interplay of relativistic effects, the confinement potential (in model $\mathcal{A}$) and 't Hooft's force. This lowering was not isolated to the Roper resonance alone but could be identified also for higher resonance states. The question arises whether these achievements are purely accidental. Of course a clear answer cannot be given for any possible phenomenological interaction, but it can be answered at least for another QCD-inspired candidate, namely one-gluon exchange. From phenomenological grounds this alternative can be discarded for light flavors: We have demonstrated this by a Bethe-Salpeter calculation in the same spirit as described in this paper, see appendix A for a short description.

The way in which we have introduced 't Hooft's interaction in our spectroscopic calculation may look a bit too *ad hoc* for experts. Indeed more elaborate treatments of the characteristic instanton effects exist in the literature [63–69]. The result is however identical in form with the final two-body force used in this paper. The difference shows up mainly in the form factor of the force which we determined in a purely phenomenological way anyhow.

There remains to compute the spectrum of strange baryons in order to complete our unified description of the light-baryon masses. This will be done in a separate paper [26].

We have profited very much from scientific discussions with V.V. Anisovich, G.E. Brown, E. Klempt, K. Kretzschmar, A.V. Sarantsev and E.V. Shuryak to whom we want to express our gratitude. We also thank the Deutsche Forschungsgemeinschaft (DFG) for financial support.

Appendix A. One-gluon exchange forces

De Rujula, Georgy and Glashow [47] initially suggested to explain the hyperfine structure of hadrons by using the OGE as a residual interaction. Later it was applied in several non-relativistic potential models. To adopt this interaction in non-relativistic quark models, the fully relativistic expression for the perturbative OGE interaction is expanded in powers of $|\mathbf{p_q}|/m_q$ up to order $\mathcal{O}(|\mathbf{p_q}|^2/m_q^2)$, leading to the so-called Breit-Fermi interaction. Although various parts of this interaction have been applied in non-relativistic quark model calculations, *e.g.*, perturbatively for each shell in a naive oscillator model by Isgur *et al.* [36,37], the full expression, however, has never been used. Moreover, due to the fact that the quarks are not really slow, *i.e* $|\mathbf{p_q}|/m_q \approx 1$, the convergence of this expansion should be quite bad at least for light quarks such that even higher-order relativistic corrections might contribute significantly. In fact, such a treatment of relativistic effects of the OGE is therefore not justified. It should be emphasized that particular terms of the Breit-Fermi expansion are *deliberately neglected*. Employing the full Breit-Fermi interaction, a severe difficulty appears, which is referred to as the so-called "*spin-orbit-problem*". While the hyperfine structure of ground-state baryons can be nicely explained by the short-range spin-spin part (Fermi contact term), the inclusion of spin-orbit forces arising from OGE leads to large splittings for excited states spoiling the agreement with phenomenology, since the experimental mass spectrum of excited baryon resonances indicates that such a strong spin-orbit force should not exist between quarks. In order to obtain a reasonable description of the spectra, these approaches are therefore forced to remove the spin-orbit components of the OGE by hand and to include as spin-dependent part the color magnetic hyperfine interaction only. However, leaving these interactions out is rather unsatisfactory and inconsistent. Isgur argued heuristically [36,18] that spin-orbit forces might cancel with the Thomas term from a confinement force with scalar Dirac structure (see also ref. [70] and references therein). But in view of several terms of the Breit-Fermi expansion that are left out anyway, this explanation is not really convincing and thus still remains rather *ad hoc*.

In order to correct the flaws in the non-relativistic model, other potential model calculations, which retain the one-gluon exchange picture of the quark interaction, have gone beyond the original model of Isgur *et al.* The so-called "relativized" extension has been investigated by Godfrey, Capstic and Isgur for mesons [5] and subsequently also for baryons [6]. Also in this attempt, which still is based on the ordinary Schrödinger equation (with the kinetic energy replaced by its relativistic expression), the usual terms of the Fermi-Breit reduction of the OGE (including spin-orbit forces) as in the non-relativistic approach have been used. But compared to the non-relativistic version the expressions have been modified in order to *qualitatively* parameterize the momentum dependence of the relativistic corrections away from the $|\mathbf{p_q}|/m_q \to 0$ limit. However, this effective parameterization of relativistic effects is at the cost of introducing several new, non-fundamental parameters which were not derived from first principles. Using the new freedom to fit the additional parameters, the spin-orbit interactions could indeed be suppressed relative to the contact interaction. These effects, along with a partial cancellation of OGE-induced spin-orbit effects with those of a scalar three-body confinement (calculated within a two-body approximation) could finally

reduce the size of spin-orbit effects to an acceptable level. Nonetheless, in view of the crude method of "relativizing" the non-relativistic quark model, the spin-orbit puzzle connected with the employment of OGE as residual interaction is in fact unsolved.

More reliable investigations ultimately require the description of baryons in a fully relativistic framework, where relativistic effects of the residual force and the confinement force are *consistently* and *fully* taken into account. In this respect, a suitable approach to investigate this problem in fact is given by our covariant Salpeter framework. We therefore used this framework to verify the statements of the relativized quark model [6] concerning the spin-orbit problem in an analogous, but fully covariant model which we shall discuss here briefly. Recall that our approach does not introduce any additional parameters; all relativistic effects are *uniquely* and *fully* determined by means of the embedding map in the Salpeter amplitudes.

According to the assumptions of the relativized quark model [6], we parameterize confinement by a Δ-type three-body string potential which is assumed to have a *scalar* Dirac structure:

$$V^{(3)}_{\rm conf}(\mathbf{x}_1,\mathbf{x}_2,\mathbf{x}_3) = \left[3a + b\sum_{i<j}|\mathbf{x}_i-\mathbf{x}_j|\right] \quad \mathbb{1}\otimes\mathbb{1}\otimes\mathbb{1}. \tag{A.1}$$

In view of the instantaneous treatment of the OGE, the natural gauge for the gluon propagator is the Coulomb gauge [71], which will be applied in the following. This specific gauge has the advantage that the gluon propagator given by

$$\gamma^\mu D_{\mu\nu}\gamma^\nu = 4\pi\left(\frac{\gamma^0\otimes\gamma^0}{|\mathbf{q}|^2} + \frac{\boldsymbol{\gamma}\cdot\otimes\boldsymbol{\gamma} - (\boldsymbol{\gamma}\cdot\hat{\mathbf{q}})\otimes(\boldsymbol{\gamma}\cdot\hat{\mathbf{q}})}{q^2+\mathrm{i}\epsilon}\right) \tag{A.2}$$

with $\hat{\mathbf{q}} := \mathbf{q}/|\mathbf{q}|$ is already instantaneous in its component $D_{00}(q)$ which describes the ordinary Coulomb potential. In the instantaneous approximation we substitute q^2 in the second term by $-|\mathbf{q}|^2$. The two-quark OGE kernel in coordinate space then reads [71]

$$V^{(2)}(x_1,x_2;\,x_1',x_2') = V^{(2)}_{\rm OGE}(\mathbf{x})\;\delta^{(1)}(x^0)\;\delta^{(4)}(x_1-x_1')\;\delta^{(4)}(x_2-x_2'), \tag{A.3}$$

with $x = x_1 - x_2$ and

$$V^{(2)}_{\rm OGE}(\mathbf{x}) = -\frac{2}{3}\frac{\alpha_s}{|\mathbf{x}|}\left(\gamma^0\otimes\gamma^0 - \frac{1}{2}\boldsymbol{\gamma}\cdot\otimes\boldsymbol{\gamma} - \frac{1}{2}(\boldsymbol{\gamma}\cdot\hat{\mathbf{x}})\otimes(\boldsymbol{\gamma}\cdot\hat{\mathbf{x}})\right), \tag{A.4}$$

where $\hat{\mathbf{x}} := \mathbf{x}/|\mathbf{x}|$. Here α_s is the running strong-coupling constant, which in momentum space is assumed to saturate at a maximal value for $q^2 \to 0$. For the sake of simplicity, we shall treat the coupling α_s as a constant. This coupling together with the other parameters listed in table 25 has been fixed by a common fit to the spin-(3/2) decuplet and spin-(1/2) octet ground-states baryons as well as to the states $\Delta\frac{7}{2}^+(1950,****)$ and $\Delta\frac{11}{2}^+(2420,****)$ of the Δ Regge trajectory in order to obtain also the correct positions of the higher band structures. The Salpeter equation has been solved by expanding the states in a rather large harmonic oscillator basis up to $N_{\rm max} = 14$ for the spin-$\frac{1}{2}$ baryons and $N_{\rm max} = 12$ for all other spins.

Table 25. Model parameters of the scalar confinement, the quark masses and the strong coupling constant

Constituent quark masses	non-strange	m_n	450	MeV
	strange	m_s	675	MeV
Confinement parameters	offset	a	-395	MeV
	slope	b	926	MeV fm^{-1}
OGE	strong coupling	α_s	1.10	

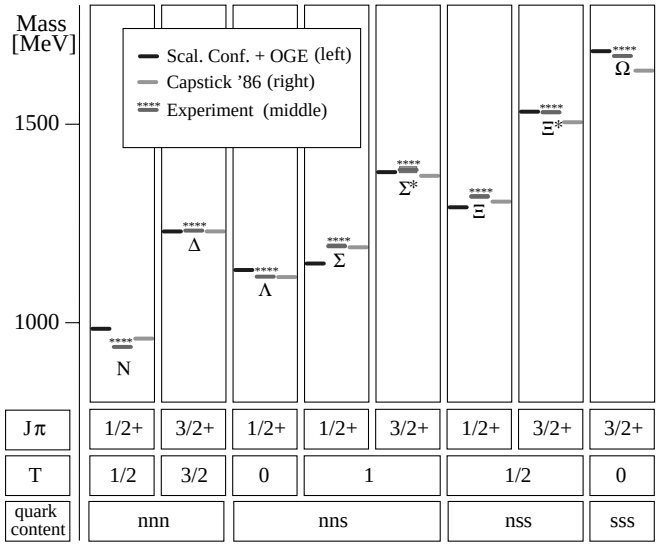

Fig. 23. The resulting spin-(1/2) octet and spin-(3/2) decuplet ground-state baryons calculated with a scalar three-body confinement and residual OGE interaction (on the left in each column). For comparison the results of the "relativized" model [6] are shown on the right in each column. In the middle of each column the experimental masses [38] are displayed.

Figure 23 shows the resulting masses of the octet and decuplet ground-state baryons in comparison with the experimentally observed positions [38]. In addition, also the results of the relativized model [6] are displayed. Since the ground states are dominantly S-wave states, the spin-orbit forces are irrelevant. As can be seen, also a fully relativistic treatment of the one-gluon exchange interaction allows a reasonable description of the hyperfine splittings $\Delta - N$, $\Sigma^* - \Sigma$ and $\Xi - \Xi^*$ which is comparable to the mass splittings generated by the spin-dependent Fermi contact interaction in the non-relativistic and relativized approach. Note, however, that the $\Sigma - \Lambda$ splitting turns out much too small in comparison to the observed splitting of roughly 75 MeV. It is worth mentioning that the value of the strong-coupling constant $\alpha_s = 1.1$ in our fully relativistic approach is *not* reduced relative to the usual values $\alpha_s \simeq 1.0$ determined in non-relativistic quark models. Treating α_s really as running coupling constant

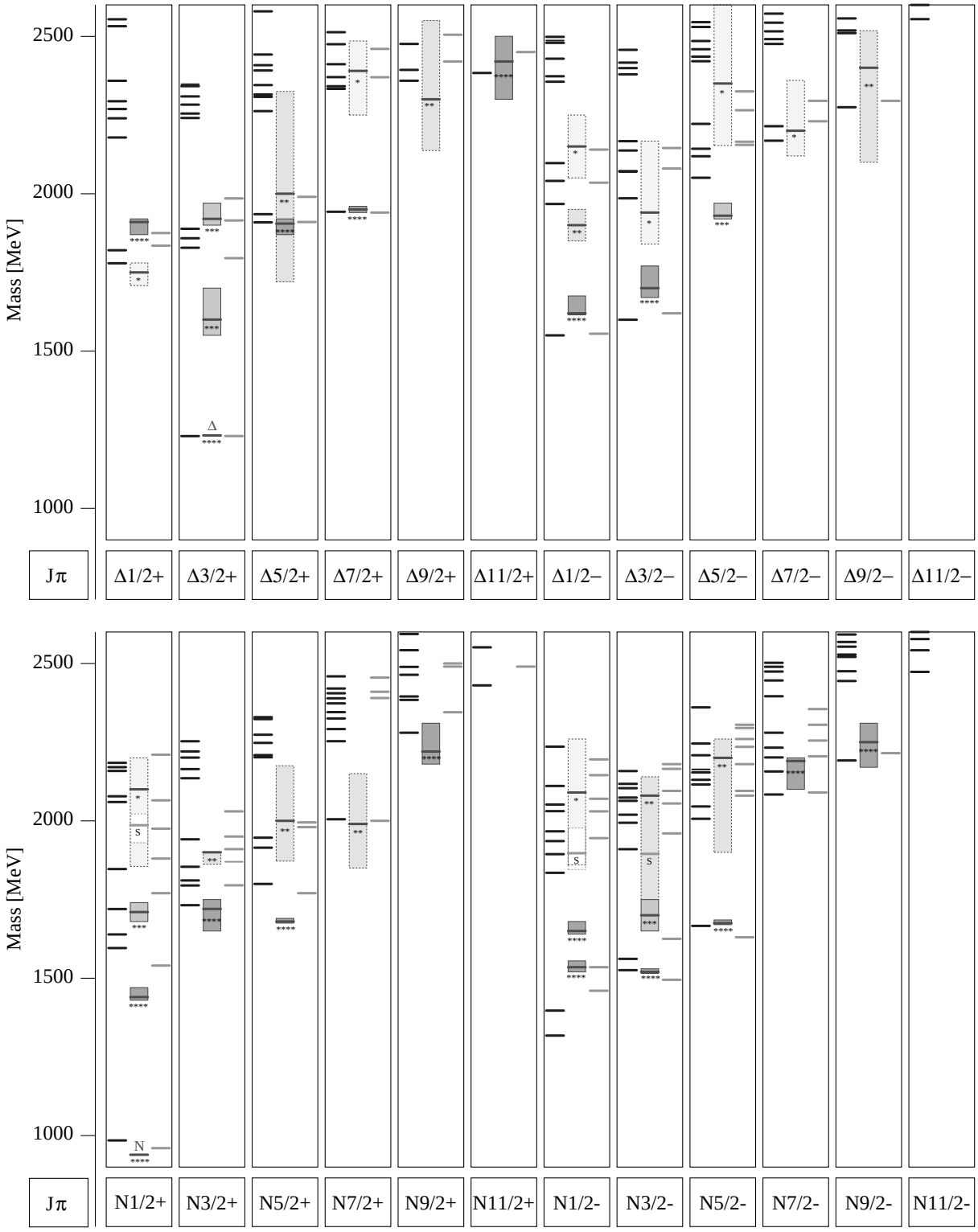

Fig. 24. The positive- and negative-parity *Δ- and N-resonance spectrum* calculated in a scalar three-body confinement model with residual OGE interaction (left in each column) in comparison to the experimental spectrum [38] (middle of each column) and the results of the "relativized" model [6,52] (right in each column). Experimental positions are indicated by a bar, the uncertainties by the shaded box which is darker for better established resonances; the rating is additionally indicated by stars.

would require a saturated value even bigger than 1.1. This is quite in contrast to the result of the relativized model [6], where this value became significantly smaller, namely $\alpha_s = 0.6$.

Concerning the spin-orbit problem, which in fact is our major interest here, let us as an example consider the spectrum of the excited non-strange baryons calculated with the parameter set of table 25. Our results for the Δ and N sector up to 2600 MeV are depicted in fig. 24, once again in comparison with the currently experimentally known resonance spectrum reported by the Particle Data Group [38] and the corresponding results of the relativized quark model [6,52]. In each column the resonances are classified by the total spin and parity J^π and in each sector from $\frac{1}{2}^\pm$ to $\frac{11}{2}^\pm$ at most the first ten predicted excitations are displayed. Altogether, the structure of the Δ spectrum can still be reasonably well accounted for. The spin-orbit effects are moderate enough to be compatible with the uncertainties of the experimentally observed Δ resonances in each band. Our calculation roughly agrees with that of the relativized quark model. For instance, the predictions for the two lowest excited $\Delta\frac{1}{2}^-$ and $\Delta\frac{3}{2}^-$ negative-parity states are quite the same. Notice however that both models predict their centroid too low with respect to the observed states $\Delta\frac{1}{2}^-(1620,****)$ and $\Delta\frac{3}{2}^-(1700,****)$. This is due to the fact that the OGE interaction shifts the Δ ground state upwards relative to these two states.

Much bigger discrepancies between the model predictions and the phenomenological spectrum emerge in the nucleon sector. First of all the predicted intra-band structures do not well agree with prominent empirical structures such as, *e.g.*, the four comparatively low-lying states of the positive-parity $2\hbar\omega$ band (including the Roper resonance) or the hyperfine splittings in the negative-parity $1\hbar\omega$ band. In fact, the most striking effect of the spin-orbit interaction is seen for the two lowest excitations of the negative-parity $N\frac{1}{2}^-$ sector. The center of gravity of these states is lowered by roughly 300 MeV with respect to the $N\frac{5}{2}^-$ state. Hence the predictions are far below the empirical positions of $N\frac{1}{2}^-(1535,****)$ and $N\frac{1}{2}^-(1650,****)$. We should note that this effect, although less pronounced, is likewise indicated in the relativized model [6], and also Isgur [36] predicted within a perturbative calculation of OGE-induced spin-orbit effects a quite large downward mass shift of roughly 500 MeV relative to the $N\frac{5}{2}^-$. However, we obviously cannot confirm the conjecture that these effects might cancel against corresponding equally large spin-orbit effects stemming from the scalar confinement force. We should remark that similar results are obtained also for the corresponding strange sectors. We tried to cure this problem by using other spin structures than scalar. In fact it turned out that hyperfine structures of excited states strongly depend on the Dirac structure chosen. But so far no appropriate choice has been found that could suppress the large OGE-induced spin-orbit effects in the $J^\pi = \frac{1}{2}^-$ sectors. In our opinion a solution of the spin-orbit puzzle connected with the residual OGE interaction thus seems highly questionable even in fully relativistic quark model. Our results concerning OGE in the Bethe-Salpeter framework indicate that it can be discarded for light flavors from phenomenological grounds.

In fact, apart from the spin-orbit problem of the residual OGE force, there are even more basic objections against the perturbative OGE interaction. Actually, it is only valid in the asymptotic-free domain of QCD, where the strong-coupling constant is small and perturbation theory is expected to work. However, baryon spectroscopy obviously belongs to the domain, where the strong coupling is large such that perturbation theory fails and therefore complicated higher-order multi-gluon exchange contributions should be of roughly the same order of magnitude as the lowest-order OGE contribution itself. The strength of OGE determined in an empirical way by a fit to the hyperfine splittings turned out to be roughly $\alpha_s \approx 1$ which indeed makes it hard to treat it as a perturbative effect. Furthermore, the OGE is explicitly flavor-independent and one thus obtains in the mesonic spectrum degenerate π and η mesons in clear contradiction to experiment. In order to cure this discrepancy, one in fact would have to take into account higher-order QCD diagrams [5]. All these arguments thus call into question the justification for applying the perturbative OGE in a non-perturbative sector of QCD. It can at best be added with a small coupling to the stronger force which we favor in this paper and would only modify the results slightly.

References

1. U. Löring, K. Kretzschmar, B.Ch. Metsch, H.R. Petry, Eur. Phys. J. A **10**, 309 (2001).
2. E.E. Salpeter, H.A. Bethe, Phys. Rev. **84**, 1232 (1951).
3. J.G. Taylor, Phys. Rev. **150**, 1321 (1966).
4. E.E. Salpeter, Phys. Rev. **87**, 328 (1952).
5. S. Godfrey, N. Isgur, Phys. Rev. D **32**, 189 (1984).
6. S. Capstick, N. Isgur, Phys. Rev. D **34**, 2809 (1986).
7. J. Resag, C.R. Münz, B.C. Metsch, H.R. Petry, Nucl. Phys. A **578**, 379 (1994).
8. C.R. Münz, J. Resag, B.C. Metsch, H.R. Petry, Nucl. Phys. A **578**, 418 (1994).
9. C.R. Münz, J. Resag, B.C. Metsch, H.R. Petry, Phys. Rev. C **52**, 2110 (1995).
10. C.R. Münz, Nucl. Phys. A **609**, 364 (1996).
11. B.C. Metsch, H.R. Petry, Acta Phys. Polon. B **27**, 3307 (1996).
12. R. Ricken, M. Koll, D. Merten, B.C. Metsch, H.R. Petry, Eur. Phys. J. A **9**, 221 (2000).
13. M. Koll, R. Ricken, D. Merten, B.C. Metsch, H.R. Petry, Eur. Phys. J. A **9**, 73 (2000)..
14. G. 't Hooft, Phys. Rev. D **14**, 3432 (1976), Erratum: *ibid.* **18**, 2199 (1978).
15. W.H. Blask, U. Bohn, M.G. Huber, B.C. Metsch, H.R. Petry, Z. Phys. A **337**, 327 (1990).
16. W.H. Blask, *Baryon-Spectroscopy and Scattering Observables in the Constituent Quark Model*, Ph.D. Thesis, University of Bonn, TK-90-07 (1990).
17. B.C. Metsch, *Instanton-induzierte Quarkkräfte und Hadronspektroskopie*, habilitation thesis, University of Bonn (1993).
18. S. Capstick, W. Roberts, nucl-th/0008028 (2000).

19. S. Mandelstam, Proc. Roy. Soc. **233**, 248 (1955).
20. V.V. Anisovich, Upton/BY, AIP Conf. Proc., Vol. **432** (AIP, New York, 1997) p. 421.
21. V.V. Anisovich, Phys. Usp. **41**, 419 (1998).
22. V.V. Anisovich, Usp. Fiz. Nauk **168**, 481 (1998).
23. A.V. Anisovich, A.V. Sarantsev, hep-ph/9705401; see also Phys. Lett. B **413**, 137 (1997).
24. V.V. Anisovich, A.V. Sarantsev, Phys. Lett. B **382**, 429 (1996).
25. V.V. Anisovich, Yu.D. Prokoshkin, A.V. Sarantsev, Phys. Lett. B **389**, 388 (1996).
26. U. Löring, B.Ch. Metsch, H.R. Petry, this issue, p. 447.
27. G.S. Bali, hep-ph/0001312 (2000).
28. J. Carlson, J.B. Kogut, V.R. Pandhariapande, Phys. Rev. D **27**, 233 (1983).
29. J. Carlson, J.B. Kogut, V.R. Pandhariapande, Phys. Rev. D **28**, 2807 (1983).
30. H.G. Dosch, V. Müller, Nucl. Phys. B **116**, 470 (1976).
31. F. Ferraris, M.M. Giannini, M. Pizzo, E. Santopinto, L. Tiator, Phys. Lett. B **364**, 231 (1995).
32. E. Santopinto, F. Iachello, M. Giannini, Nucl. Phys. A **623**, 100c (1997).
33. M.A. Shifman, A.I. Vainshtein, V.I. Zakharov, Nucl. Phys. B **163**, 46 (1980).
34. E.V. Shuryak, Nucl. Phys. B **203**, 93; 116 (1982).
35. C.G. Callan, R.F. Dashen, D.J. Gross, Phys. Rev. D **17**, 2717 (1978).
36. N. Isgur, G. Karl, Phys. Rev. D **18**, 4187 (1978).
37. N. Isgur, G. Karl, Phys. Rev. D **19**, 2653 (1979).
38. Particle Data Group, *Review of Particle Physics*, Eur. Phys. J. C **15**, 1-878 (2000).
39. L.Ya. Glozman, D.O. Riska, Phys. Rep. **268**, 268 (1996).
40. L.Ya. Glozman, Nucl. Phys. A **663-664**, 103 (2000).
41. D.M. Manley, E.M. Saleski, Phys. Rev. D **45**, 4002 (1992).
42. T.P. Vrana, S.A. Dytman, T.S. Lee, Phys. Rep. **328**, 181 (2000).
43. Particle Data Group, *Review of Particle Physics*, Eur. Phys. J. C **3**, 1-794 (1998).
44. V. Kanavets *et al.*, *Spectrum and parameters of isobars in the second resonance region–analysis of the experimental data* in *Proceedings of the 8th International Conference on the Structure of Baryons*, edited by D.W. Menze, B.Ch. Metsch (World Scientific, Singapore, 1999) p. 99.
45. I.G. Alekseev *et al.*, Phys. Lett. B **351**, 585 (1995).
46. I.G. Alekseev *et al.*, Phys. Rev. C **55**, 2049 (1997).
47. A. De Rujula, H. Georgi, S.L. Glashow, Phys. Rev. D **12**, 174 (1975).
48. E.V. Shuryak, J.L. Rosner, Phys. Lett. B **218**, 72 (1989).
49. A.E. Dorokhov, Yu.A. Zubov, N.I. Kochelev, Sov. J. Part. Nucl. **23**, 522 (1992).
50. B.C. Metsch, *Hadron Spectroscopy with Instanton induced Forces* in *Proceedings of the 99th WE-Heraeus Seminar on Quark Cluster Dynamics*, edited by K. Goeke, P. Kroll, H.R. Petry, *Lect. Notes Phys.*, Vol. **417** (Springer-Verlag, Heidelberg, 1992) p. 72.
51. O. Krehl, C. Hanhart, S. Krewald, J. Speth, Phys. Rev. C **62**, 025207 (2000).
52. S. Capstick, W. Roberts, Phys. Rev. D **47**, 1994 (1993).
53. E. Klempt *et al.*, *Photon excitations of baryon resonances* in *Proceedings of the 8th International Conference on the Structure of Baryons*, edited by D.W. Menze, B.Ch. Metsch (World Scientific, Singapore, 1999) p. 25.
54. Particle Data Group, *N and Δ Resonances*, revised by R.L. Workman in *Review of Particle Physics*, Eur. Phys. J. C **15**, 696 (2000).
55. R. Plötzke *et al.*, Phys. Lett. B **444**, 555 (1998).
56. M.Q. Tran *et al.*, SAPHIR Collaboratrion, Phys. Lett. B **445**, 20 (1998).
57. T. Mart, C. Bennhold, Phys. Rev. C **61**, 012201 (1999).
58. S. Capstick, W. Roberts, Phys. Rev. D **49**, 4570 (1994).
59. S. Capstick, W. Roberts, Phys. Rev. D **58**, 074011 (1998).
60. R. Bijker, F. Iachello, A. Leviatant, Ann. Phys. (N.Y.) **236**, 69 (1994).
61. R. Bijker, F. Iachello, A. Leviatant, Ann. Phys. (N.Y.) **284**, 89 (2000).
62. K. Kretzschmar, *Electroweak Form Factors in a Covariant Quark Model of Baryons*, Ph.D. Thesis, University of Bonn, TK-01-01 (2001).
63. T. Schäfer, E.V. Shuryak, Rev. Mod. Phys. **70**, 323 (1998).
64. D.I. Dyakonov, V.Y. Petrov, Nucl. Phys. B **245**, 259 (1984).
65. D.I. Dyakonov, V.Y. Petrov, Sov. Phys. JETP **62**, 204, 431 (1985).
66. D.I. Dyakonov, V.Y. Petrov, Nucl. Phys. B **272**, 457 (1986).
67. D.I. Dyakonov, V.Y. Petrov, *Diquarks in the Instanton Picture* in *Proceedings of the 99th WE-Heraeus Seminar on Quark Cluster Dynamics*, edited by K. Goeke, P. Kroll, H.R. Petry, *Lect. Notes Phys.*, Vol. **417** (Springer-Verlag, Heidelberg, 1992) p. 288.
68. M.A. Nowak, J.J.M. Verbaarschot, I. Zahed, Nucl. Phys. B **324**, 1 (1989).
69. M.A. Nowak, M. Rho, I. Zahed, *Chiral Nuclear Dynamics* (World Scientific, Singapore, 1996).
70. A.J.G. Hey, R.L. Kelly, Phys. Rep. **96**, 71 (1983).
71. T. Murota, Progr. Theor. Phys. **69**, 181 (1994).